Lukas Sterner, BSc

3D CFD simulations for Tonstad surge tanks upgrade

MASTER'S THESIS

to achieve the academic degree of a

Diplom-Ingenieur

Master's degree program: Geotechnical and Hydraulic Engineering

submitted to

Graz University of Technology

Supervisor

Univ.-Prof. Dipl.-Ing. Dr.techn. Gerald Zenz

Co-Supervisor

Dipl.-Ing. Wolfgang Richter

Institute of Hydraulic Engineering and Water Resources Management

Graz, March 2018

Supervisor:

Univ.-Prof. Dipl.-Ing. Dr.techn. Gerald Zenz

.....

Co-Supervisor:

Dipl.-Ing. Wolfgang Richter

.....

Statutory declaration

I declare that I have authored this thesis independently, that I have not used other than the declared sources/resources, and that I have explicitly marked all material which has been quoted either literally or by content from the used sources.

Graz, March 2018 .....

Eidesstattliche Erklärung (Ehrenwörtliche Erklärung)

Ich erkläre an Eides Statt, dass ich die vorliegende Arbeit selbstständig und ohne fremde Hilfe verfasst, andere als die angegebenen Quellen nicht benutzt und die den benutzten Quellen wörtlich und inhaltlich entnommenen Stellen als solche kenntlich gemacht habe.

Ich versichere, dass ich dieses Masterarbeitsthema bisher weder im In- noch im Ausland (einer Beurteilerin oder einem Beurteiler) in irgendeiner Form als Prüfungsarbeit vorgelegt habe.

Graz, im März 2018 .....

Acknowledgements

Zu Beginn dieser Arbeit möchte ich mich bei all jenen bedanken, die mich während meines Studiums und bei der Erstellung dieser Masterarbeit unterstützt haben.

Zuerst gilt mein Dank, Herrn Univ.-Prof. Dipl.-Ing. Dr. techn. Gerald Zenz und ganz besonders Herrn Dipl.- Ing. Wolfgang Richter für die im Laufe dieser Arbeit sich ergebenen konstruktiven Diskussionen und in weiterer Folge auch für die gebotenen Hilfestellungen. Ebenso gilt mein Dank dem Sira-Kvina Energieunternehmen für die Bereitstellung diverser Unterlagen, ohne welche diese Arbeit nicht in diesem Ausmaß realisierbar gewesen wäre.

Was wäre das Leben ohne Familie und Freunde, an dieser Stelle möchte ich mich bei meinen Eltern für die jahrelange Unterstützung in moralischer und finanzieller Hinsicht bedanken.

Ein besonderer Dank gilt auch meiner Freundin Carola, welche mir immer Rückhalt und Unterstützung geboten hat. Danke im speziellen auch für das entgegengebrachte Verständnis während der Erstellung dieser Arbeit.

Weiters möchte ich meinem Studienkollegen Marc danken. Ohne die gemeinsamen, produktiven Kaffeepausen, hätte mein Studium sich wahrscheinlich um etliche Semester verlängert.

Am Schluss möchte ich mich noch bei meinen Kollegen/innen des Beton-Holzbau Zeichensaals bedanken. Danke für die schöne gemeinsame Zeit und die dadurch entstandenen Erinnerungen.

Kurzfassung

Diese Arbeit befasst sich mit der hydraulischen Untersuchung eines möglichen Upgrades der Wasserschlösser des Tonstad Wasserkraftwerks in Norwegen.
Das Kraftwerk Tonstad hat eine Ausbauleistung von 960 MW, und liegt im Süd-Westen Norwegens. Es ist das größte Kraftwerk in Hinsicht auf die jährliche Stromproduktion mit etwa 4 TWh. Es besteht aus 5 Francis Turbineneinheiten, drei Druckrohrleitungen, drei Wasserschlössern und zwei Oberbecken in einem komplexen Triebwasserwegsystem mit etlichen Bacheinleitungen. Das norwegische Elektrizitätsnetz steht in den kommenden Jahren vor großen Veränderungen aufgrund der Konstruktion von neuen Hochspannungsleitungen wie z.B. dem Nord Link (1400 MW) und dem North Sea Link (1400 MW).
Diese beiden Leitungen werden das Festland mit Deutschland und Großbritannien verbinden. Der Stromhandel und die mögliche Nivellierung der variablen Quellen ist ein Hauptziel dieser Verbindung. Aufgrund dieser Veränderungen kann es notwendig sein, eine Aufrüstung der Ausgangsleistung vorzunehmen um den Marktanteil in Zukunft zu erhöhen.

In dieser Arbeit wurde ein Versuch unternommen, solch eine Aufrüstung durch eine Durchflusserhöhung vorzunehmen und auf die Notwendigkeit von Modifikationen an den Wasserschlössern anhand von 3D CFD Simulationen zu untersuchen.
Das 3D Modell der Wasserschlösser basiert auf Ausführungsplänen und besteht aus den Wasserschlössern, den verbundenen Entsandern und Druckrohrleitungen. Vorhergehende 1D Simulationen zeigten, dass eine Erhöhung von 25% des Ausbaudurchflusses bei zumindest Stauziel möglich ist, wenn die Installation einer Erweiterungskammer in der Höhenlage der bestehenden Unterkammern durchgeführt wird.

Diese Erweiterungskammer wurde direkt an eines der Wasserschlösser angeschlossen. Die Kammer wurde modelliert und hydraulisch untersucht, um die Notwendigkeit von Adaptionen festzustellen und soll als eine Machbarkeitsuntersuchung für die Erzielung einer Leistungserhöhung dienen.

Abstract

The present work deals with a hydraulic detail study on the possibility of an upgrade of the surge tanks of the Tonstad hydropower plant (HPP) in Norway.
Tonstad HPP with a capacity of 960 MW, situated in the south west of Norway is the largest power plant according to the annual energy production of about 4 TWh. It consists of 5 power units, three penstocks, three surge tanks and two main upper reservoirs in a complex water system with additional several brook inlets.
The Norwegian energy grid is facing major changes in the oncoming years, due to the construction of several interconnectors such as the Nord Link (1400 MW) and the North Sea Link (1400 MW). These two new power lines will connect the mainland with Germany and the UK. Electricity trade and possible levelling of variable source is a main goal of the interconnection. These grid changes make it necessary to upgrade power plants in means of the power output to increase market participation in the future.

In this thesis the approach for such an upgrade is made by increasing the discharge by 25% and investigating the needed modifications at the surge tanks of Tonstad HPP by the use of 3D CFD simulations.
The 3D model of the surge tanks of Tonstad HPP was built based on design plans and consists of the surge tanks itself and the associated sand traps and penstocks. Foregoing 1D simulations showed that an upgrade can be realised by the installation of an additional lower chamber defined as extension chamber that is directly connected to one of the surge tanks. This extension chamber was modelled and hydraulically investigated for the need of adaptions and should serve as a feasibility study of such an upgrade.

Table of contents

1. Introduction

One of the main targets of the European Union regarding the energy policy to improve an integrated energy market is to ensure the flow of energy throughout the whole union without any restrictions or adaptations. In this way it is secured that all energy providers can compete and offer the best price to their consumers. One other goal is a high achievement of renewable energy potential for all member states (European Commission , n.d.).

In Norway, an associated country to the EU, Statnett is the transmission system operator (TSO), in charge for achieving this requirements (Vereide , et al., 2017). Norway is regarding renewable energy a forerunner within the union, because 99% of the energy is generated by hydropower (Statkraft, n.d.). Norway is blessed with much rainfall and high mountains and a well-established engineering culture.

The Norwegian grid is also facing major changes due to the construction of two new HVDC interconnectors. The first one is the Nord Link, connecting Norway and Germany, with a capacity of 1400 MW, which should be put in service by the year 2020. The second one is the North Sea Link, connecting Norway and the UK, with the same capacity of 1400 MW, which should be completed by the year 2021 (Statnett & Fingrid, 2016).

On this basis the power plant operators are forced or invited to adjust to the emerging new challenges in the demand of energy. Due to the huge energy storage capacity of about 84 TWh in the Norwegian grid by the potential energy of the reservoirs, Norway can balance a significant amount of power indirectly. The safety of the whole grid is depending on the power output and the corresponding flexibility of each power plant. The operators could on the one hand, just build new power plants or on the other hand upgrade the existing ones. Due to the idea of the sustainable thinking, the second method an upgrading of existing power plants can provide power increase by using existing facilities. Obviously, not every power plant is suitable to be upgraded due to technical or other restrictions e.g. water resources, installed machinery etc.

In this thesis, an approach is made at an existing power plant to upgrade the power output and the corresponding flexibility at the power plant Tonstad. In particular, the hydraulic upgrade of existing surge tank facilities is investigated. The investigations are made by the use of 3D CFD simulations.
The possible hydraulic upgrade of the Tonstad surge tanks is an outcome of the ongoing research initiative Flexible Sand Traps (FlekS). The Tonstad surge tanks are directly connected to the pressurized sand traps that are included in the power water conduits (Richter , et al., 2017).

1.1 Tonstad Hydropower plant

The municipality Tonstad is situated in the Sirdal valley, in the south west of Norway at the northern end of the lake Sirdalsvann. The power plant is part of the Sira-Kvina development project and owned by the Sira-Kvina hydro power scheme and owned by the Sira-Kvina power company. The power plant is part of a series of seven power plants illustrated in Figure 1.

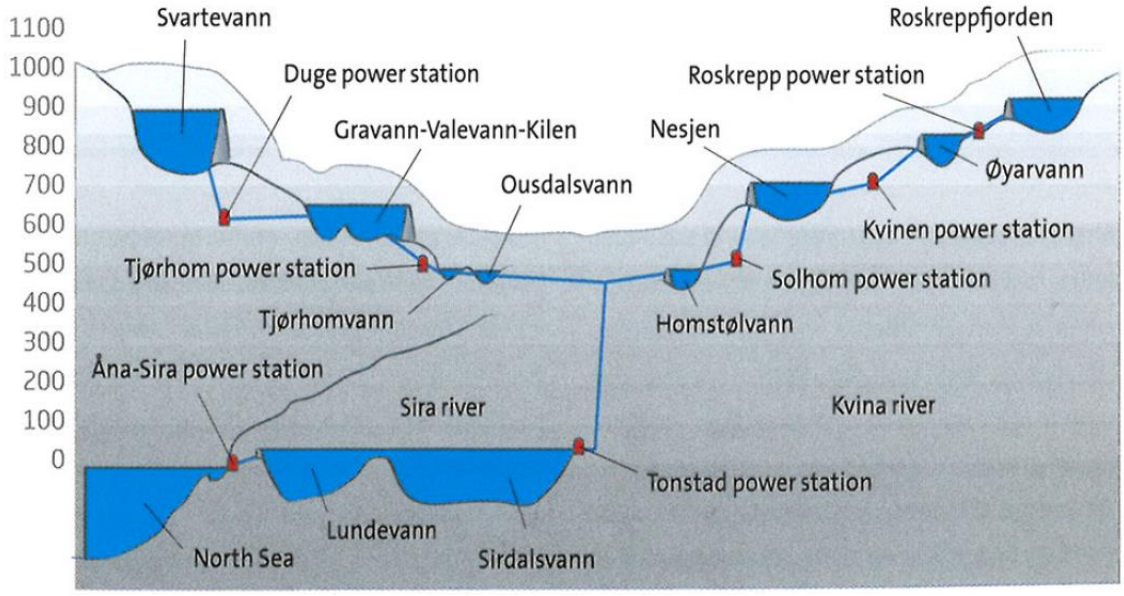

Figure 1 - Overview Sira-Kvina waterway system (Møller, 2009)

All seven power plants together have an installed capacity of 1760 MW and provide a large portion of the Norwegian power output (Møller, 2009). The installed capacity of the Tonstad power plant is 960 MW and is in respect to the annual produced energy of nearly 4 TWh the largest power station in Norway.

The capacity is distributed to five vertical Francis turbines that have a combined discharge of about 250 m^3/s and a gross head of 450 m.

The power plant was put in service in 1968 by starting energy production with two turbines, each with a capacity of 160 MW. In 1971 two additional turbines with a capacity of 160 MW were commissioned. The final addition until now was the fifth turbine with a capacity of 320 MW in 1988 (Sira-Kvina Kraftselskap, n.d.). Table 1 should sum up the key information.

Table 1 - Key information Tonstad power plant (Sira-Kvina Kraftselskap, n.d.)

Units	Capacity	Design discharge
M1 & M2	each 160 MW	each 42.5 m^3/s
M3 & M4	each 160 MW	each 42.5 m^3/s
M5	320 MW	80 m^3/s
Overall	960 MW	250 m^3/s

1.1.1 Development

From commissioning until the 1990s the power plant was mainly operated as a base load power plant, this situation changed then because of the deregulation of the northern power market (Nordpool). Due to the deregulation and the additional installation of the fifth machinery in the end of the 1980s, the power plant started operating as well as a peaking power plant. In the last years, the power plant has additionally started to supply frequency restoration reserves (FRR) to the national transmission system operator (TSO) Statnett (Vereide , et al., 2017)

These changes influenced the hydraulic loading and thus the sediment transport in the headrace system and at the existing sand traps. This means that the interval of the frequency of the inspections or emptying of the sand traps decreased to under two years. The water tunnels of the Tonstad power plant are mainly unlined tunnels with large flow sections.

As many other Norwegian tunnels, they were constructed by drill and blast, leaving some of the blasted material on the invert to have smooth driving conditions for the machines. This saved much time of cleaning and resulted in an earlier power plant commissioning. This material is most likely still the main contributor of sediments in the sand trap. The amount of material coming from the eight creek intakes is unknown.

The experience shows that due to the operational changes the mass oscillation in combination with the high head losses in the headrace system has led to at least one situation with free surface flow in the sand trap. Such a free surface flow is not helpful at any point of operation because it may cause a flushing of sediments down to the turbines and thus damages. Because of these events it was decided to establish a minimum water level in the surge tank at steady operation of 470 m a.s.l. This limitation results in a reduction of the maximum power output and influences the flexibility of the power plant (Vereide, et al., 2015).

1.1.2 Components of the power plant

The power plant can be divided into three main components, which will be described in the following sub-chapters. The first part is the waterway and the reservoirs, followed by a description of the surge tanks. The last components are the sand traps. These are placed directly before the water enters the pressure shafts.

1.1.2.1 Waterway and reservoirs

The power waterway is part of a greater system. This system gets fed by the Sira and Kvina rivers. There are two power stations along the Sira river and three along the Kvina river (Figure 1). The two upper reservoirs of Tonstad power plant are the downstream reservoirs of the foregoing power stations.

The Tonstad power plant gets mainly fed by two upper reservoirs and additional eight brook inlets along large headrace tunnel. The reservoir on the Kvina river

side is the Homstølvann and the respectively on the Sira river side the Ousdalsvann. Due to the excellent rock quality, the main part of the system consists of unlined tunnels, only small sections with poor rock or weakness zones had to be lined.

The tunnel branch from the Ousdalsvann has a length of 16 km and a flow section area of 65 m^2, the water tunnel from the Homstølvann reservoir has a length of 7.5 km and a flow area of 55 m^2. These two merge into one tunnel with a cross section of 100 m^2 and a length of 6 km until it splits into three branches. All three branches have the same structure and consist of a surge tank with an associated sand trap. The brook inlets have a significant impact on the behaviour of the power plant because of the dampening effect, which is connected to them. The brook inlets function as small surge tanks along the headrace system (Vereide , et al., 2017).

Figure 2 shows the full Sira-Kvina hydropower system in ground view. The specific area of the Tonstad scheme is indicated.

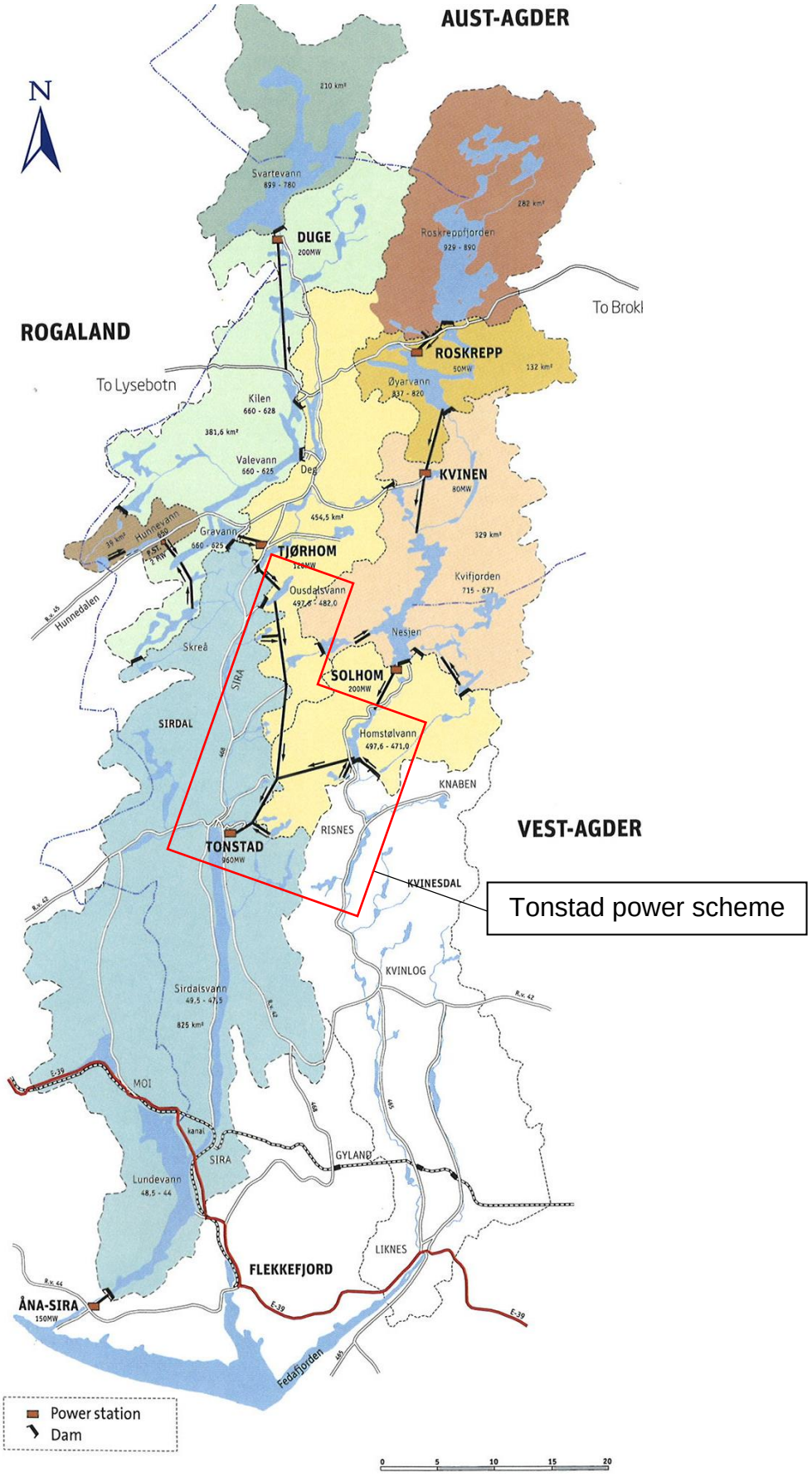

Figure 2 - Overview Tonstad power plant waterway (Møller, 2009)

1.1.2.2 Surge tanks

The power plant has a total of six surge tanks, three of them on the upstream side and three at the downstream side of the turbines. The main focus in this present work is regarding the three upstream surge tanks.

Surge tanks no.1 & no.2

The numbering of one and two is based on the machinery they are affiliated with; e.g. Machinery M1 & M2 → Surge tank no.1, Machinery M3 & M4 → Surge tank no.2. These two surge tanks are identical constructed with one exception according the orientation of the lower chamber. The lower chambers are orientated in a right angle to the main tunnel axis. In the following the lower chambers are referred as start-up chambers, due to the fact how they are commonly called in Norway. This also indicates that those chambers were not designed for a resonance load cases with reloading events.

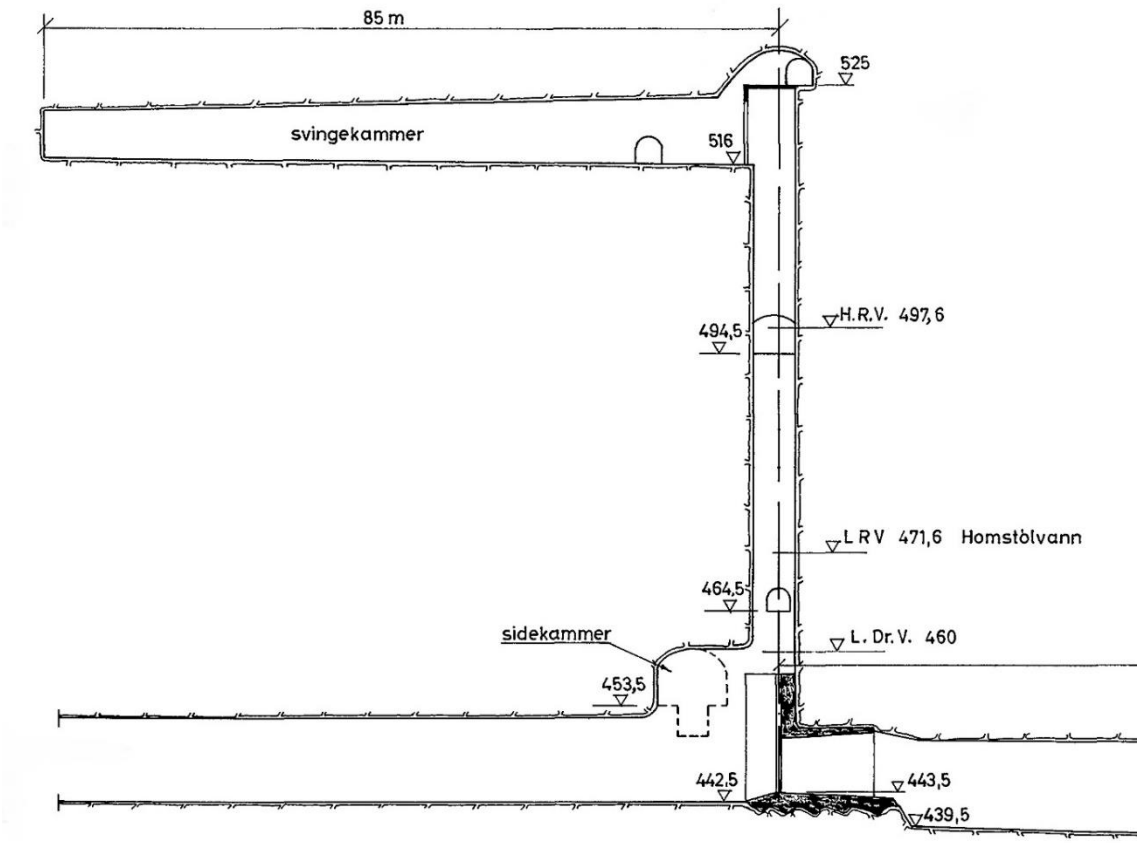

Figure 3 - Surge tank no.1 & no.2 elevations and dimensions

The two surge tanks are connected via three transverse tunnels, one situated in the upper chamber and two along the surge shaft. The top section of the surge shaft contains a maintenance tunnel and a platform that is used for the control of the sand trap gates and the hydraulics needed for the operation. The elevations of the tunnels are shown in Figure 3. A throttle is situated at the beginning of the upper chamber to increasing the differential effect of the surge tank. The width of the throttle opening is 2.3 m and has height of about 9 m. The Figure 4 shows a cross section at the position of the larger transverse tunnel and shows that the two surge shafts are very much identical and have an section area of approximately 35 m^2 (Figure 4).

Most of the surge tank is unlined rock due to the good rock quality. Only the lower part where the gates are placed, directly before the sand traps is lined with concrete.

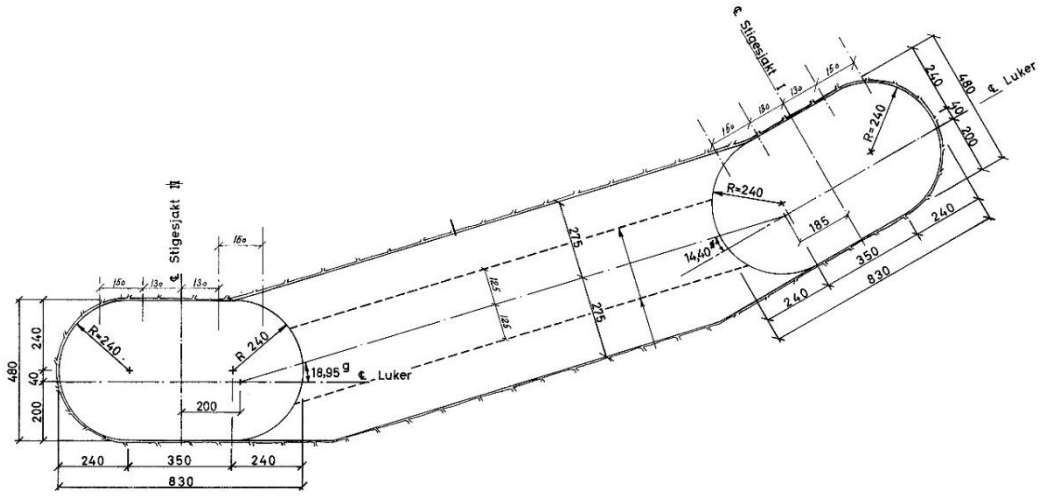

Figure 4 - Surge shaft no.1 & no.2 cross section

Surge tank 3

This surge tank is the largest and newest, it is connected to the pressure shaft leading to machine no.5 and has some different layout aspects compared to the surge tanks no.1 and no.2. The upper chamber as well as the start-up chamber have a larger volume. The upper chamber splits into two tunnels. In contrast to the start-up chambers of surge tank no.1 and no.2 this one is an extension of the headrace tunnel. As well as mentioned before the top section of the surge shaft consist of an access tunnel and the space for the control devices needed. The throttle at the entry of the upper chamber has a slightly greater opening width than the ones from surge tank no.1 and no.2. The elevations and dimensions of the surge tank are shown in Figure 5.

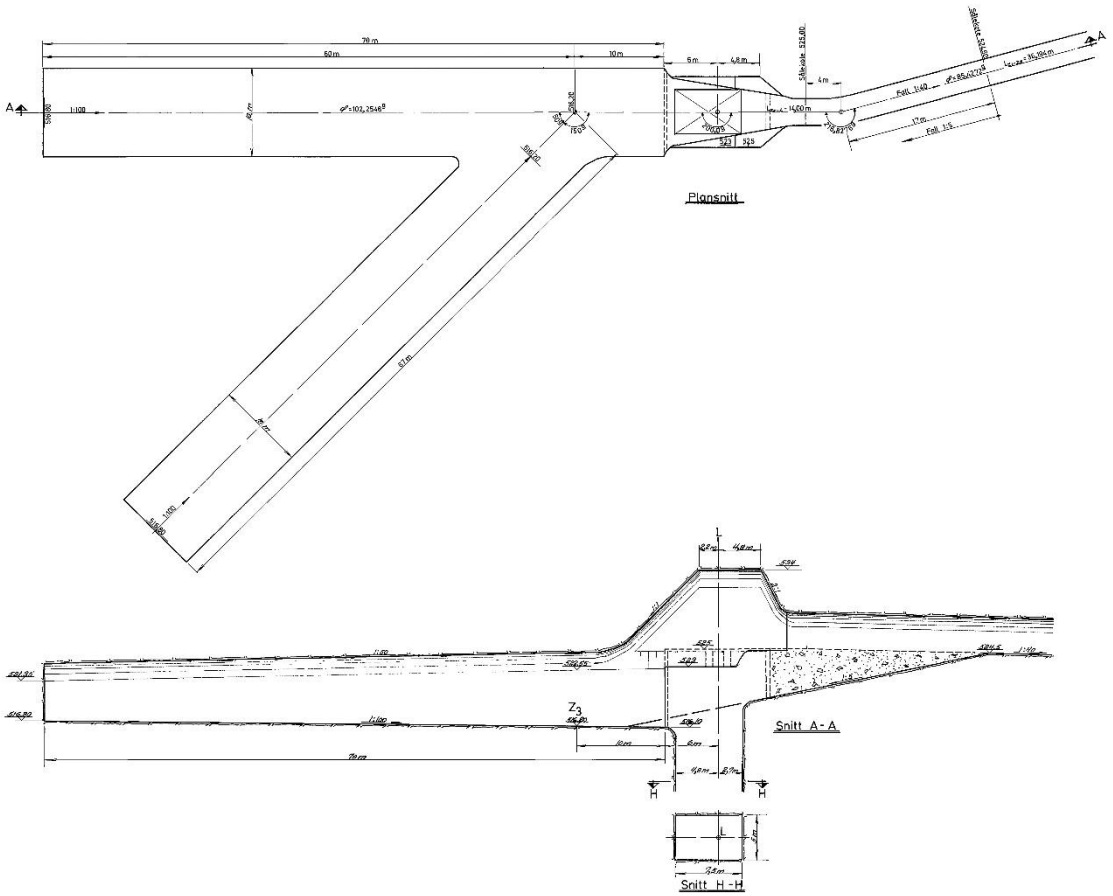

Figure 5 - Upper chamber surge tank no.3

As mentioned in the chapter before the third surge tank also consist of unlined rock with the exception of the lower part in the area of the gates.

1.1.2.3 Sand traps

In Norway it is typical to construct unlined hydropower tunnels, this is possible due to very good rock quality and advantageous rock pre-stress conditions. It is common that parts of the excavated material are left at the tunnel bottom to allow access road during construction. Then to spare the time of cleaning the material is left inside the tunnel (Vereide , et al., 2017). Due to this fact the sediment transport is an issue and is the main reason of the sand trap need. All three surge tanks are directly equipped with a pressurized sand trap. This is noticeable by the widening of the cross section after the gates to 100 m^2. The tunnel sections are used for the deceleration of the water and allow sedimentation before entering the penstocks. The walls are unlined rock and the floor is paved with concrete. There is a possibility of different installations within the sand trap, to increase the efficiency (Vereide , et al., 2017), the Tonstad power plant has none of such automation installations yet. In case of maintenance it is possible to reach the sand trap via access tunnels to clean the deposited material out.
The layout is nearly identical for all three of them, as example the sand trap from surge tank no.1 is shown in Figure 6.

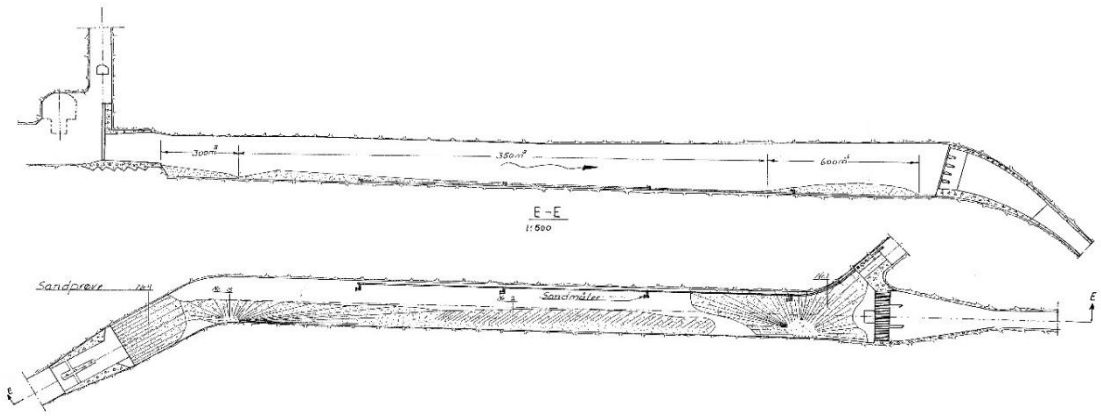

Figure 6 - Sand trap no.1 layout

1.2 Thesis objectives

In this thesis it is investigated to increase the total discharge of the power plant by 25%. This would lead to an increase of the power output of up to about 20 %. Thus, the discharge is investigated with an increase of 62.5 m^3/s. A higher discharge leads to higher losses in the power water way. Therefore, the increase in power is not equal to the increase in discharge. Still the possible power upgrade is significant. The advantage is that the overall upgrade of the power plant is possible by upgrading the surge tank. Since usually it is very difficult to upgrade power water ways owing to long outage of the hydropower plant . In consequence is the power plant challenged with higher losses due to the increased discharge and flow velocity. Due to the possible upgrade the sediment transport also evolves to an important issue and should be investigated further. At all circumstances, should free surface flow in the sand traps be avoided to reduce the chance of sediment or rock transport down the penstocks to the turbines.

The aim of this thesis is to investigate the needed structural adaptions at the surge tank of power plant to secure a proper operation with a higher discharge. This is done by investigating a design load case with means of 3D CFD including a quick start-up and shutdown at maximum flow in the headrace tunnels. The sediment transport itself is neglected.

2. Theoretical basis

This part gives a brief explanation of the hydraulic theories behind this thesis. The phenomena of the water hammer and the resulting idea of a surge tank is explained. The main hydraulic losses appearing at the given system of Tonstad are defined and explained by the use of the affiliated equations.

2.1 Water hammer

Every change in flow velocity at an open channel or pipe leads to pressure fluctuations. In an open channel this change leads to a raising or lowering of the water surface (up- or down surge), within a pressurized pipe this change leads to a conversion from motion energy to pressure energy (Giesecke , et al., 2014).
In Figure 7; the concept of the water hammer is demonstrated at a simple system, consisting of a tank with pipe and a valve at the end.

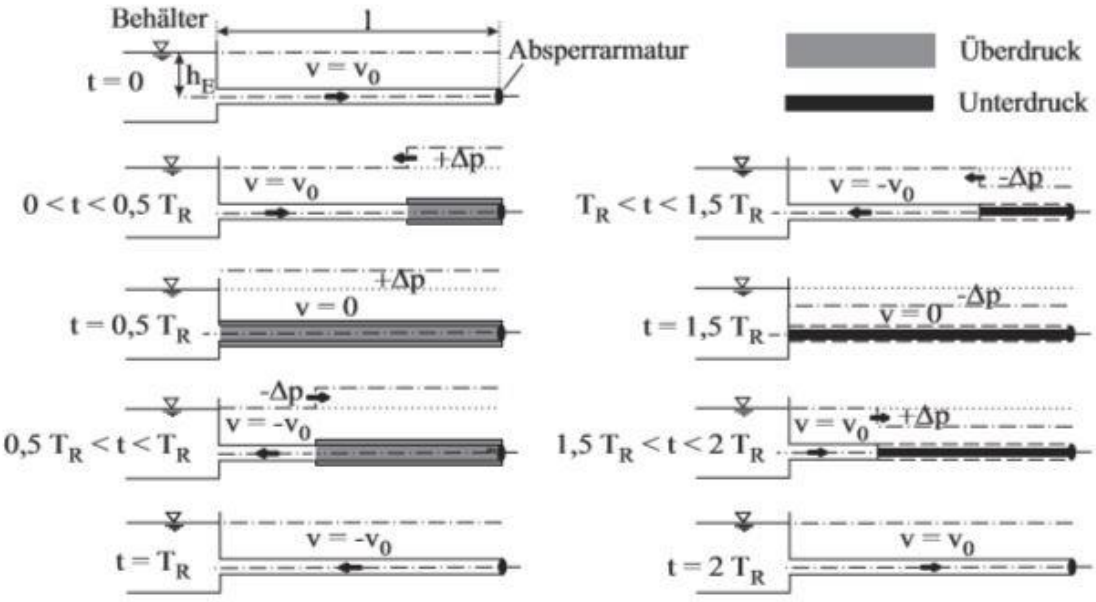

Figure 7 - Chronological sequence of the water hammer (Giesecke et al.,2014)

After the sudden shut down and the affiliated sudden delay of the flow velocity, a water hammer *Δp* (pressure increase) is formed. The water hammer now spreads as a pressure wave along the pipe with the velocity *a* [m/s] until it reaches the free surface at the tank. At the moment the water hammer reaches this free surface, it gets fully reflected and so the sign changes negative. This change in sign leads an under pressure wave. This wave is again reflected at the

free surface and the sign changes again. Figure 7 represents a theoretical assumption without any losses or dampening. In reality the pressure wave will be dampened by the wall friction of the pipe. Due to this dampening the first oscillation will be the largest and is therefore the crucial one. The first oscillation or the maximum water hammer can be estimated per the following equation after Joukowsky (Giesecke , et al., 2014).

$$maxh_a = \pm \frac{a \cdot \Delta v}{g} \; [m] \tag{2-1}$$

$maxh_a$ maximum water hammer

a wave propagation velocity [m/s]

Δv velocity difference [m/s]

g force of gravity [m/s²]

The reflection time T_R is the needed time until the pressure wave is back at the starting point. The closing time t_s of a valve has a significant impact on the size of the amplitude of the water hammer. If the closing time t_s is greater than the reflection time T_R a water hammer reduction occurs due to the overlap at the open end. If the closing time t_s is smaller than the reflection time T_R, the full water hammer occurs at the valve independent on the closing mechanism. The calculation of the reflection time is easily calculated by the following equation (Giesecke , et al., 2014).

$$T_R = 2 \cdot T_L = {}^{2 \cdot l}/_{a} \; [s] \tag{2-2}$$

T_R reflection time

l length to the nearest free water surface [m]

Therefore, the first peak or the water hammer can be estimated via the following linear equation.

$$maxh_a \approx \frac{a \cdot \Delta v}{g} \cdot \frac{T_R}{t_s} \; [m] \quad \text{for } t_s > T_R \tag{2-3}$$

It can be seen that the only variable term in this equations is the reflection time or in the broadest sense the distance to the nearest free water surface. The idea of the shortening of the distance leads to the concept of a surge tank in sense of a water hammer protection device (Giesecke , et al., 2014).

2.2 Surge tank

A surge tank has to be situated as close as possible to the penstocks. A surge tank ensures a stable operation of a power plant (Vereide , et al., 2017). Therefore, when significant tunnel lengths appear is it crucial to construct a surge tank. For the decrease of the water hammer some effects may be taken into account. First, the reduction of the length until the nearest free water surface. Second, a surge tank improves the acceleration of the water volume during the start-up of the turbines and the deceleration at turbine closing. These effects have a main and positive impact on the stability and the flexibility of a hydropower plant.

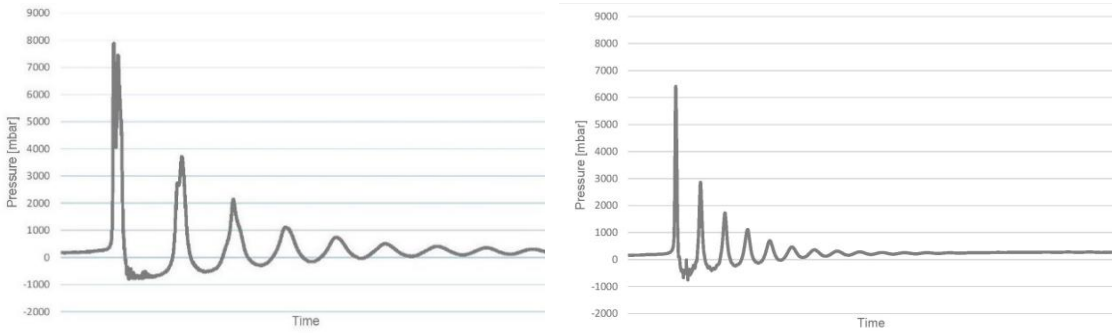

(a) surge tank disconnected (b) surge tank connected

Figure 8 - Water hammer comparison (measurement at valve)

The effect of the dampening on the mass oscillation as well as on the water hammer is shown in Figure 8 above. The data was collected during a laboratory test at the Hydraulic institute at the Technical University Graz during the course of a lecture. The set-up consists of a water reservoir, a pressure tunnel and shaft and a surge tank. Valves are situated at the bottom of the surge tank and at the end of the pressure shaft. This set-up makes it possible to connect or disconnect the surge tank and the simulating of a sudden closing of the shaft. The time intervals for the two tests were the same.

In Figure 8a the surge tank is not connected and the system only experiences the water hammer with the peak value at the beginning and due to no superposition of two wave structures the effect lasts longer before it dampens out. In Figure 8b, the peak value of the first oscillation is slightly smaller and decreases at a faster rate.

2.3 Hydraulic losses

The base equation for the movement of a fluid is the Bernoulli equation

$$H = z + \frac{p}{\gamma} + \frac{v^2}{2 \cdot g} = const. \tag{2-4}$$

H	total height [m]	γ	specific weight [N/m^3]
z	height above reference plane [m]	v	flow velocity [m/s]
p	pressure [N/m^3]	g	gravitational force [m/s^2]

This equation is based on the idea of an ideal fluid. In the following equation the term of losses is added to represent real fluid behaviour.

$$H = z + \frac{p}{\gamma} + \frac{v^2}{2 \cdot g} + \sum_0^x h_v = const. \tag{2-5}$$

The term h_v should describe all the losses occurring within a pipe flow. The losses can be divided into two parts.

$$\sum h_v = \sum Throttle\ losses + \sum Friction\ losses \tag{2-6}$$

Their characteristics as well as the formulas for the calculation of the two are described in the following sub-chapters (Bollrich, 2013).

2.3.1 Throttle losses

The term "throttle losses" is a general term for the sum of hydraulic losses associated with flow through throttles, for example: at inlets or a sudden/gradual expansion or contraction. The losses, independent of which type, are defined via the following formula. The coefficient of loss ζ is defined depending on the given situation, and is a convenient simplification of the real situation (Bollrich, 2013).

$$h_v = \zeta_i \cdot \frac{v^2}{2 \cdot g} \tag{2-7}$$

2.3.1.1 Inlet losses

The coefficient of entry loss ζ_e is determined based on the shape of edges at the inlet. The difference of the values is shown in Figure 9.

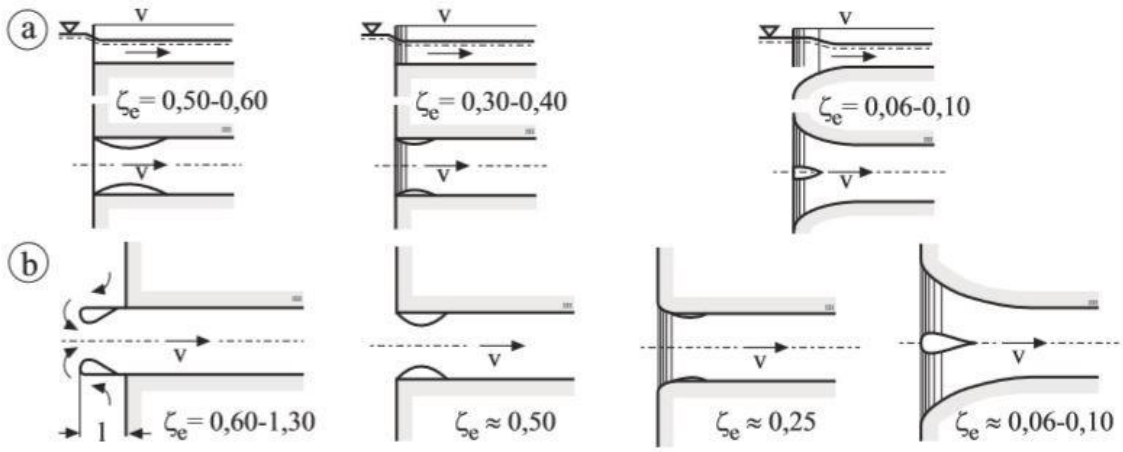

Figure 9 - Coefficient of loss ξ_e for (a) channel or (b) pipe inlet (Giesecke et al., 2014)

The values for the coefficient are based on in situ test and empirical values. It should always be the intention to form rounded edges to provide a smoother transition and therefore lower losses at inlets (Giesecke , et al., 2014). Except there is a special need for local losses, such as in surge tanks.

2.3.1.2 Expansion/Contraction

There has to be a differentiation between a sudden or a gradual expansion resp. contraction. If the cross-section change is a sudden or a gradual one, has a significant impact on the size of the coefficient. The turbulences at a sudden change and therefore the coefficient is larger than for a gradual one (Bollrich, 2013).

Sudden expansion/contraction

This case can be described as Borda-Carnot impact loss. The coefficient of loss ζ_v is mainly depending on the ratio between the two cross sections. The Figure 10 gives an impression of the situation at a sudden expansion (Bollrich, 2013).

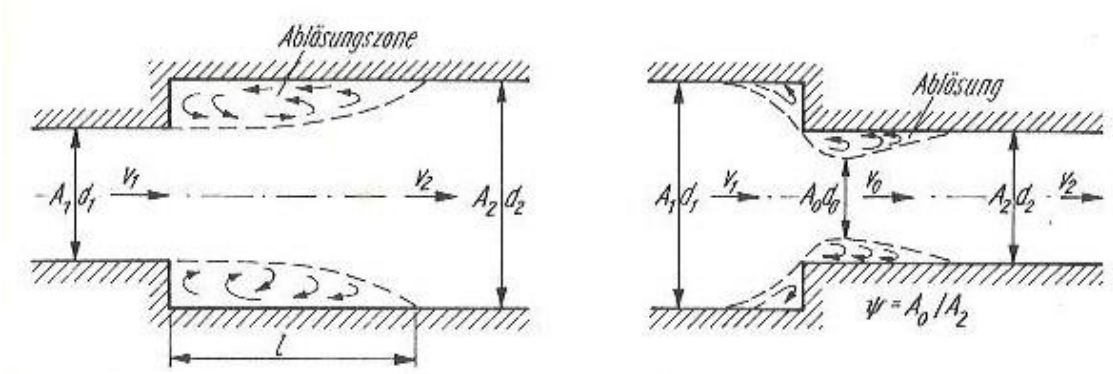

a) Sudden expansion b) Sudden contraction

Figure 10 - Sudden expansion/contraction - Borda-Carnot (Bollrich, 2013)

Sudden expansion:

$$\zeta_v = \left(1 - \frac{A_1}{A_2}\right)^2 \qquad (2\text{-}8)$$

Sudden contraction:

$$\zeta_v = \left(1 - \frac{A_1}{A_2}\right)^2 \qquad (2\text{-}9)$$

The coefficient of loss ζ_v is calculated via the equations above, it can be seen that the value of it is strongly depending on the ratio of the cross-section change.
In Figure 10a can It be seen that due to the sudden expansion, sort of a jet is formed and separates from the remaining fluid and leads to turbulences along the bigger cross section. These turbulences are the reason for the local losses. In the case of a sudden contraction (Figure 10b), the jet is also formed but now in the smaller cross section. The turbulences appear due to the expansion of the jet, also some recirculation zones are formed and dissipate energy.

Gradual expansion

A gradual expansion is also known as diffuser. The main equation for the coefficient of loss ζ_v is the same as for the sudden expansion with the exception that it is multiplied by a reduction factor η. The factor η is depending divergence angle β. If the angle is smaller than 8°, this means that no separation of the stream appears and therefore the factor η is zero. In the case of an angle larger than 20° the factor η is 1, this leads to the case of sudden expansion. Figure 11 gives an impression of the situation (Bollrich, 2013)

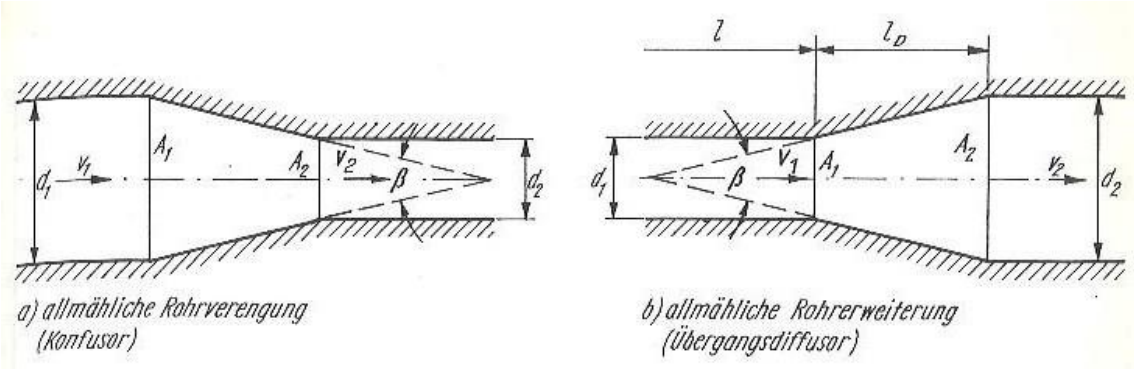

Figure 11 - Gradual expansion or contraction (Bollrich, 2013)

Figure 12 represents a more detailed flow situation at the expansion. It indicates that the length, until the flow is without vortices is longer than at a sudden expansion (Idel'chik, 1994). The losses for a sudden cross section change are indeed bigger than for a gradual one but depending on the different applications it is sometimes wiser to prefer one over the other.

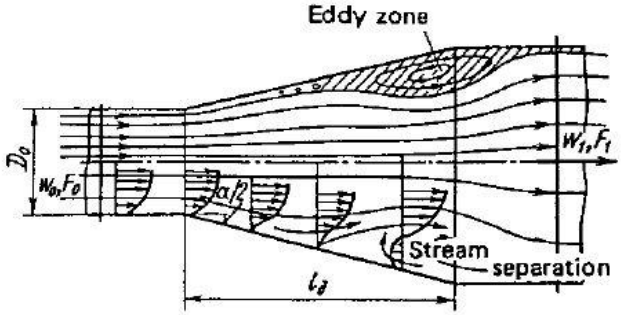

Figure 12 - Gradual expansion flow separation and formation of diffuser (Idelchik,1994)

2.3.2 Friction losses

The friction losses represent a large portion of the losses in pipes, especially for hydropower tunnels. The determination of the losses is based on the Darcy-Weisbach equation. The value of the coefficient of loss ζ_v is depending on.

$$\zeta_v = \lambda \cdot \frac{L}{D} \tag{2-8}$$

λ	Friction factor [-]	D	Diameter of pipe [m]
L	Length of pipe [m]		

The friction factor *λ* can be determined via the MOODY- diagram or per formula. In both cases it is needed to determine the Reynolds number *Re* and the roughness *k* [mm] of the pipe. The Reynolds number *Re* is determined via the following formula.

$$Re = \frac{v \cdot D}{v} \tag{2-9}$$

v	flow velocity [m/s]
v	kinematic viscosity of water [m^2/s]

The kinematic viscosity of water at a temperature of 10° is about $1.31 \cdot 10^{-6}$ m^2/s. For the determination by the use of MOODY- diagram it is needed to know the Reynolds number *Re* as well as the ratio of the roughness to diameter of the pipe. The MOODY-diagram is shown in Figure 13, the abscissae represents the Reynolds number. The right ordinate represents the ratio of roughness to diameter and the left one the friction factor *λ*.
Depending on the ratio a curve is chosen and blended with the Reynolds number value. The intersection of these two is then transferred to the left ordinate to read the friction factor *λ*.

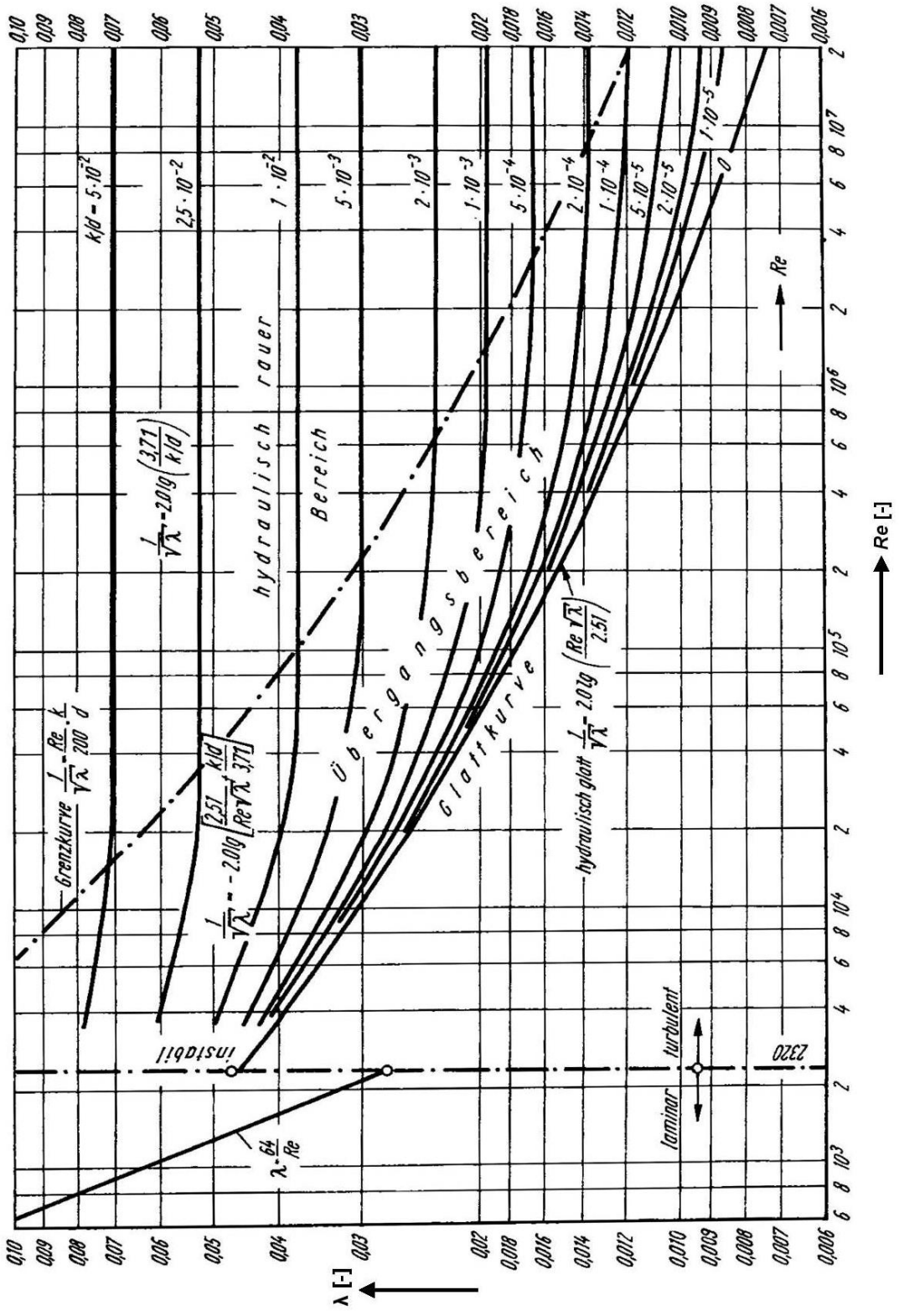

Figure 13 - MOODY diagram for the determination of drag coefficient λ (Bollrich, 2013))

The second method to determine the drag coefficient determination is by formula. This method represents an iterative way to get to the right result. The identification if the flow is laminar or turbulent is indicated by the critical Reynolds number (Re_{krit} = 2320 [-]). If the number is higher than the critical one, it can be stated that the flow is turbulent. The turbulent flow is further distributed into hydraulic smooth or hydraulic rough area and a transition area. Depending which situation is given the formula for the drag coefficient is adapted.

Hydraulic smooth area $$\frac{1}{\sqrt{\lambda}} = -2 \cdot \left(\frac{2.51}{Re \cdot \sqrt{\lambda}}\right) \quad (2\text{-}10)$$

Transition area $$\frac{1}{\sqrt{\lambda}} = -2 \cdot \left(\frac{2.51}{Re \cdot \sqrt{\lambda}} + \frac{k}{2.71 \cdot D}\right) \quad (2\text{-}11)$$

Hydraulic rough area $$\frac{1}{\sqrt{\lambda}} = -2 \cdot \left(\frac{k}{3.71 \cdot D}\right) \quad (2\text{-}12)$$

The sand grain roughness values *k* can be taken from Table 2. This table shows both the sand grain roughness values as well as the roughness values regarding the Manning-Strickler approach. In the investigation cases for the Tonstad surge tanks the chosen roughness values vary between 0.20 m for unlined rock and 0.20 mm for concrete.

Table 2 - Roughness values of different conditions (Bollrich, 2013)

wall conditions	k [mm]	k_{st} [$m^{1/3}/s$]
particular smooth	≤ 0.002	100
smooth	≤ 0.05	80
less smooth	0.25 - 0.50	60
rough	0.50 -2.00	35 -50
extremely rough and irregular	10 – 500	≤ 25

2.4 CFD Simulation

Computational fluid dynamics (CFD), is the numerical investigation of fluids based on the laws of conservation for mass, impulse and energy. CFD simulations can be used to simulate nearly every flow situation around or within an object. Therefore, it's used in nearly every region of the natural- or engineering sciences (Schwarze, 2013).

A CFD Model is the mathematical description of a flow, in particular of the turbulences within a flow. It needs to be discretised by the means of time and spatial. It consists in detail of the following parts (Schwarze, 2013):

- **Mesh**
  The geometry of the flow region as special discretisation

- **Mathematical model of the flow**
  The base equations of the flow description. This includes the laws for conservation of mass, impulse and energy as well as the fluid dynamic base equation.

- **Material values**
  Examples: density, viscosity and thermal conductivity of the fluid

- **Boundary conditions**
  Description of the hydraulic conditions at the inlet and outlet of the model.

- **Turbulence model**
  Numerical methods and algorithms that are used to transform the differential equations to model the turbulence in the flow.

2.4.1 Navier-Stokes equations

The mathematical model of the flow is based on the conservation equations for mass, impulse and energy or also referred as Navier-Stokes equations. By the use of these equations is it possible to fully describe the flow, fully means that the smallest turbulences and swirls are included in the description.
Due to the full description of the flow with all its turbulences the data mass and calculation time reaches an enormous amount and are therefore simplified for the technical application. These simplified equations are the Reynolds-averaged Navier-Stokes equations (RANS) (Lecheler, 2014).

2.4.2 Reynolds-averaged Navier-Stokes equations

The time dependent fluctuations of the flow are taking into account but not the turbulences itself. The not accounted turbulences are described via turbulence models. The accuracy of the of the equations and thus the results depend therefore heavily on the chosen turbulence model and the discretisation.
The turbulence models based on the RANS also called turbulent viscosity models and can be split into (Lecheler, 2014):

- Zero equation model:
  The turbulence viscosity is described via a simple algebraic equation and the differential equation for the turbulence is not solved.
- One equation model
  The turbulence viscosity is solved via one differential equation for the transport of the turbulent kinetic energy.
- Two equation model
  The turbulence viscosity is solved by the use of two differential equations.

The last one is the most common used equation model and can be split into the following three turbulence models:

k-ε turbulence model

This model uses two additional transport equations, one for the turbulent kinetic energy *k* and one for the turbulent dissipation ε. It was the long term standard for the industry. The model may provide too optimistic results for flows which separate at walls (Lecheler, 2014).

k-ω turbulence model

This model may give more accurate results in wall proximity as the *k*-ε model. It is possible to generate more accurate results at separated flows by only using a small interface dissolution. In terms of the accuracy in the middle of the flow it is stated not to be as good as the *k*-ε model (Lecheler, 2014).

SST-model

The SST-model (Shear-Stress-Transport) is the new standard for the industry because it combines the good characteristics of the two models mentioned before. Therefore, the results over the whole flow field are more accurate and the calculation time remains at an acceptable range (Lecheler, 2014).

3. Methodology

The main idea of the investigations, is the possibility of an additional lower chamber, in the following called extension chamber. This is planned to be placed at surge tank no.3 directly at the diffusor that leads into the connected pressurized sand trap. This extension chamber takes account for the higher hydraulic losses and serves therefore as an extension of the existing start-up chambers for all three surge tanks.

This new chamber allows the operation of the power plant without any constraints. The access tunnel for the chamber can be connected by the existing access tunnel for sand trap no.3. The layout as well as positioning of the chamber will be described in the related chapter. In the following the different steps from the modelling over the simulation until the results and the related analysis is further described. Figure 14 represents the course of the a CFD simulation and the steps needed till the results.

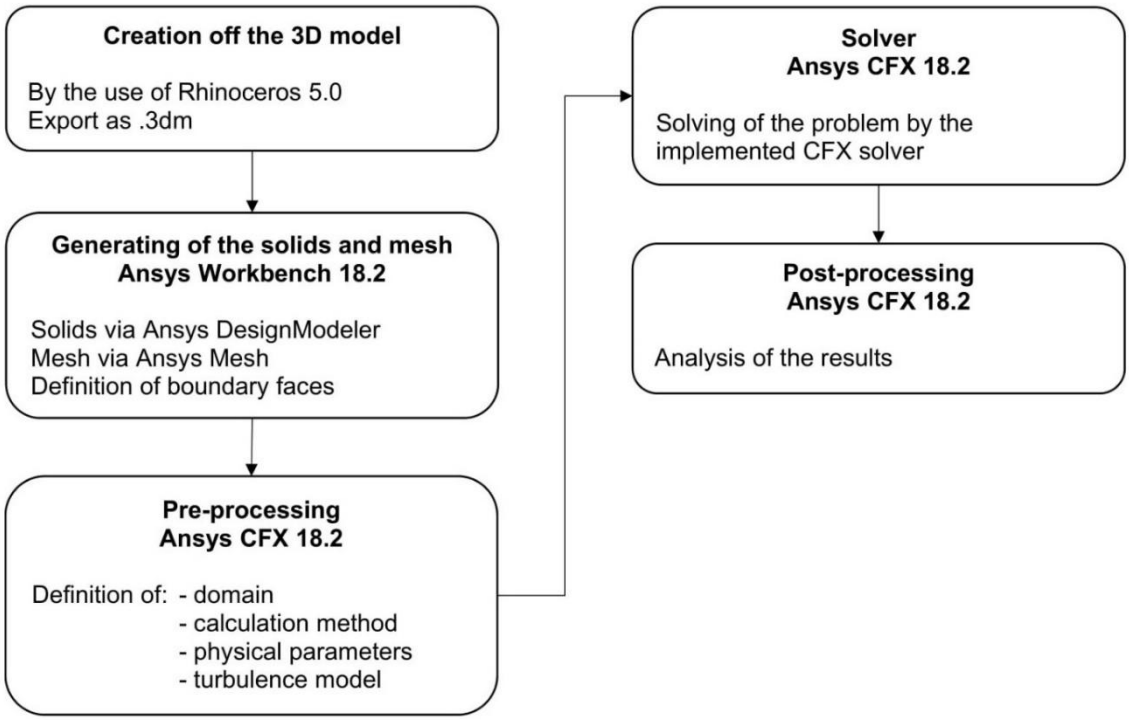

Figure 14 - Procedure of a CFD simulation

The chosen software for the modelling of the geometry of the CFD Model is *Rhinoceros V5.0*. It is a user friendly program and easy to use, if one is familiar with any similar drawing program. It is possible to generate surfaces with multiple curves with relatively little effort, thus this makes it a very good match for the modelling of a headrace system with multiple changes within the geometry. Additionally, a direct file communication between *Rhinoceros V5.0* (.3dm) and *Ansys Workbench 18.2* and *CFX 18.2* is conveniently possible.

The simulation as well as the analysis of the results is done by *Ansys Workbench 18.2 and Ansys CFX 18.2*. These programs are one of the most common used software for the investigation of fluid dynamics.

4. Geometry

The 3D model generated within the present work is based on provided 2D plans from Sira-Kvina Power company, the dimensions and plan views are collected in the Appendix A. The whole structure of the model is idealized and the roughness of different surfaces was simulated via boundary conditions in the 3D CFD model, these are further explained in chapter 5.2.2.1. The idealizations are an important approach for the present work, since the real system is unlined and thus the surface very unstructured. Previous work was done to investigate 3D CFD simulations to account for most accurate simulation approach (Bråtveit & Olsen, 2015) and (Brevik, 2013).

Part of the present work is to evaluate the efficiency of a 3D CFD model with smooth geometry and imposed roughness conditions in the simulations. Due to the oncoming changes and adaptions at the power plant system, the different stages of development are specifically designated in the form of a numbering, e.g. V0 (variant 0 – initial geometry), V1 (variant 1 – first adaptions), etc.

4.1 Current system – variant V0

The initial geometry design model represents the current state of the surge tank. It consists of the three surge tanks and the related sand traps and penstocks. In Figure 15, the different machines as well as the tunnel branches are explained.

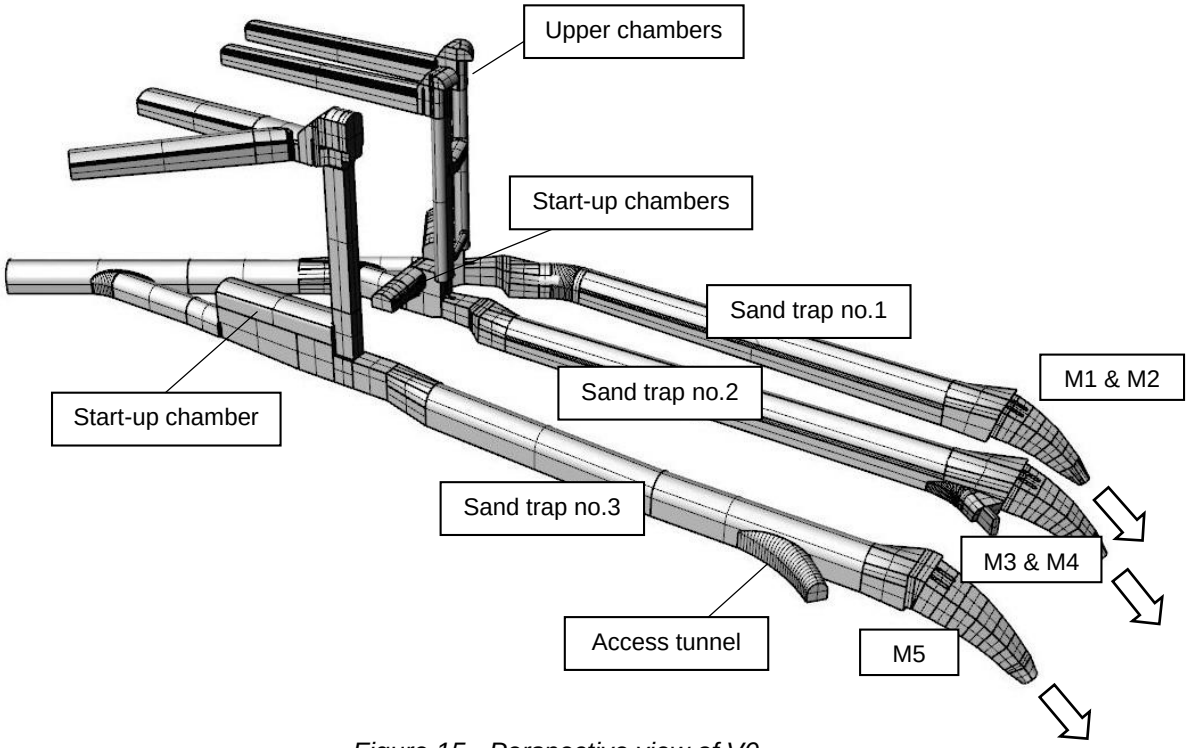

Figure 15 - Perspective view of V0

Following some of the features of the current state design is described.

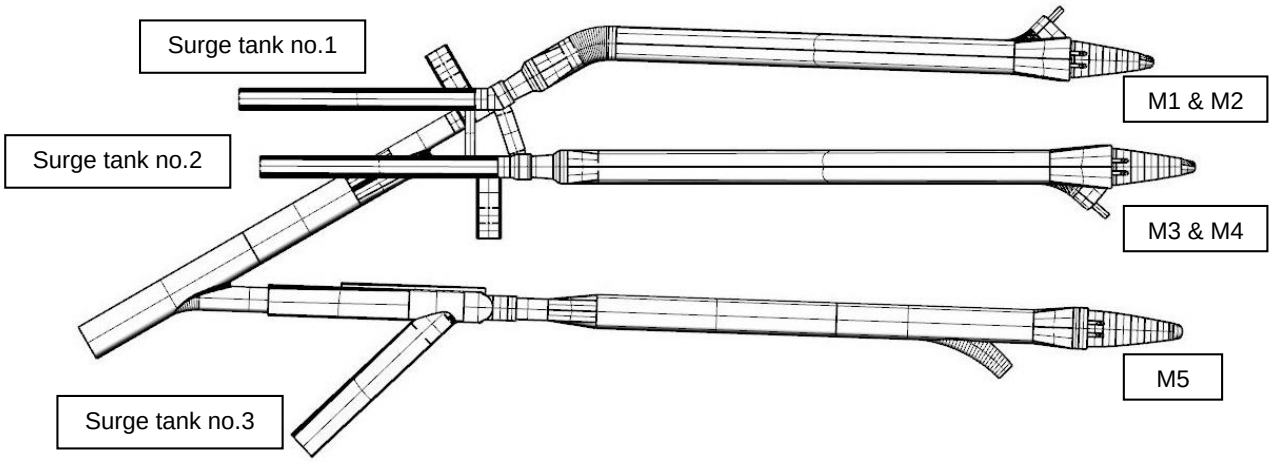

Figure 16 - Ground view of V0

Some of the characteristics of the system can be seen best in the ground view, which is shown in Figure 16. The main headrace tunnel has a flow area of about 100 m^2. According to the flow direction, the first diversion from the main tunnel is surge tank no.3. After the diversion the main tunnel splits into two separate branches, each branch leading to one of the surge tanks no.1 and no.2. Sand trap no.2 and no.3 follow the direction of the headrace. Sand trap no.1 is an exception, the route of this trap bends parallel to sand traps no.2 and no.3 shortly after the widening of the cross section.

The important elevations of the system are shown in Figure 17. Additional marked is the water level limitation of the current system. This limitation was defined to mitigate the danger of free surface flow in the sand traps. This limitation is the limit water level for steady state flow in full operation. One aim of this work is to find a structural way to avoid this limitation.
For the 3D CFD simulations a reference coordinate system was defined with the origin at 0,0,0 [x,y,z] at the middle of the main tunnel invert. All elevations in the 3D CFD simulations are referring to this coordinate system.

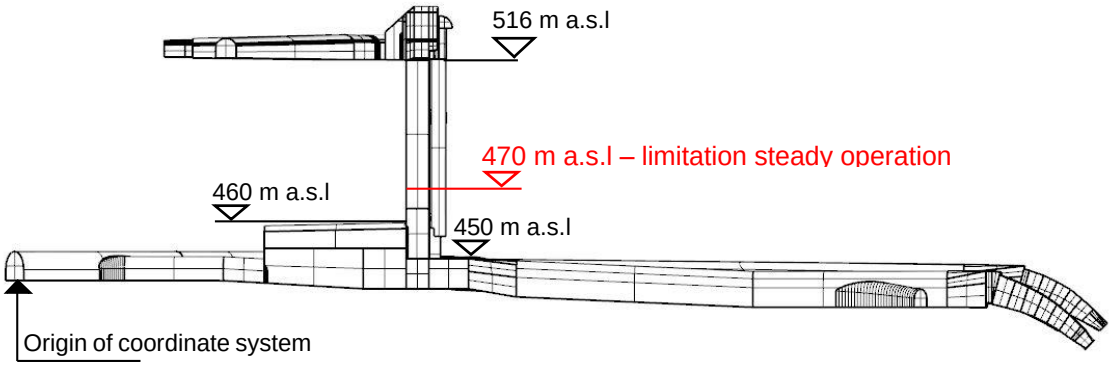

Figure 17 - Side view of V0 with elevations

4.1.1 Start-up chambers

The design for surge tank no.1 and no.2 is very similar, the only difference is the orientation of the chambers. The chambers are aligned in a 90° angle to the tunnel axis. The cross sections are shown in Figure 18.

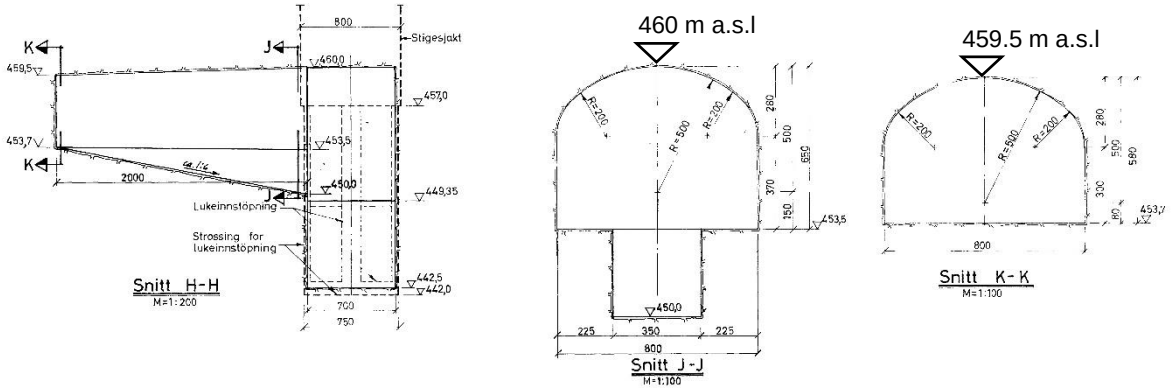

Figure 18 - Start-up chamber layout surge tank no.1 & no.2

The design of the start-up chamber for surge tank no.3 is different and constructed as an extension of the lower tunnel cross section and is shown in Figure 19. This shape is somehow disadvantageous regarding an increased possibility of sediment deposition due to decreased flow velocity.

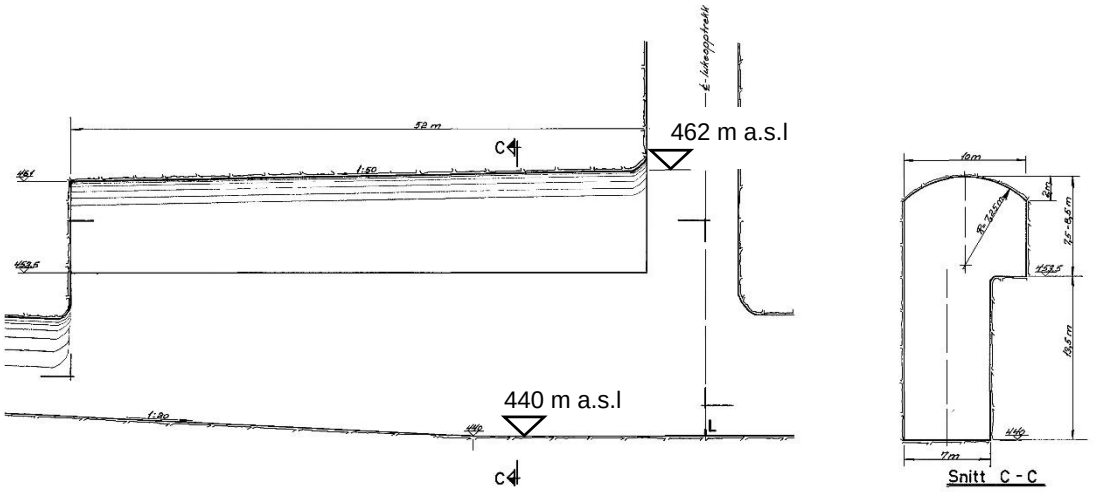

Figure 19 - Start-up chamber layout surge tank 3

4.1.2 Upper chambers

The shape as well as size of the upper chambers were discussed before in 1.1.2.2. In this part, the focus will be on the design of the throttle in the upper chambers. All upper chambers are equipped with such a throttle at the inlet, only the opening size varies. These throttles limit the run-off into the chamber at filling and into the surge shaft at emptying. The reason for their existence is the fact that the limited run-off into the chamber keeps the upsurge water level higher. The higher the water level in the surge improves the situation for the decelerating of the water mass in the main tunnel in sense of improving the differential effect of the surge tank. The same goes for the other way, the limited run-off back into the surge shaft leads to a lower water level in the shaft that corresponds as pressure level in the system.

The width of the opening is 2.3 m for the surge tanks no.1 and no.2 and slightly larger at surge tank no.3 with the width of 2.5 m. The opening height is from the chamber floor until the maintenance platform. This platform was neglected in the model because it is not attached to water. Obviously is it strictly forbidden that water can overflow the platform.
Figure 20 gives an impression of the throttles, as example only the throttle of one surge tank is shown due to the fact that they are nearly the same for all three.

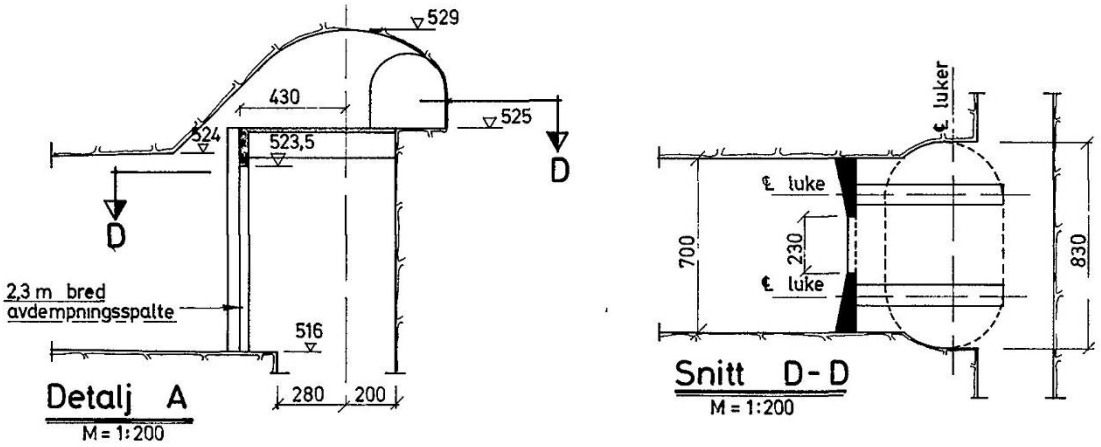

Figure 20 - Upper chamber throttle surge tank no.1

4.1.3 Penstocks

The penstocks are connected at the end of the sand traps. The inlet edges are about 1.5 m higher than the floor of the sand trap. Due to the position at the end of the sand trap, this space is needed for the deposited material. The two penstocks for the machines M1 & M2 and M3 & M4 have a diameter of 3.7 m and the one for M5, a diameter of 4.8 m. The entries of the penstocks start with a rectangular shape and evolve into a circle shape. Each penstock inlet is covered by an inclined rake (13.5 m by 11 m), which is supported by two pillars. Each pillar has a width of about 1.5 m and extends over the whole cross section. The rake covers as well as the pillars have nearly the same area for all three inlets. The rakes are not modelled because they have little to no effect on the mass oscillation and the investigated issue.

Figure 21 provides an impression of the transition to the penstocks.

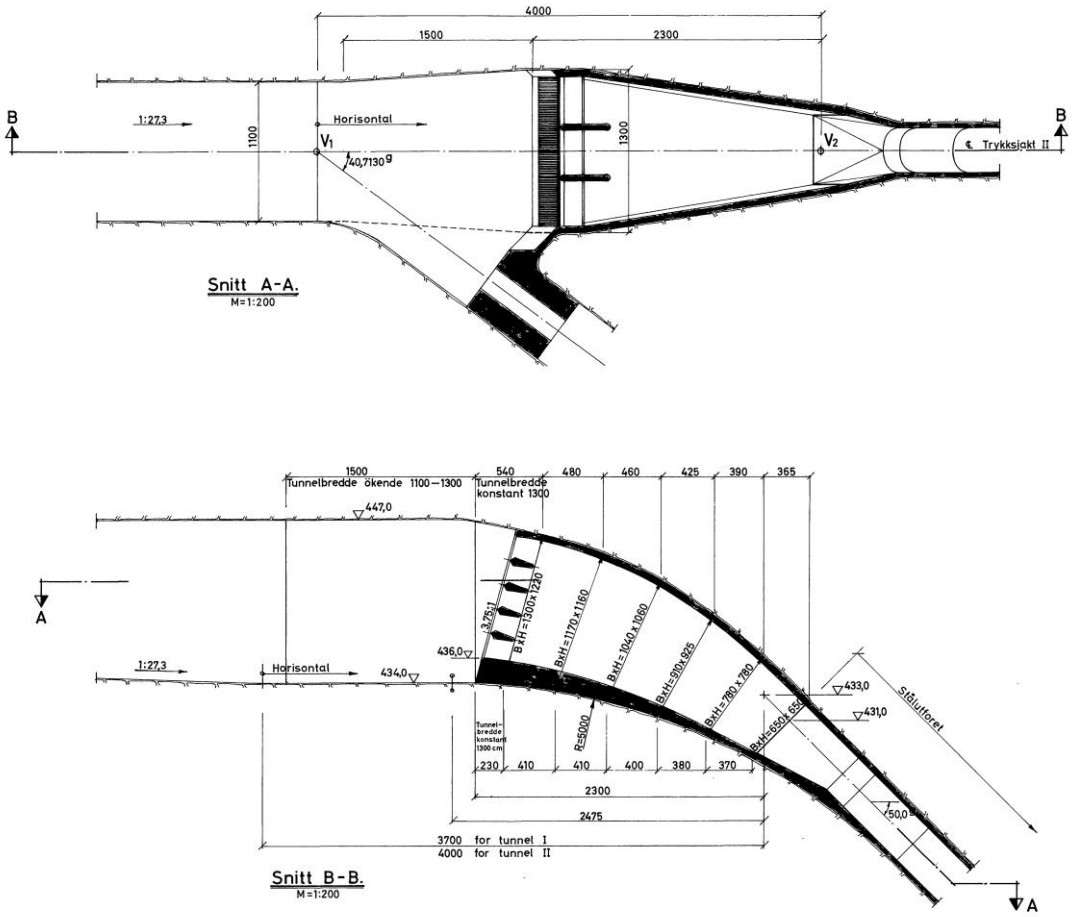

Figure 21 - Penstock layout of surge tank no.2

5. Extension chamber

Figure 22 shows the system of the Tonstad surge tanks with the implemented final geometry of the extension chamber investigated in this thesis.

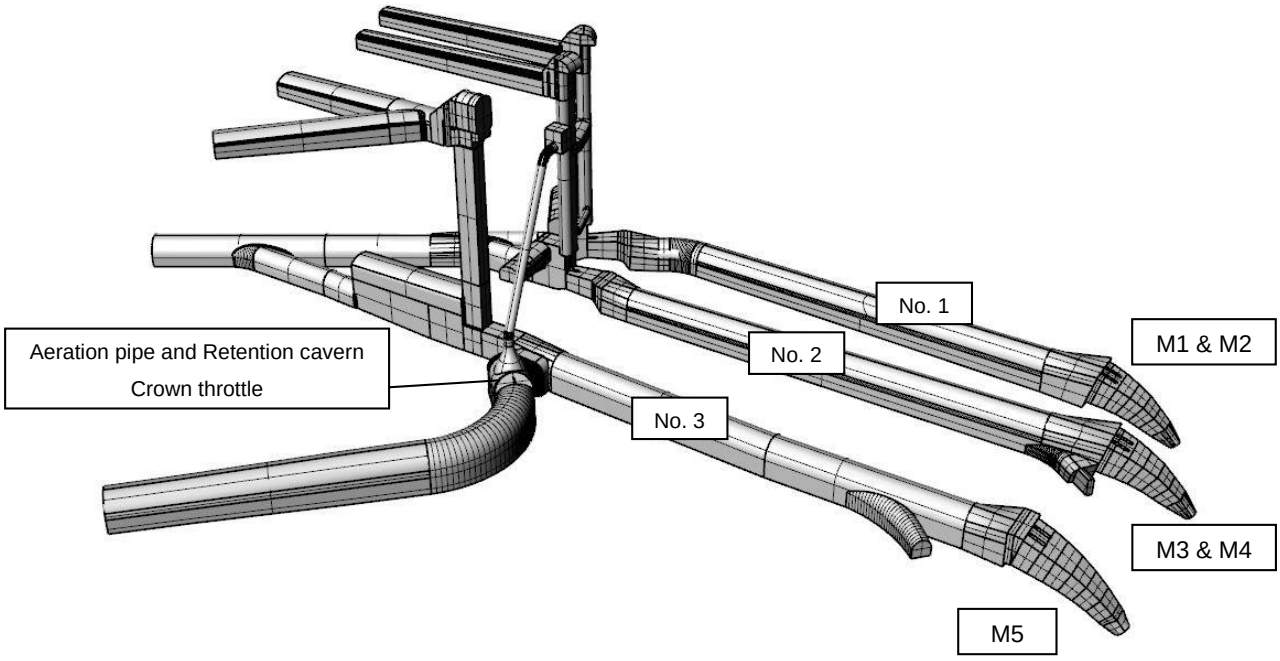

Figure 22 - Perspective view final extension chamber

The following figures represent V3 in different views. The different variants (V1, V2) leading up to this final one (V3) are further explained in this chapter.

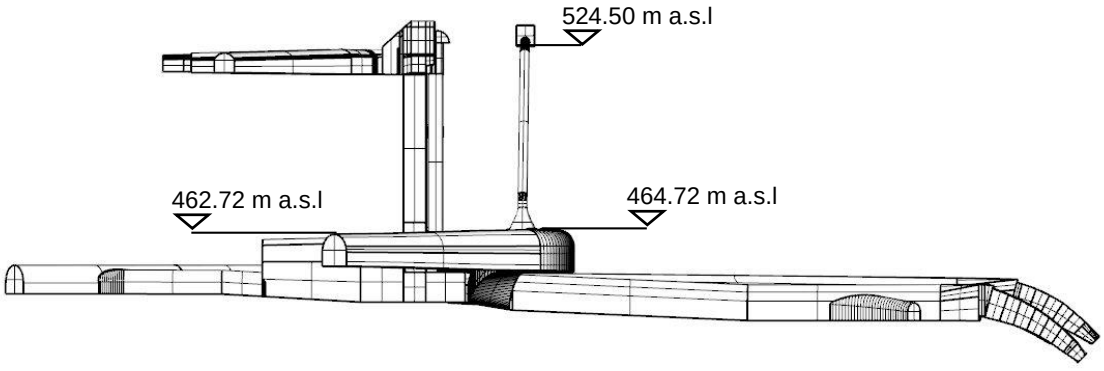

Figure 23 - Side view final extension chamber

Figure 23 provides an overview of the elevations of the extension chamber as well as of the foreseen adaptions. All suggested adaptions, such as an aeration pipe and associated small retention cavern on top plus the aerated crown throttle can be seen in Figure 24 and Figure 25. The different adaptions shown, will be described in subchapters.

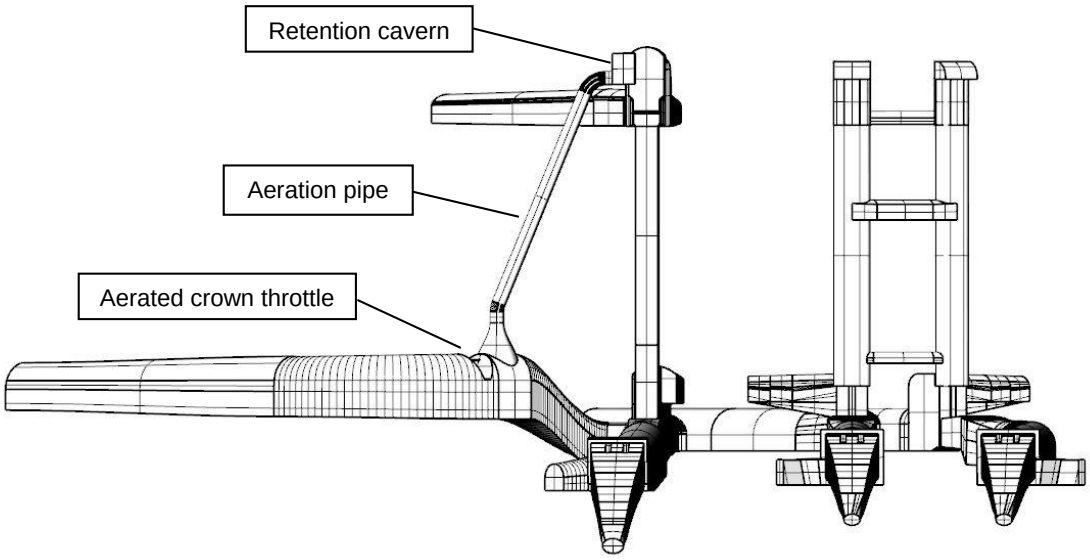

Figure 24 - Front view final extension chamber

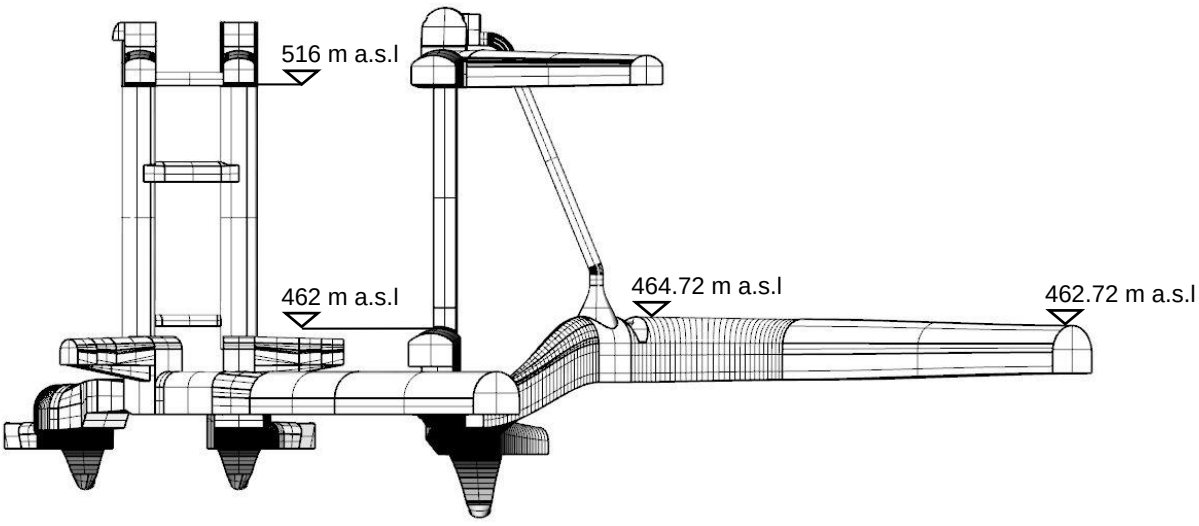

Figure 25 - Rear view final extension chamber

5.1 Extension chamber – V1

The input data for the first approach (V1) of the extension chamber is taken from a 1D simulation with the software WANDA. The initial chamber based on the 1D simulation is a 200 m long tunnel with a diameter of 10 m. Additional to this first dimensioning further specifications are made by the investigation.

One of the specifications is, that a new access tunnel has to connect to the existing one of surge tank no.3. Additionally, the extension chamber is required to be in a reasonable distance to the existing system. The impact on the power plant during the construction of the extension chamber has to be as little as possible, since the idea is to construct the extension chamber without major outage. The connection to the existing system has to be situated shortly after the gates of surge tank no.3. This is at the initial unlined section.
On the basis of this specification the first attempt is to position the chamber parallel to the sand trap no.3. The needed height difference between the tunnel inverts of the chamber and the sand trap has an additional impact on the positioning. In addition, enough rock has to be kept to allow sufficient stability.

Sand trap no.3 has a maximum length of approximately 170 m. A parallel positioning of a chamber with the same length right next to it is hardly possible. The water pressure in the chamber can reach a significant value equal to the maximum water level inside the surge shafts. This means that a satisfying amount of overburden has to be secured.
After considerations of the specifications, the decision is made to modify the length and cross section of the chamber to maintain enough space for the positioning. The volume of the new design stays the same as for the input data of 200 m length and 10 m diameter (net. volume 15700 m^3).
The diameter was increased from 10 m to 12 m, which results in a length of 146 m. The round cross section is then redesign to a more frequent used layout in tunnelling. The redesigned layout with dimensions and elevations can be seen in Figure 26.

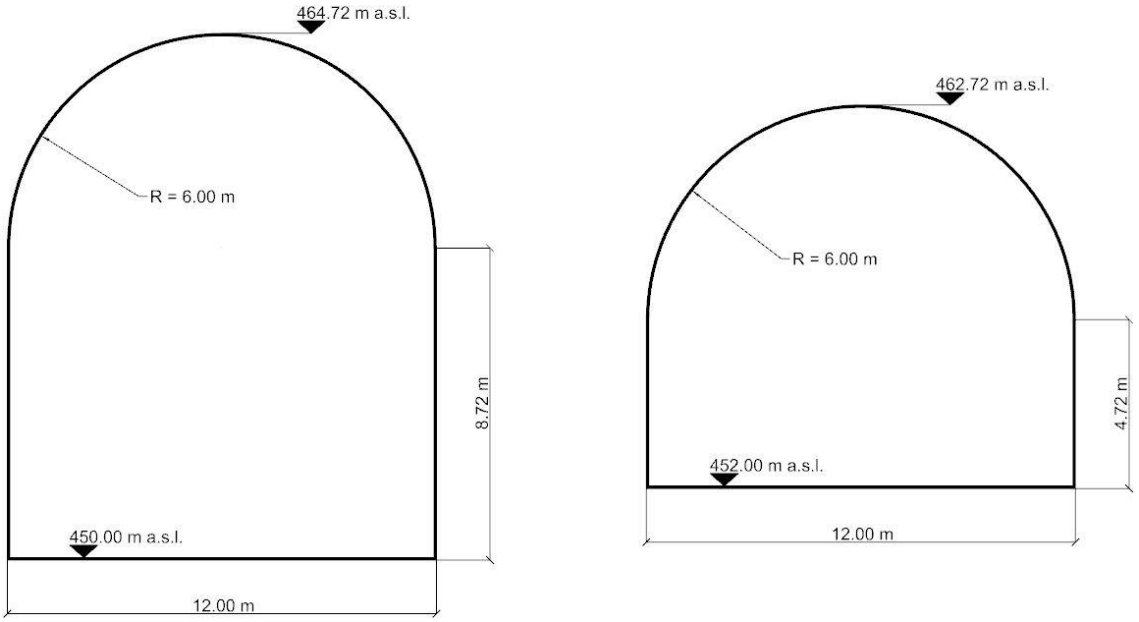

Cross-section 1 Cross section 2

Figure 26 - Cross sections 1 and 2 extension chamber, creating crown inclination

Figure 26 shows the two cross sections of the extension chamber. Cross section 1 is situated at the beginning of the chamber and develops to the smaller cross section 2 across the chamber length. This is done to generate an inclination between the two cross sections at the crowns. This inclination is needed to allow efficient de-aeration.

The water level in the chamber fluctuates and therefore the chamber needs to be aerated. If the water level lowers, air is needed to flow into the chamber and if it rises, the air needs to escape. In the case of a mass oscillation, a massive amount of entrapped air needs to escape in a short period of time through a relatively small de-aeration pipe. The crown inclination makes it necessary to place the aeration pipe at the beginning of the chamber. Owing to the massive amount of air during mass oscillation has the pipe a diameter of min. 2 m. The aeration pipe connects to the access tunnel of the upper chamber of surge tank no.3.

5.1.1 Variation study extension chamber

In variant V1, the proximity of the new chamber is the main focus. Therefore, the first chamber drafts are placed in the space between the surge tank no.3 and the associated access tunnel. Based on the specifications eight different routes of the main tunnel axis are sketched. Out of this eight, the one who meets most of the specifications is chosen, indicated in Figure 27.

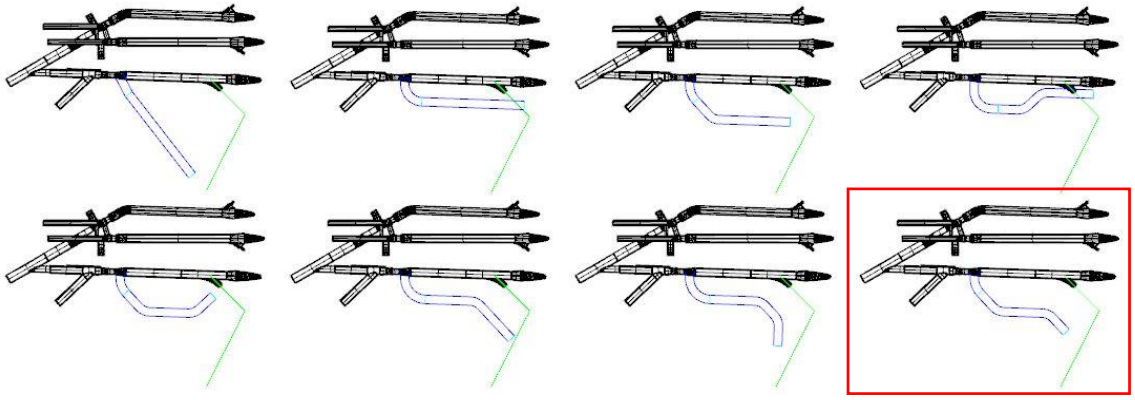

Blue – Planned route Green – Access tunnel

Figure 27 - Variation study for the chamber axis (in red, the chosen variant)

The blue lines are the sketched chamber routes plus the connection tunnel. The green lines represent the axis of the access tunnel; these are shown to get a better understanding of the planning area.

After the definition of the chamber layout, the connection between chamber and existing system is the next focus. The connection has to be as large as possible to not negatively influence the hydraulic behaviour. The largest cross section is realisable, if the connection tunnel has a right angle to the tunnel axis of the existing sand trap. The resulting inlet area of the extension chamber is approximately 137 m^2. The height difference between the tunnel inverts is approximately 11.5 m. The length of the connection tunnel is approximately 30 m, this results in a steep inclination.

Figure 28 and Figure 29 show the resulting variant V1, which is used for the first simulations.

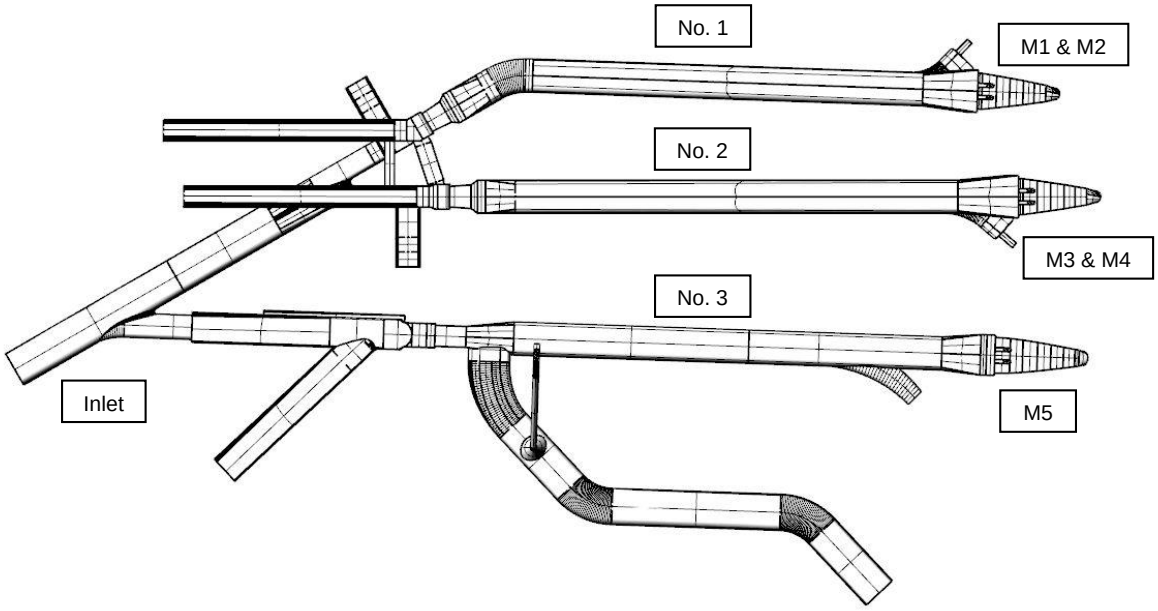

Figure 28 - Ground view of V1

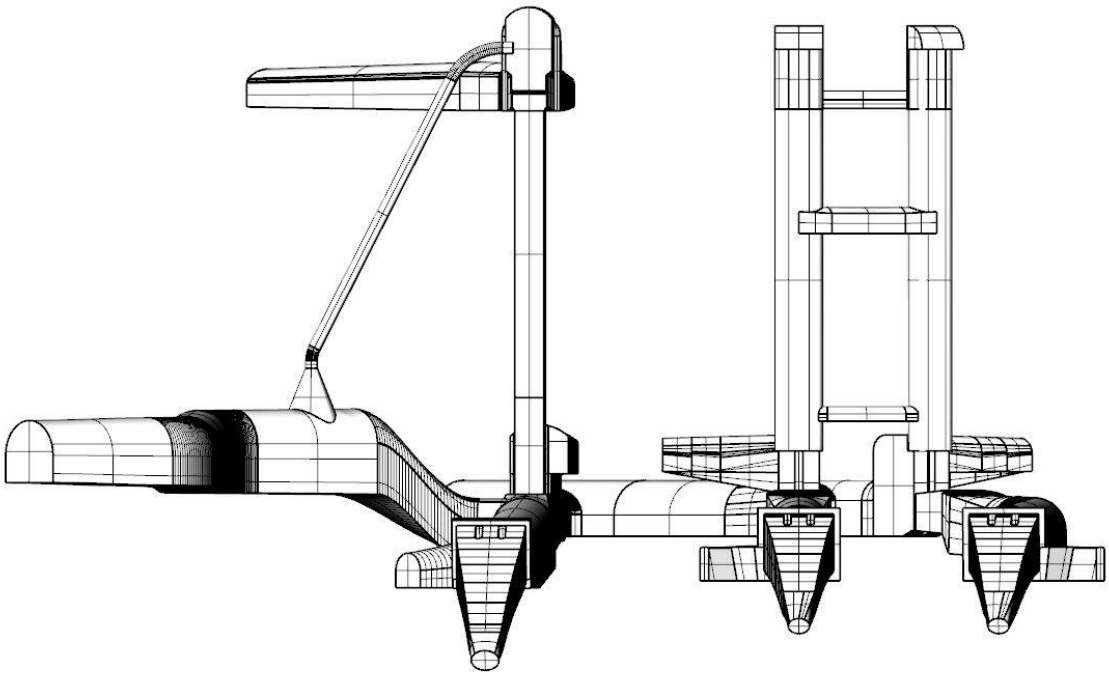

Figure 29 - Front view of V1

5.2 3D CFD Simulation Ansys Workbench 18.2

The *Ansys Workbench 18.2* combines all needed programs for a 3D CFD simulation in one clear surface. This combination makes it possible to easily understand the procedure of a CFD simulation.

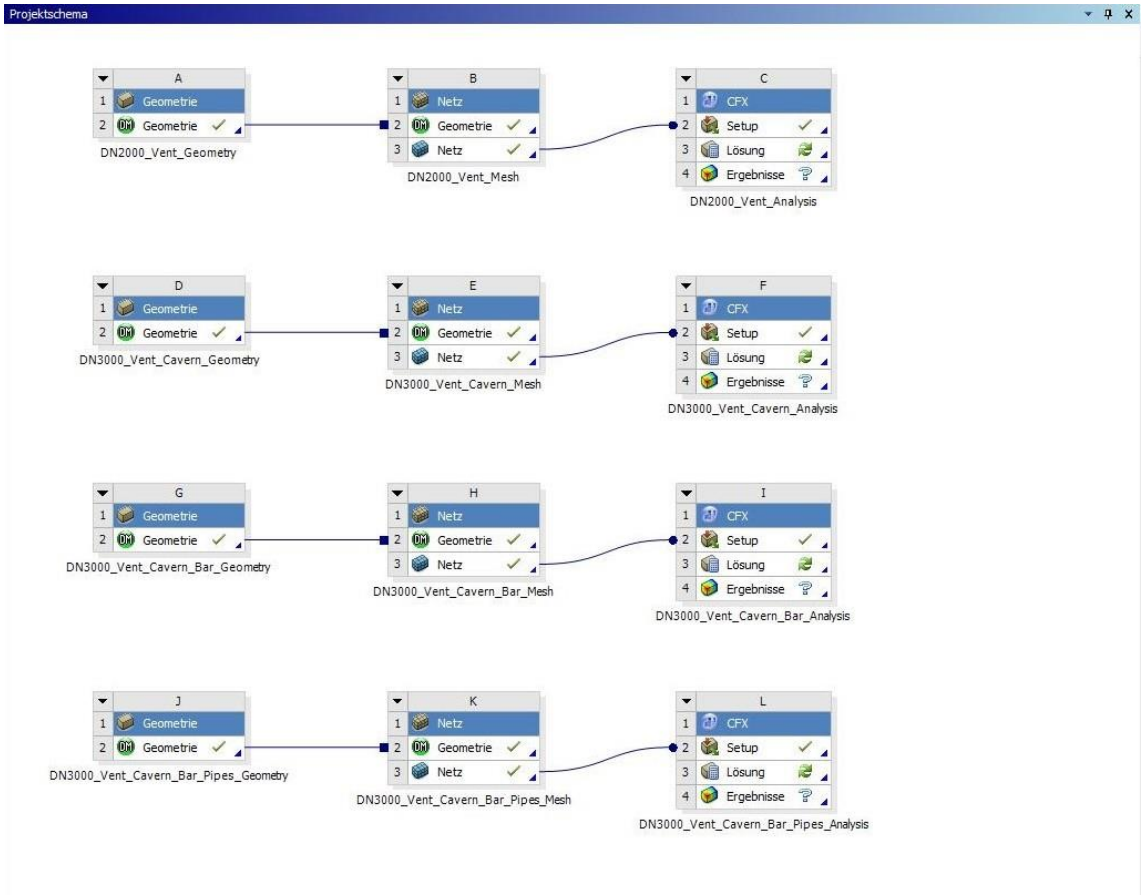

Figure 30 - Project scheme Ansys Workbench 18.2

The scheme (Figure 30) provides an overview of the interface. It can be seen that the different parts are connected to each other. Thus, makes it possible to change the geometry or mesh and the data is automatically updated in all connected parts. As example, one of the branches represents a CFD simulation from start to end, consisting of geometry, mesh and the pre- processing. All the figures in the following subchapters are illustrative for the process of setting up the CFD simulation.

5.2.1 Generating solids and mesh

The generating of the solids is done by the importing of the geometry file from *Rhinoceros V5.0* into the *Ansys DesignModeler*.

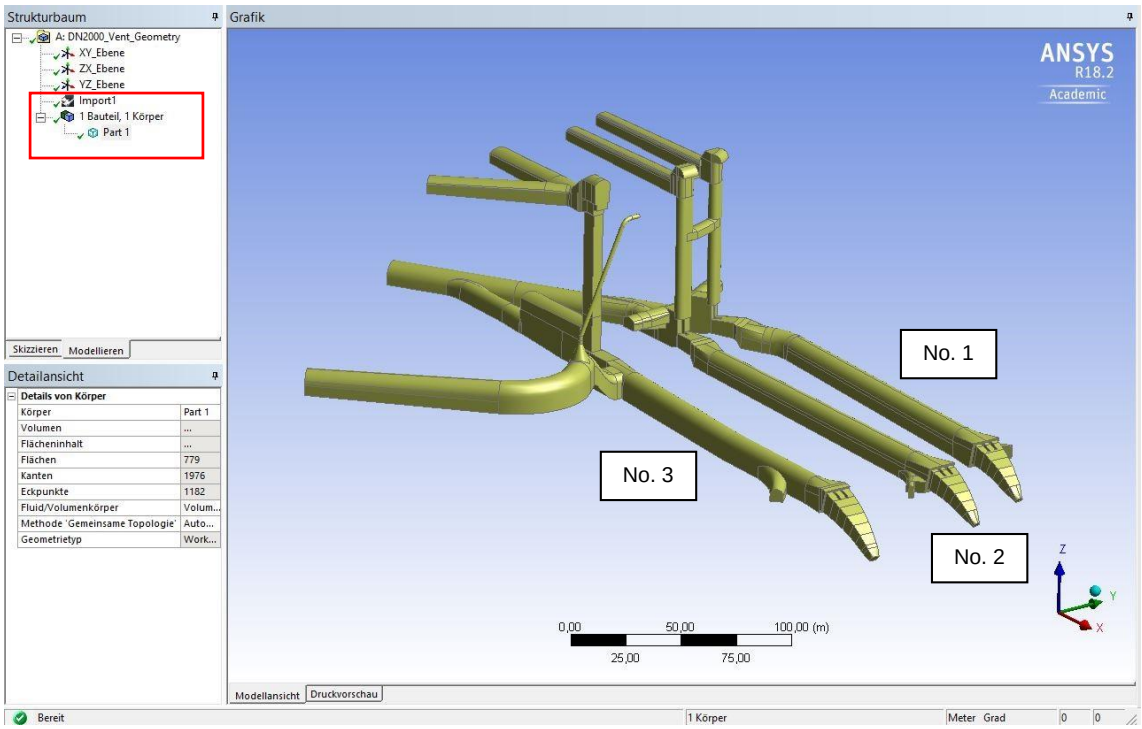

Figure 31 - Generating of the solids in Ansys DesignModeler

Figure 31 gives an overview of the user interface of the *DesignModeler*. On the left side, marked red, the generated parts can be seen. In this case the generated model represents the final variant of the extension chamber with the updated layout.

If there are more parts of a model, it is possible to suppress individual parts. In the present case, this option is not used. Therefore, the whole model consists of one part. The focus is on the interaction of the existing system with the new chamber and needs to be investigated entirety. It is possible to change parts or generate the whole geometry in the *DesignModeler*. It turns out that the changing of the geometry by the use of *Rhinoceros 5.0* is found to be the convenient approach.

The next step is the generation of the mesh by the use of the *Ansys Meshing* tool. Since the whole surge tanks are needed to be modelled in an efficient manner. The chosen approach is a balance between a mesh rough as possible but also as fine as needed to get suitable results with a reasonable calculation time. The automatic mesh generating was found to lead to a trustworthy mesh. In the case of this thesis, the *Ansys CFX* solver was chosen and turned out to serve as a very powerful tool.

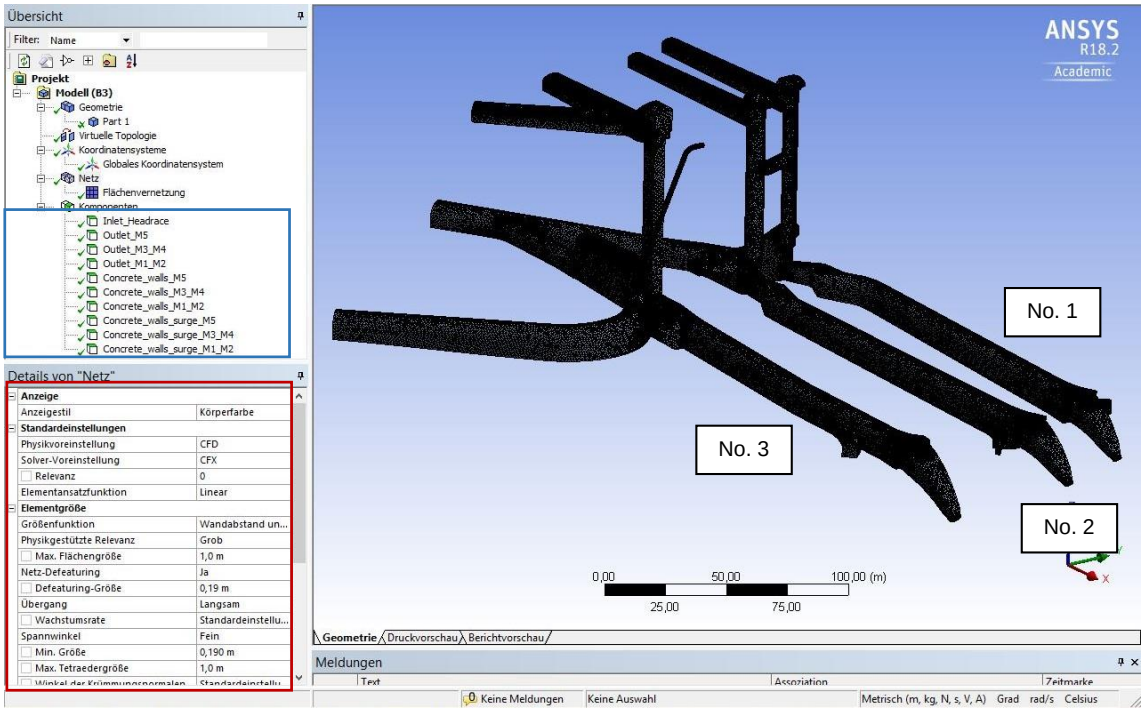

Figure 32 - User interface Ansys Meshing 18.2

Figure 32 shows the interface of the Meshing program, on the left side marked red, the section of input parameters can be seen. In the blue marked area another important feature can be seen, the so-called components. These components make it possible to define single surfaces or polysurfaces, which is very useful in the following pre-processing to assign boundary or physical conditions. As example in Figure 32, the inlet, the outlets as well as the areas of concrete were defined.

In addition, it is easy to edit the settings of the mesh, e.g. the possibility of the integrating of a virtual topology or an inflation (generating of prismatic layers) can be done very conveniently.

5.2.2 Pre-Processing

The main purpose of the pre-processing is the addressing of the physical parameters and the boundary conditions. This includes the type of calculation method, in means of stationary or transient, as well as the turbulence model.

The boundary conditions are defined via functions and expressions, for example to define the in- or outflow in the model. The monitoring of relevant physical parameters is defined in the output control, such as the discharge and the pressure at the surge tank base which indicates the water level in the surge tank.

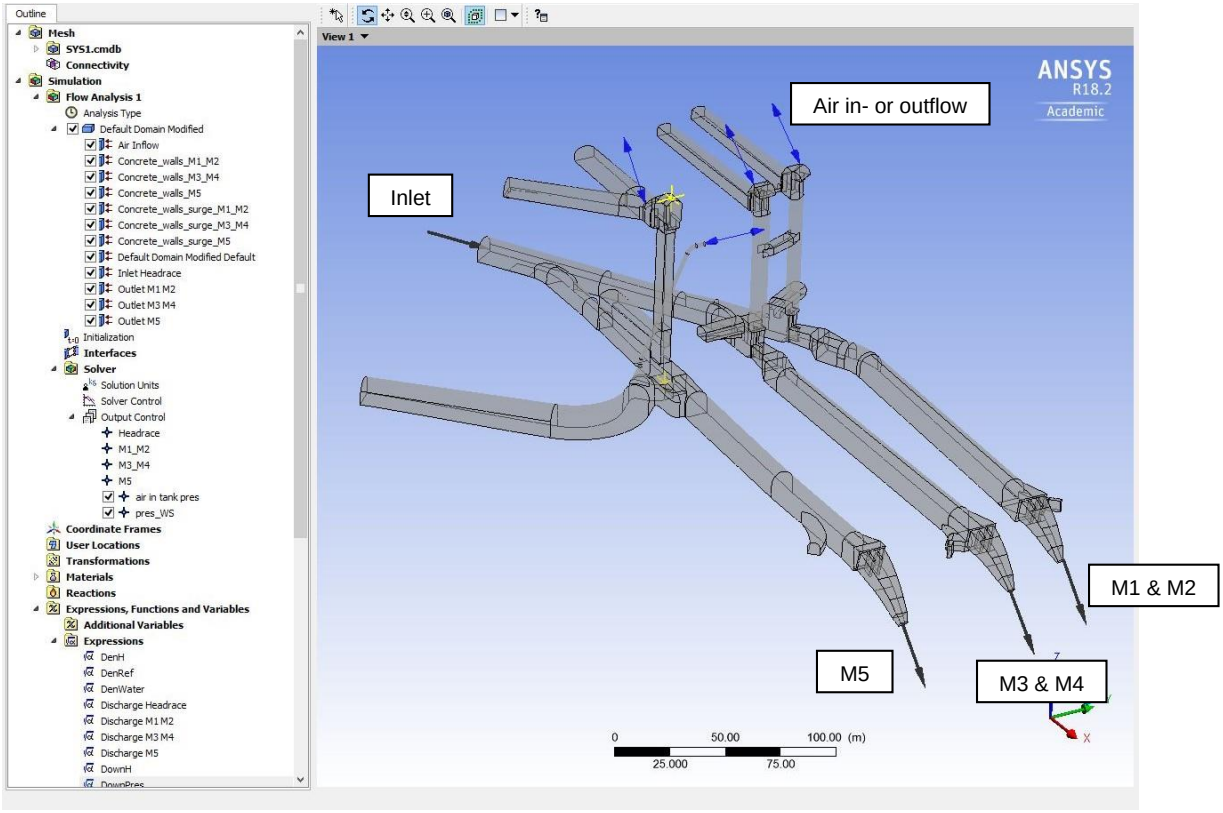

Figure 33 - Pre-processing overview AnsysCFX 18.2

Figure 33 shows the pre-processing interface. For example, the headrace inlet and the penstocks are marked with arrows. The blue arrows represent the areas where air is able to flow in or out.

5.2.2.1 Boundary conditions

The results of a simulation are highly depending on boundary condition inputs. The conditions need to be chosen carefully, in fact they need to represent the given situation at the site or in our case the power plant. These conditions and parameters are the same for all simulations of the different variants. Therefore, the variants are good comparable. It has to be stated that the impact on the mass oscillation from different chamber designs is not taken into account.

Calculation method

The simulations of the model will be transient, due to constant change of the inflow as well as the outflow. The simulation time is equivalent to 700 s in real time and a time step of 0.45 s was found as a good approach to safe calculation time. Due to the size of the model, with an average of about 3 Mio elements, the time needed for the iterations is already very long. For the purpose of an investigation of the feasibility, this time step is small enough to make a meaningful statement. The comparison with the results of the 1D model show that this approach is constructive.

Physical parameters

All the simulations are done by the use of two phases, water and air. The temperature of the fluids has very little to no effect on the results and was therefore neglected. The densities used in the model are the ones at 20°C for water and air.

All simulations are done under the influence of gravity and therefore must be accounted in the boundary conditions. The gravitational force acts in the negative z-direction in all simulations, this is owed to the given reference coordinate system. Therefore, the gravity force was put in with a negative sign (-9.81 m/s^2).

The initial water level is set at the height of 54.25 m. This means that the initial model status consists of water and air and it is needed to define a reference pressure. In the model this reference pressure is set to 1 atm.
The height of 54.25 m in respect with the origin of the coordinate system in the middle of the main tunnel results in a water level of 497.6 m a.s.l. Which corresponds with the capacity level of the water reservoirs and represents a system at rest.

The simulation at the model will lead to free surface flow in some areas, e.g. upper chambers, surge shaft. Therefore, a surface tension coefficient is needed. The coefficient is set to a value of 0.072 N/m, which represents the surface tension for water at 20°C. Indeed, an effect that also can be neglected for the result.

The last condition, which needs to be set is the turbulence model. In all cases the SST-model (Shear Stress Transport) is used. The decision is based on the fact that the model combines the good characteristics of the k-ε and the k-ω turbulence models (Lecheler, 2014).

Boundary surface conditions

Basically, it is possible to define the input parameters via velocity, pressure or flow. In this particular case the in- and outflow is defined on the basis of the water velocity and are given as transient data. The values for the in- and outflow are provided via a foregoing 1D-simulation. The values represent a starting up and a stopping of the turbines. The input values are provided via an excel sheet and are further explained and shown via a graph in the oncoming chapter 5.3.1. Boundary surfaces can be defined as openings, inlets, outlets, symmetry or wall. In the present case the inlets as well as the outlets are defined as such, due to the needed in- and outflow. The surfaces for air to flow in or out, are defined as openings. Most of the system consist of unlined rock and just smaller areas are made of concrete. Therefore, just the areas of concrete are assigned with a roughness value of 0.20 mm. The rest of the system, which represents unlined rock was assigned with a roughness value of 0.20 m.

Figure 34 gives an overview of all the assigned boundary conditions at the system. The green surfaces represent the concrete and the grey ones the unlined rock. The Inlet at the headrace as well as the penstocks are indicated by the grey arrows. The arrows additional represent the flow direction within the system. The blue arrows at the surge tanks as well as at the aeration represent the air in- or outflow of the system.

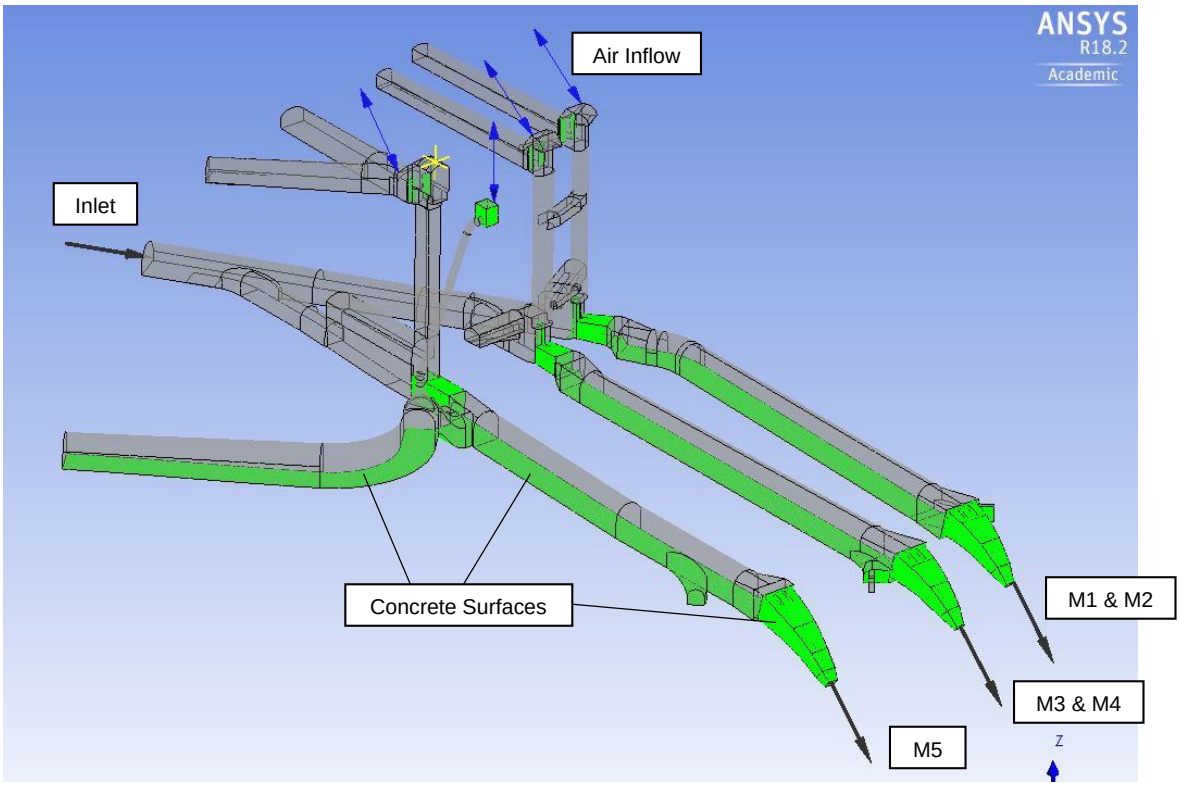

Figure 34 - Overview of the assigned boundary conditions

5.3 Simulation V1

In this subchapter the simulation itself as well as the results of variant V1 will be further described. On the basis of the gained knowledge useful and meaningful changes are made and their influence on the system is stated.

5.3.1 Initial status

As mentioned in chapter 5.2.2.1, the system is filled to a water level of 54.25 m (497.6 m a.s.l.). The discharge at the outlets as well as at the inlet is initially zero and represents a system at rest.

The start-up of the turbines is represented by a linear increasing of the discharge to 125% of the design discharge in 130 seconds. The associated accelerating of the water mass in the main tunnel is simulated with a 1D model (external information – not part of this thesis). After 360 seconds the turbines are shut-down in 10 seconds. This triggers the upswing of the mass oscillation and the filling of the surge tank. The whole time interval of the simulation is about 700 seconds and is large enough to make a meaningful statement. The velocity over time for the outlets and the inlet is shown in the graph below (Figure 35)

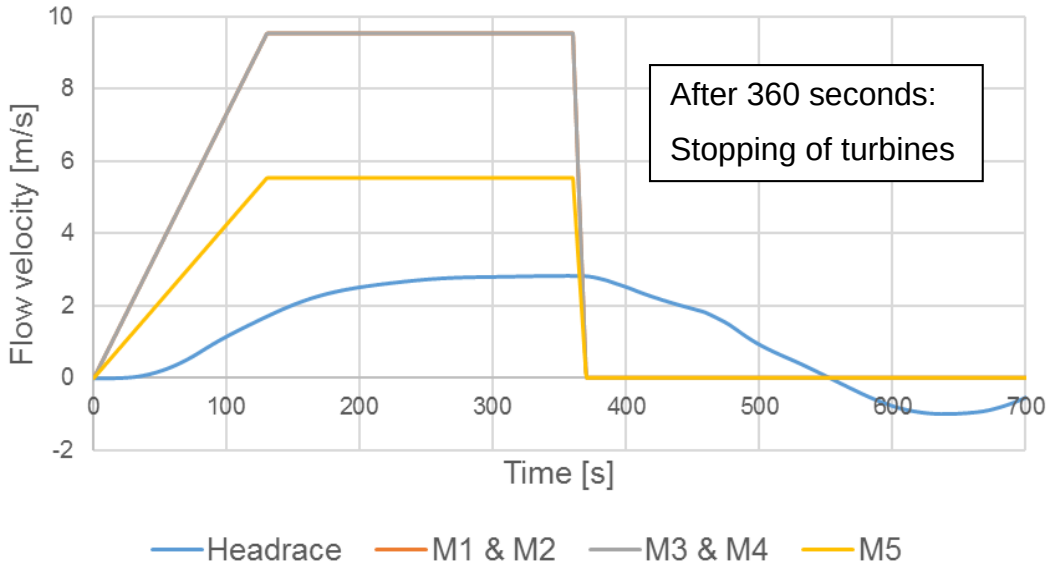

Figure 35 - Discharge input for simulation

It can be seen that as soon as the simulation starts, the discharge in the machines is increased until about 300 m^3/s within 130 seconds and after 360 seconds the emergency closing of the turbines is initiated. The closing time is set to 10 seconds. The headrace discharge starts with a time delay due to the massive inertia of the water mass inside. The simulation shows how slowly the water in the main tunnel is accelerated. This already indicates the importance of an extra chamber. The negative velocity at the end is due to the oscillation of the surge tank.

5.3.2 Areas of interest

The first area or point of interest that is investigated more detailed, is the starting up of the turbines. Under all circumstances is it needed to avoid a free surface flow within the sand traps at any time. Therefore, the focus is at the possible lowest water level in the surge shafts. The second point is the behaviour and impact of the mass oscillation and upsurge due to the shutting down of the turbines. The resulting upsurge and the behaviour of the existing upper chambers are at special attention, since these existing chambers also need to function sufficiently for the anticipated discharge upgrade of 25%.
In all cases investigated, the extension chamber represents the specific area of interest. At start-up, the chamber is needed to allow a quick and quite long downsurge. This significantly supports the existing three start-up chambers. The shut-down generates first a refilling of the lower chambers and then an upsurge into the upper chambers.

5.3.3 Insufficient overburden

An issue, which evolved already before the start of the first simulation is the insufficient overburden provided by the surrounding terrain for this extension chamber variant. This fact is observed by the comparison of V1 with the given terrain model. Whether a variant is desirable, can only be verified if the terrain provides the needed rock mass above the extension chamber to securely capture the internal pressure. Figure 36 illustrates the positioning of the model in the surrounding terrain.

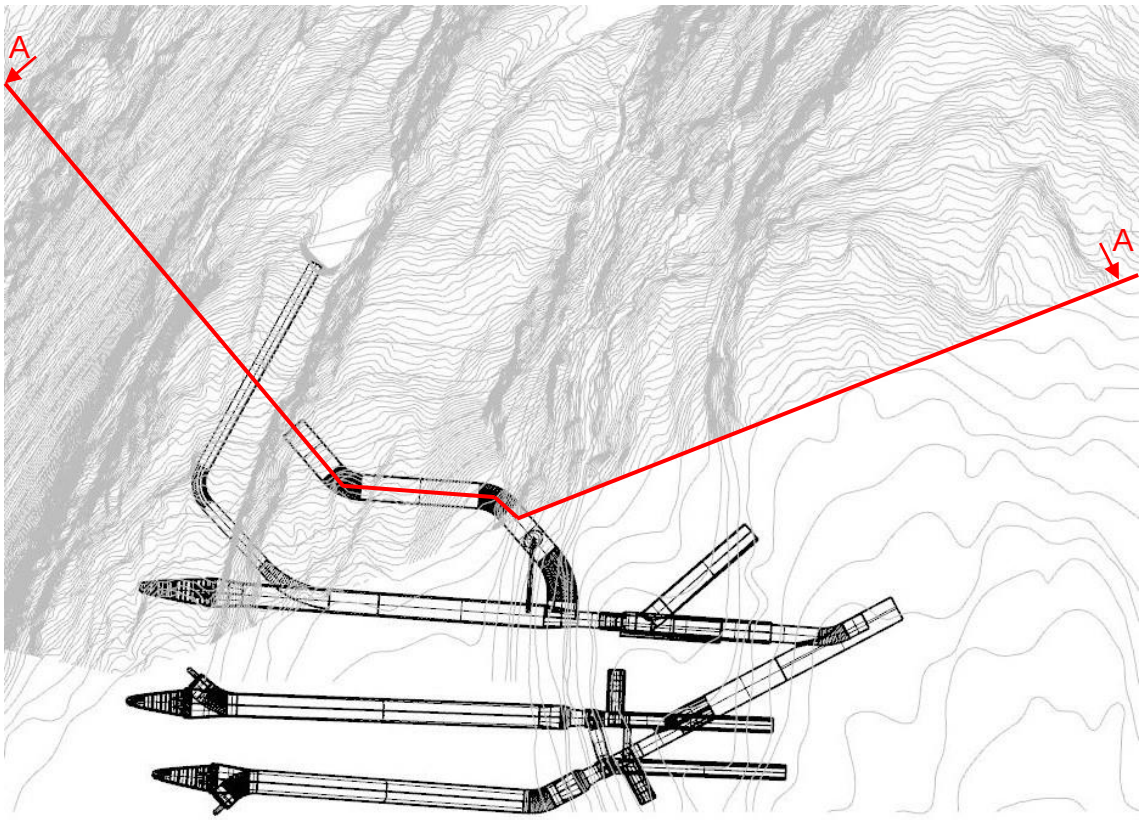

Figure 36 - Comparison V1 – Terrain / Section course A-A

As already indicated by the contour lines, the terrain at the site has a steep inclination at the end of the extension chamber. The plan section A-A can be seen in Figure 37. The plan section route is based on the more detailed presentation of the contour lines at the terrain model.

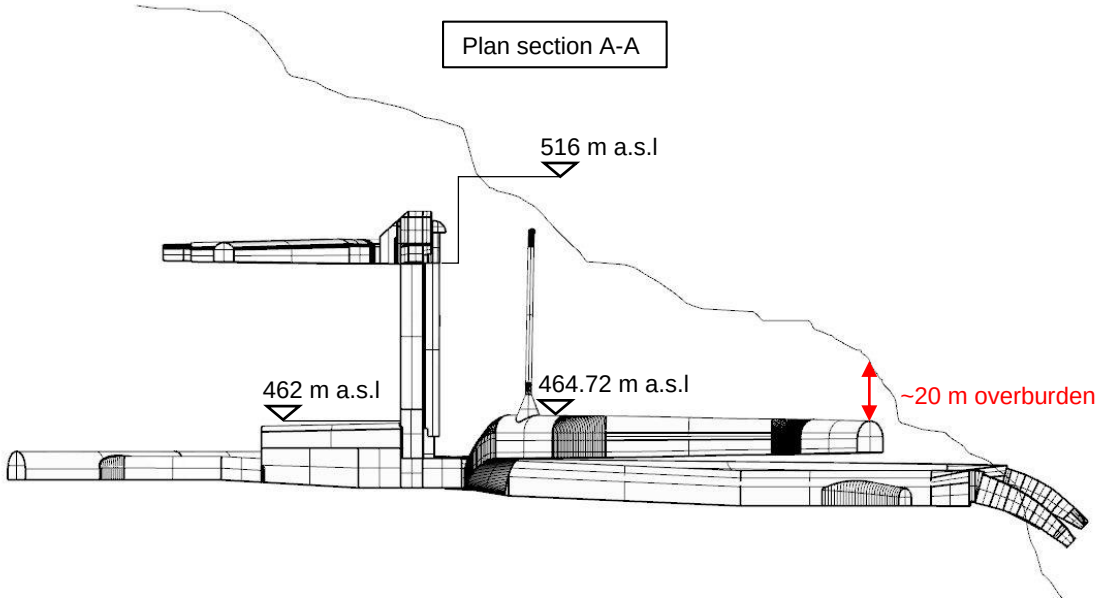

Figure 37 - Plan section A-A / Comparison of V1 with Terrain

The provided overburden at the end of the extension chamber is approximately 20 m. The pressure in the chamber is depending on the water level in the surge shaft and can reach up to a height of approximately 518 m a.s.l. The resulting water column in the case of mass oscillation will be about 56 m. The Norwegian rock mass is very good, but it also might not take tension forces. The criterion is the minimal rock stress, which needs to be in balance with the maximum hydraulic stress, if the water tunnel is not steel lined. Thus, a redesigning of the route of the chamber has to be considered.

Nonetheless, the variant (V1) is simulated to get a feel and idea of the impact and effects of the extension chamber on the power plant or surge tanks. As long as the total volume at different elevation is equal, the orientation of the extension chamber does not have a significant effect on the hydraulics.

5.3.4 Results and Findings of V1

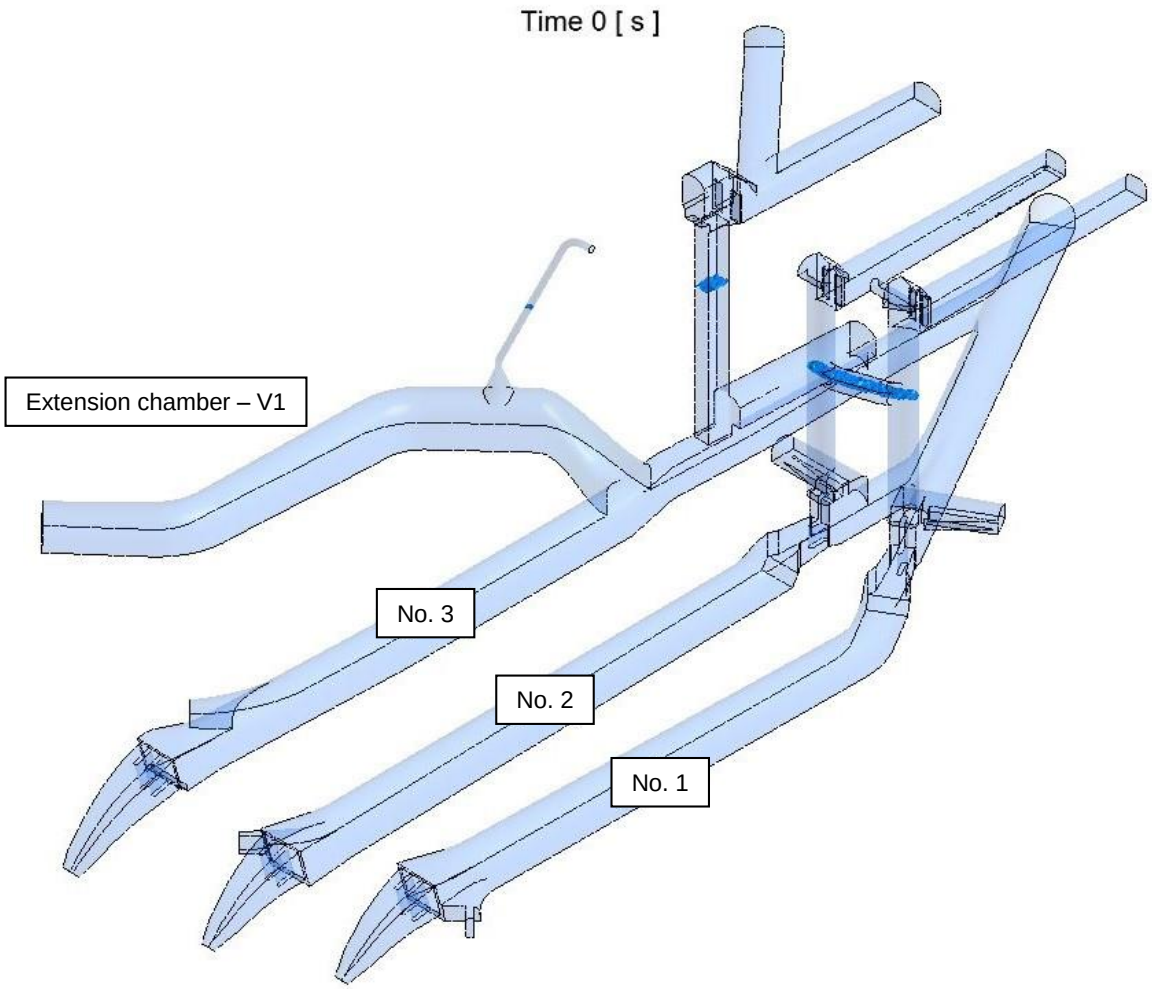

Figure 38 - Initial status of V1 (time 0 [s])

Figure 38 represents the initial status of the model. The initial water level of 54.25 m is shown. At the start, the transverse tunnel between surge tank no.1 and no.2 are filled nearly to the maximum. Additionally, it is shown that the water level throughout the model is the same. In the following particular time steps are chosen to show the effects as well as issues during the simulation.

The starting up of the turbines shows no special incidents for the first minute of the simulation. After 60 seconds, a noticeable change at the junction of surge tank no.3 and main tunnel can be seen. The streamlines indicate that the extension chamber starts to supply water not only to machine M5 but also to the other machines via surge tank no.1 and no.2.

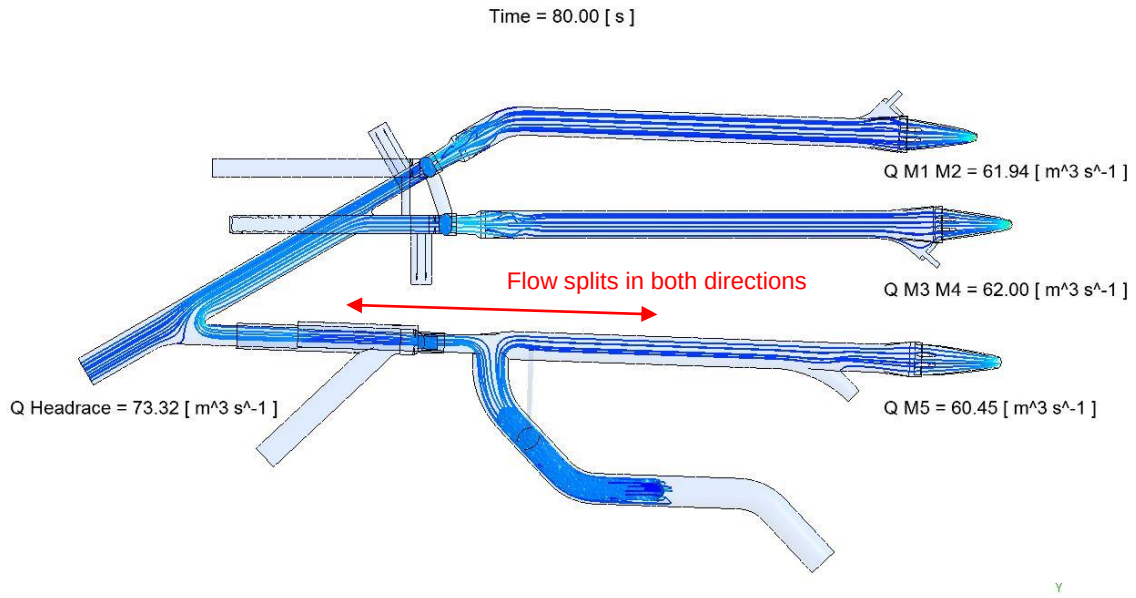

Figure 39 - Streamlines at start-up (V1 - full system ground view)

An impression of the developing streamlines can be seen in Figure 39. The streamlines originating from the extension chamber split at the area of the chamber inlet into two ways. This means that the water is distributed to machinery M5 and also to the machineries M1 – M4. This effect fades away at the point the water mass in the main tunnel is sufficiently accelerated.

The next selected time step is at 360 seconds of the simulation. At this point the lowest water level is reached. The discharge at the outlets has reached the maximum and the water is supplied only by the main tunnel or reservoirs.

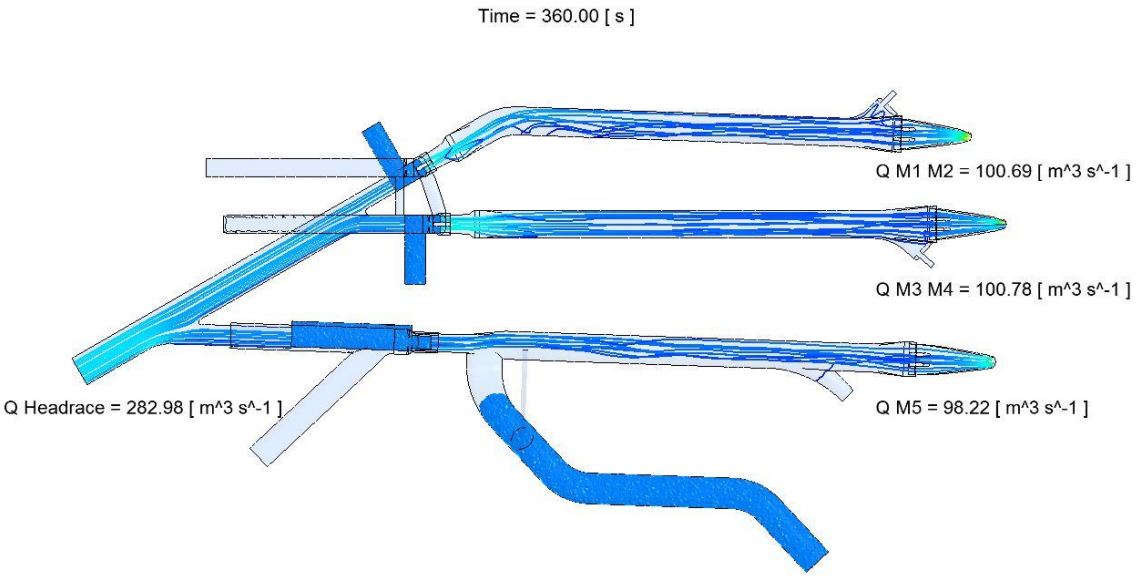

Figure 40 - Streamlines after 360 seconds (V1 - full system ground view)

Figure 40 shows the streamlines at the mentioned time step. The time step at 360 seconds represents exactly the point where the stopping of the turbines is initiated. It can be seen that the streamlines are only originating from the headrace inlet and show a very steady state flow towards the outlets. Further on are no streamlines originating from the extension chamber, which means that almost no water is supplied from it.

Figure 41 shows that the minimum water level during steady operation. The water level is clearly situated above the tunnel crowns of the sand traps. Therefore, the specification according the prevention of free surface flow in the sand traps is fulfilled.

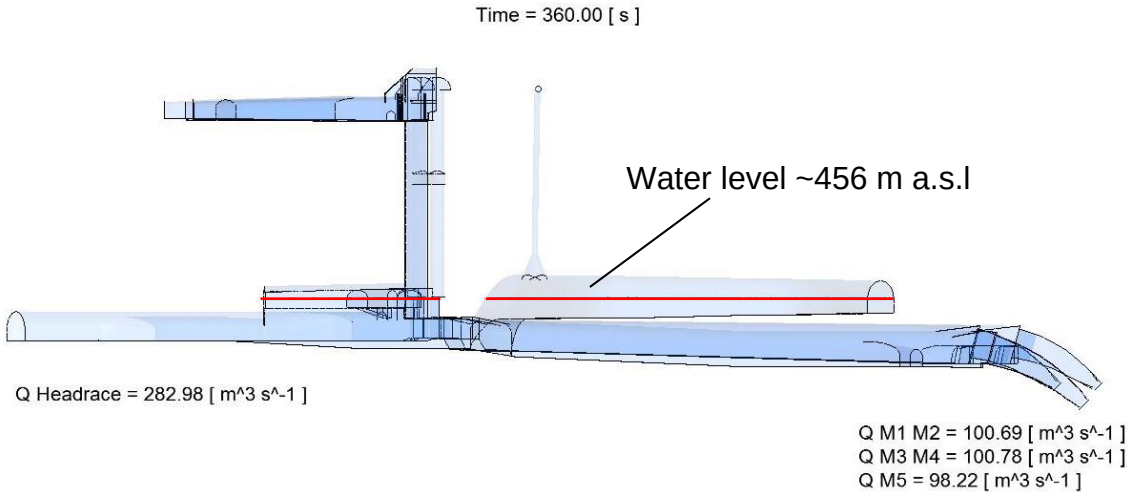

Figure 41 - Water level after 360 seconds (V1 - full system side view)

At 360 seconds the stopping of the turbines is initiated. The discharge decreases within 10 seconds from full load, in this case 125% of the current turbine flow, with 300 m^3/s to 0.0 m^3/s. This abrupt closing of the outlets leads to the initiation of the mass oscillation. An upsurge can be noticed in the whole system and spreads from the outlets upwards the flow direction and is governed by the large inertia of the water mass in the headrace tunnels. The upsurge is noticed by the fast rising of the water level. The counter pressure by the upswing above the reservoir level triggers the backflow.

The effects of the mass oscillation are shown via a two-minute sequence (120 seconds). In the following figures, the two-minute sequence is split into 40 second intervals to show the main process of the mass oscillation.

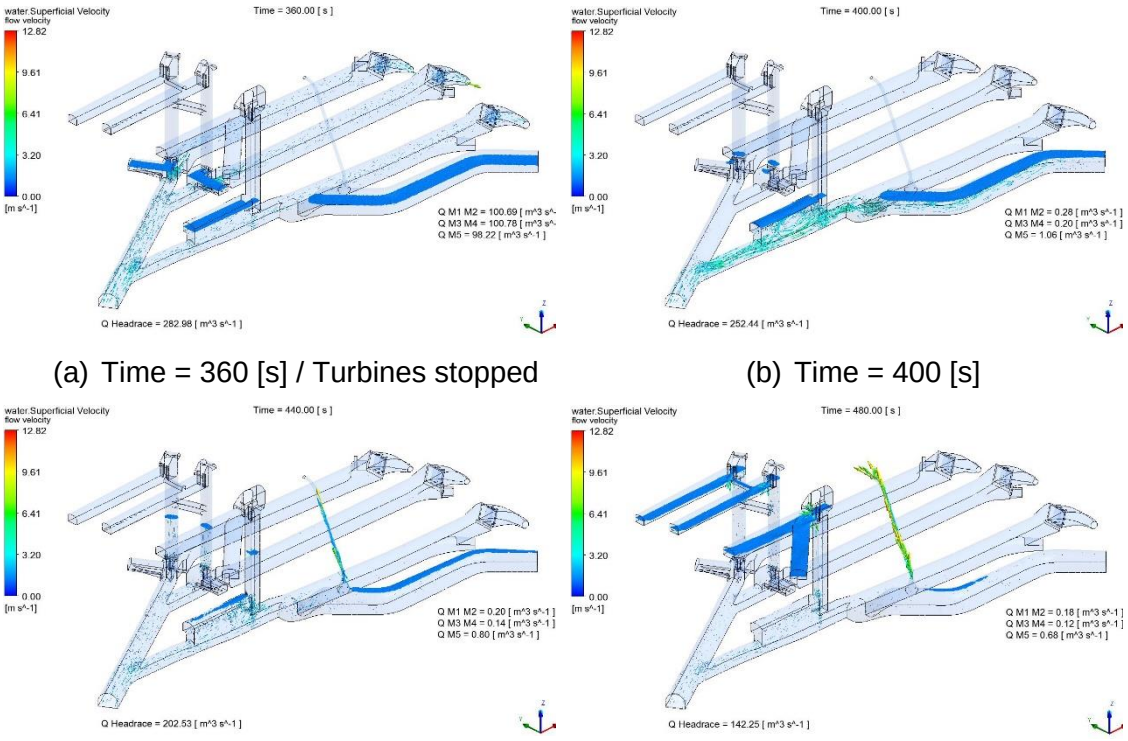

(a) Time = 360 [s] / Turbines stopped

(b) Time = 400 [s]

(c) Time = 440 [s]

(d) Time = 480 [s] / ~max. upsurge

Figure 42 - Sequence of mass oscillation (V1 - full system)

Figure 42 represents the two-minute sequence. Figure 42a shows the system at 360 seconds, the exact moment when the stopping of the turbines is indicated. In the first 40 seconds (Figure 42b) the water level increase is not significant due to the large additional volume provided by the extension chamber. The filling of the extension chamber can be noticed by the velocity vectors, these are mainly distributed at the chamber inlet. The rising water level can be noticed throughout the system after another 40 seconds (Figure 42c). Additionally, can be observed that an air water mix is travelling upwards the aeration pipe. In reality this might be also a pulsation process with bubble escape. The last time step shown, is at 480 seconds and represents the maximum upsurge noticed (Figure 42d). It can be seen that mentioned air water mix is spraying out of the aeration pipe. This fact needs to be further investigated and a corresponding modification needs and is part of the next steps showed.

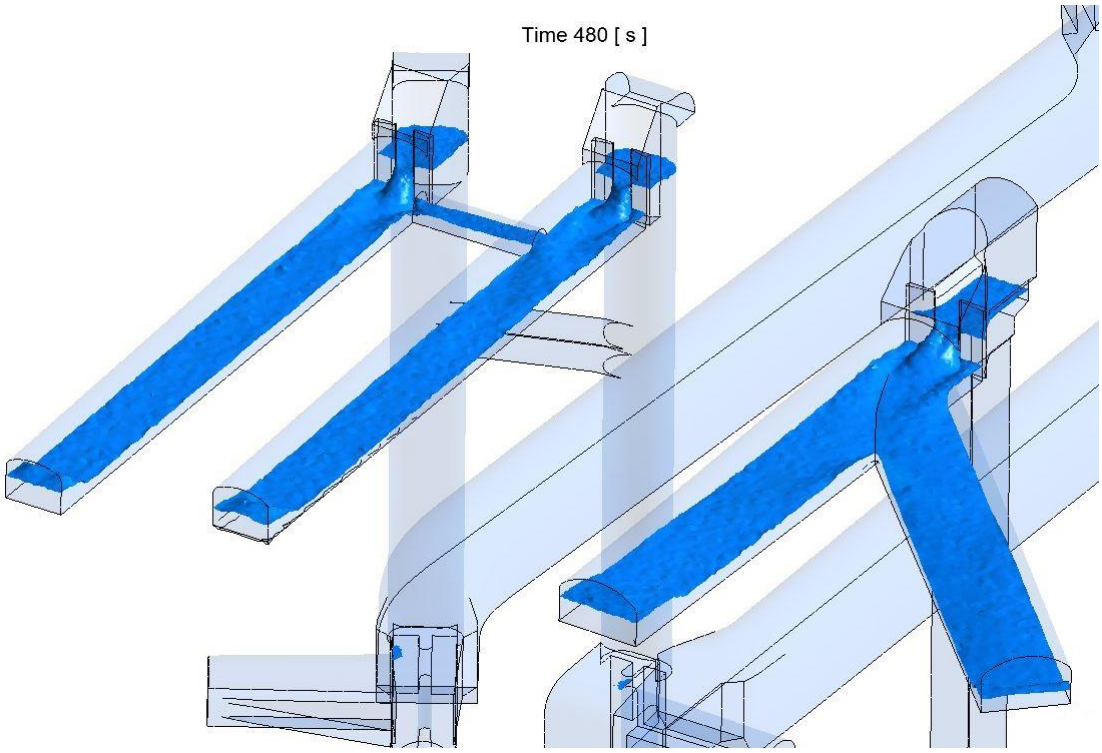

Figure 43 - Entry throttles at the upper chambers

The mode of action of the throttles at the upper chambers is mentioned in 1.1.2.2 but is best shown in Figure 43. The throttling of the filling into the upper chambers has the effect that the water level in the surge shafts is held at a higher level for a longer period, this increases the differential effect of the surge tanks. Resulting in a larger counter pressure available to slow down the water coming from the main tunnel.

The result of the first simulation looks promising for the upgrade of the discharge in combination with the extension chamber. However, the problem of the insufficient overburden as well as the evolved issue with the aeration pipe needs to be solved.

The next variant of the system has to solve the issue according to the overburden. Additionally, a modification of the aeration pipe is done to improve the issue of the air water mix spraying out of it.

5.4 Extension chamber – V2

Variant no.2 (V2) of the extension chamber has to solve the discovered issues of V1. The overburden problem is taken care of by a redesign of the ground layout. The issues in relation to the air water mix spraying out of the aeration pipe is to be solved by changes at the structure.

5.4.1 Redesign ground layout

V1 of the extension chamber provided a too small overburden at the end of it. This knowledge made it necessary to think of a new and better fitting chamber route. In the new variant the direction as well as the layout of the connection to the existing system is the same. The cross sections and the length of the chamber are also the same. Only the route of the chamber is changed. The focus is to provide a satisfying degree of overburden throughout the whole chamber to capture the internal pressure.

Therefore, the whole structure is moved further into the mountain. The relocation of the chamber made it possible to provide the required rock mass above the chamber. The new layout is based on the terrain comparison of V1 and with respect to the required specifications. The new route starts with a 90° bend shortly after the aeration pipe. The rest of the chamber route follows the direction after the turn. The resulting chamber route has sort of a L-shape and can be best seen in Figure 44.

The relocation not only has the benefit of solving the overburden problem but also is a much better fit to the specifications. An unmentioned problem in V1 is that the inclination of the resulting access tunnel is realisable but is very steep. The new chamber V2 provides a much gentler slope for the access tunnel but therefore longer. All in all, this variant represents a good compromise between the needed specifications and the given feasibility of the chamber.

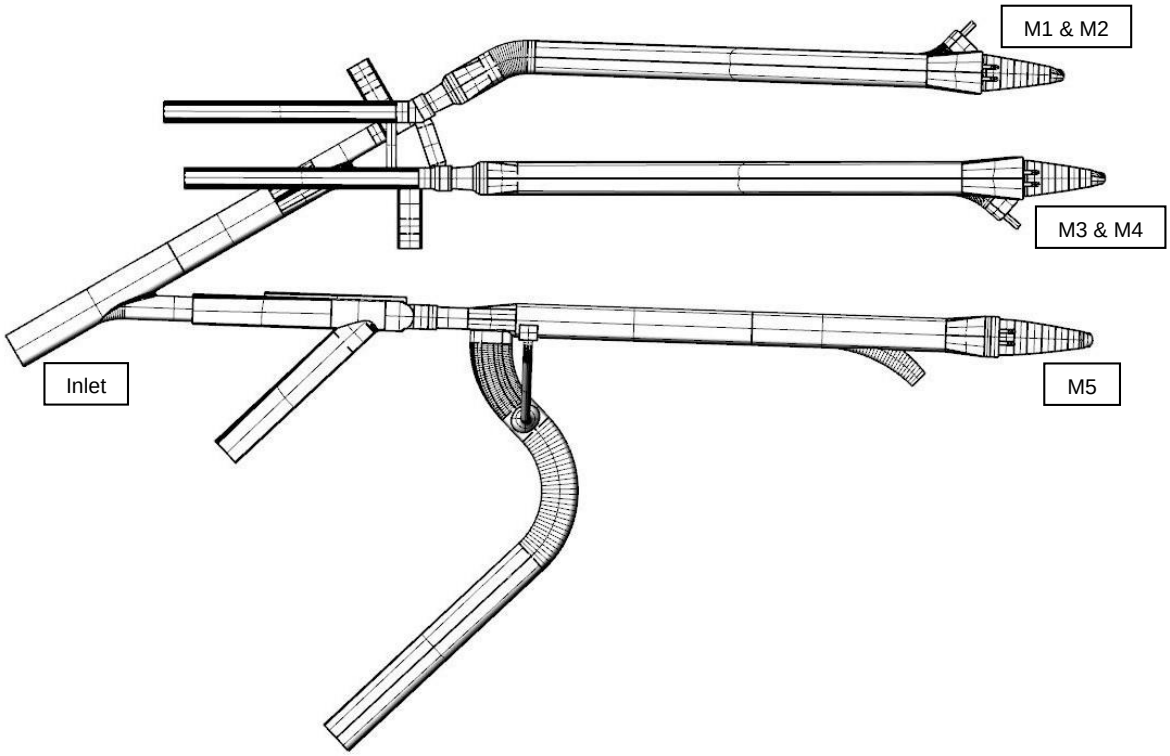

Figure 44 - Ground view V2

Figure 45 represents the system in a front view and should serve for the sake of completeness. It shows that the elevation of the chamber and the connection to the existing system stayed the same and the only change made is the route.

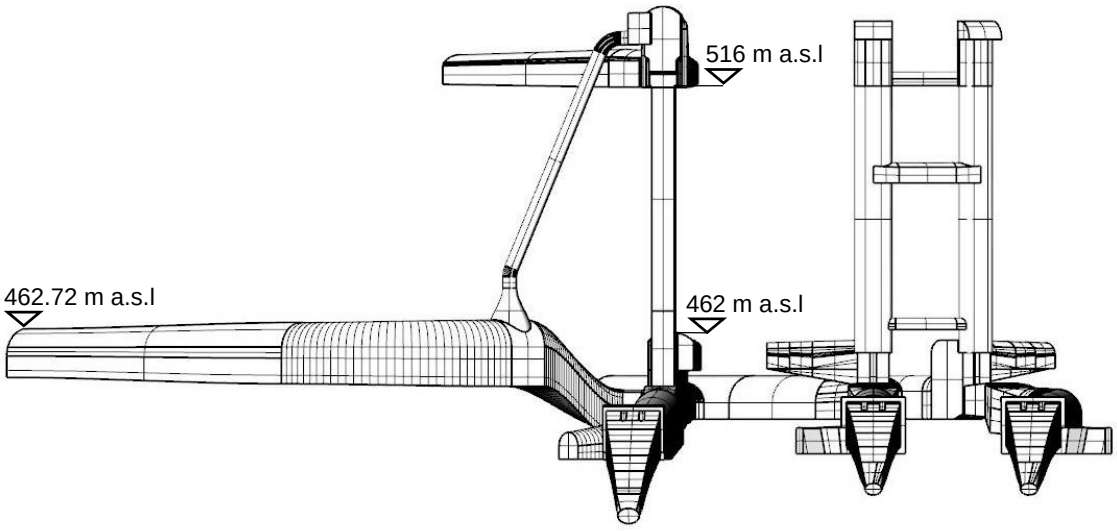

Figure 45 - Front view of V2

The variant V2 provides a satisfying degree of overburden throughout the route. The comparison between the terrain model and the improved variant V2 can be seen in Figure 46.

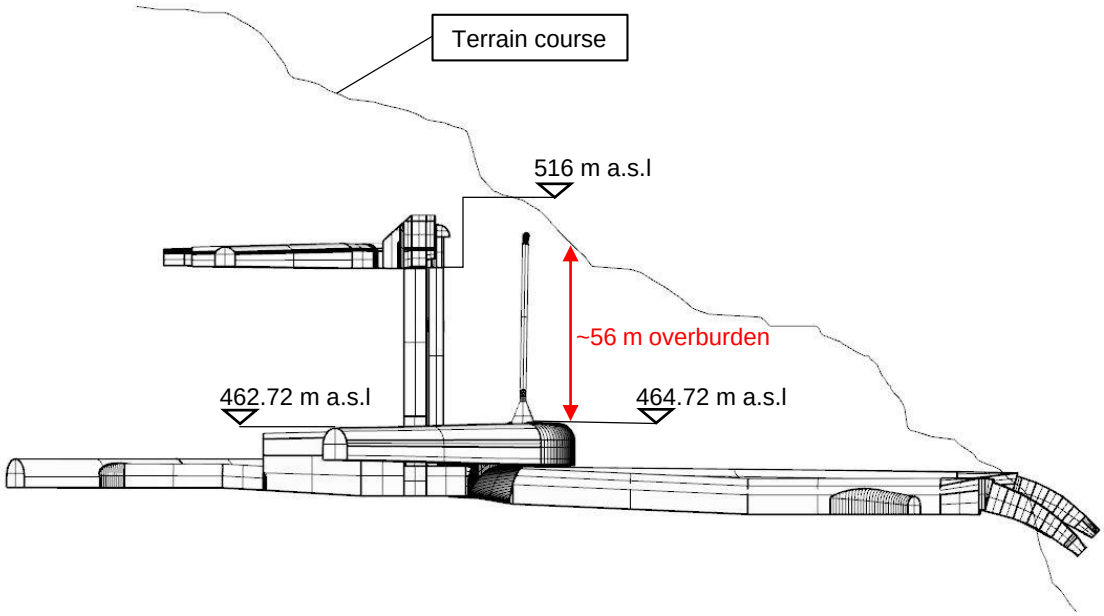

Figure 46 - Comparison of V2 with terrain

V1 provides an overburden at the end of the chamber of about 20 m. The new variant V2 has at least an overburden of about 56 m. This means that the overburden was increased by 36 m due to the relocation. As mentioned in the chapter 5.3.3 the water column can reach a height of 56 m. The general procedure would be to construct an unlined chamber with concrete on the bottom. In Norway, due to the very good rock quality it was already often proven that lower ratios of 1.0 between overburden/internal pressure is possible (Palmstrom, 1987) (Kjørholt, 1991).

This means that the pressure in the chamber can be slightly higher or equal than the provided coverage. Additional can it be seen that the surrounding terrain has a very steep inclination at the end of the sand traps.
The newly designed route of the chamber is the final change in this regard. All further adaptions will only involve adaptions on this basis.

5.4.2 Aeration pipe

In the course of the simulations of V1, it was found that the aeration pipe may have an insufficient size. This effect is noticeable by the spraying of an air water mix out of the pipe. The diameter in V1 is 2.0 m and is widened to 3.0 m. Additional to the widening of the diameter the shape of the cone at the beginning is changed too. The shape is now more rounded and provides additional volume, this should mitigate pulsations at filling.
If that's not the case, an additional security device is situated at the end of the pipe. The security device is further described further in the following subchapter. The adapted aeration pipe in combination with the security device, which is a small chamber can be seen in Figure 47.

5.4.3 Retention cavern

Additional to the change of the size of the aeration, sort of a retention cavern is modelled as security device. This cavern is situated at the end of the aeration pipe for the case of a spraying of the air water mix. This cavern can be integrated in the access tunnel of the upper chamber at surge tank no.3. The caverns floor is slightly inclined ~1% to avoid standing water in the cavern and to keep it maintenance-free. The cavern has the form of a cube with a ground area of 6.0 m by 4.0 m and a height of 7.0 m. Figure 47 gives an impression of the ratio between the widened aeration pipe and the retention cavern to the extension chamber.

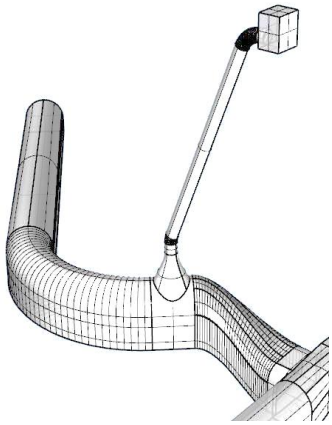

Figure 47 - Adapted aeration pipe with connected retention cavern

5.4.4 Results and Findings V2

At the start of the simulation, the adapted system V2 behaves the same as the foregoing variant V1.

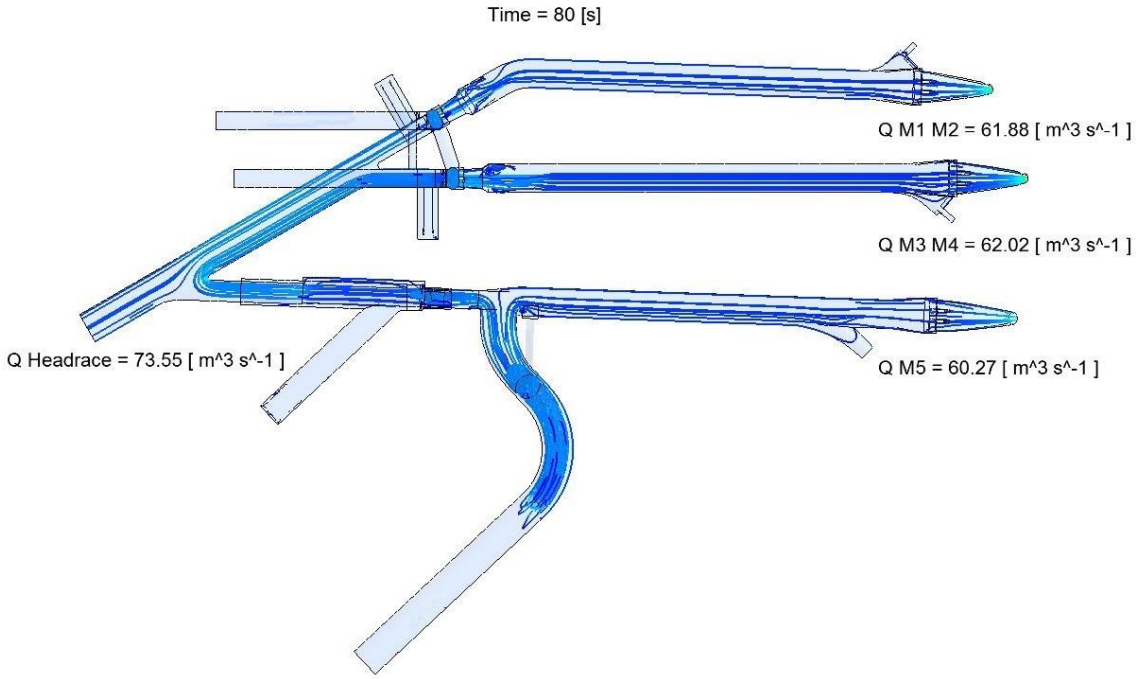

Figure 48 - Streamlines at start-up (V2 - full system ground view)

As in V1, the extension chamber starts to supply water to all three start-up chambers shortly after the simulation start. The turbines are fed on the on side by the reservoirs and on the other side by the extension chamber until full acceleration of the headrace tunnel. This is indicated by the streamlines in Figure 48 originate from the extension chamber as well as from the headrace inlet.

Figure 49 shows a two-minute sequence (120 seconds) picked of the effects during the mass oscillation. Start of the sequence is at 360 seconds after the start (Figure 49a) and the end at 480 seconds (Figure 49d). It can be seen that at the start of the sequence, the needed water is only provided by the headrace inlet or reservoirs. This is indicated by the velocity vectors in sand trap no.3.

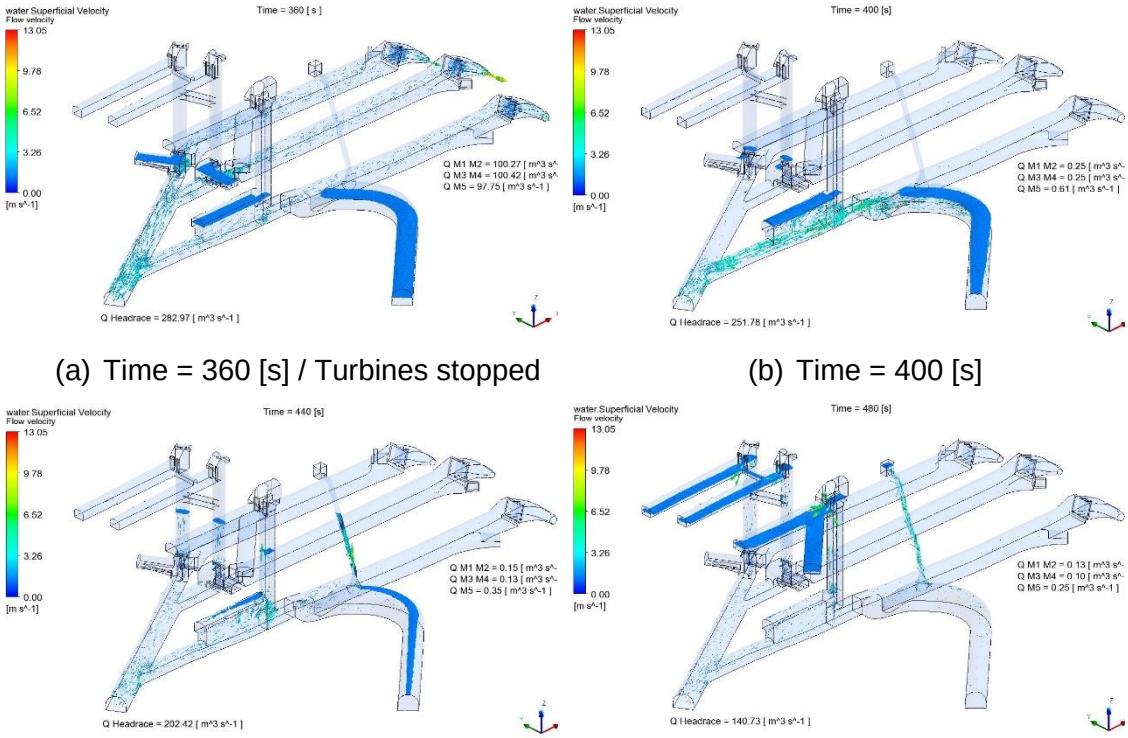

(a) Time = 360 [s] / Turbines stopped (b) Time = 400 [s]

(c) Time = 440 [s] (d) Time = 480 [s] / ~max. upsurge

Figure 49 - Sequence of mass oscillation (V2 - full system)

The upswing can be noticed after 40 seconds of the turbine stopping (Figure 49b). The rise of the water level is until this time step only limited to the lower chambers. The additional volume of the extension chamber takes on a large portion of the mass oscillation at the beginning. After 80 seconds (Figure 49c) the mass oscillation can additionally be noticed in the surge shafts as well as in the aeration pipe. The maximum upsurge can be seen two minutes after the stopping of the turbines (Figure 49d). The retention cavern is needed, due to the continuing issue of the air water mix spraying. The widening of the diameter of the aeration pipe does not provide the desired result indicated by the relative high water level in the cavern.

On the basis of these observations it is needed to investigate the issue of the air water mix further. The forming of the air water mix can be best seen at the time step of 440 seconds. The result of the air water mix is shown at the time step of 480 seconds. Therefore, a time step between these two is picked to explain the development.

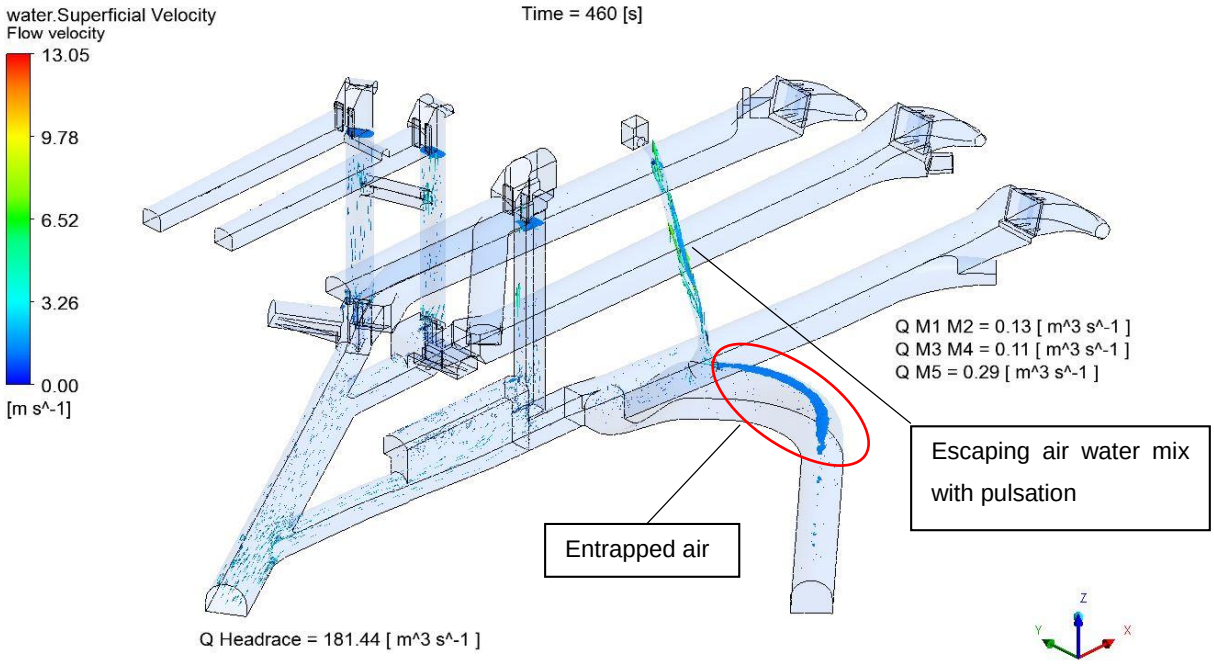

Figure 50 - Development of the air water mix spraying (V2 - full system)

Figure 50 represents the time step of 460 seconds and illustrates the reason for the evolving air water mix.

During the rising of the water level air gets entrapped in the extension chamber crown. This is a very natural behavior since the crown is not steep inclined. In addition, the surge wave influences the creation of entrapped air. The surge waves travel towards the end of the chamber and get reflected at the end. These waves push some amount of air in front of them due to the reflection. This leads to a pulsation effect at the aeration cone. This effect gets amplified by the oncoming waves due to the entrapped air. The pulsation in combination with the amplification leads to the unsteady air-water release in the pipe. This is seen to make no damages but also is not a beneficial and desirable property.

These findings show that there is space for improvement especially for the aeration pipe. The additional results show that an ongoing widening in small steps of the pipe diameter is not purposeful, since the idea is to keep the aeration pipe as small as possible. The root of the problem is the entrapped air in the rear part of the extension chamber. The next variant is meant to introduce a modification, which intends to solve the problem.

5.5 Extension chamber – V3

The results of V2 showed that there is still potential for improvement according the aeration pipe. The taken measures up to this point are not sufficiently solving the problem with the air water mix spraying out of the pipe. Further considerations on the issue lead to the introduction of an aerated crown throttle.

5.5.1 Aerated Crown throttle

After the simulations of V1 and V2, it could be investigated that the effect of the pulsating air release and significant spraying (geyser effect) has its roots in the entrapped air in the rear part and along the chamber crown. This entrapped air causes a sloshing of water into the aeration cone at the beginning of the chamber. The resulting spraying effect is based on the pulsation of the surge waves and the accompanied amplification due to the high interval of the waves. Based on this investigations, a structure is needed to calm down the surge waves, which results in a decreasing of the sloshing effect. The concept is to place a bar shortly after the aeration pipe. In the following is this bar referred as crown throttle. The throttle reduces the cross section of the chamber and creates a large cavity behind, that is only de-aerated by a small pipe (Figure 51).

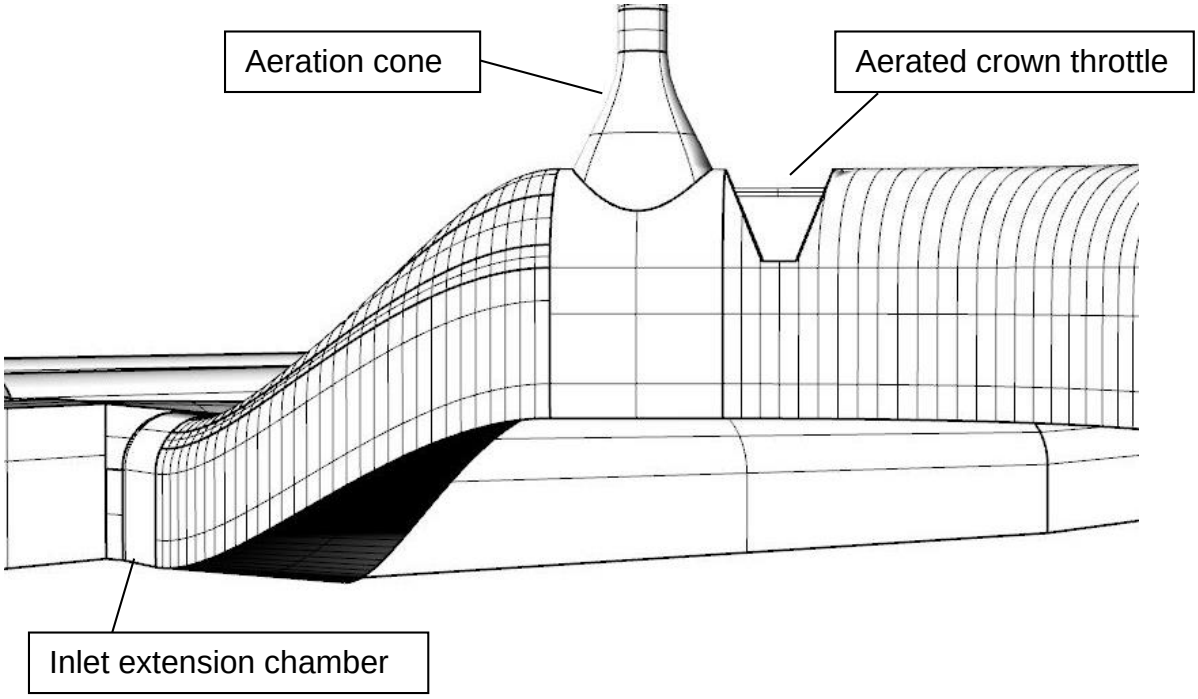

Figure 51 - Aerated crown throttle in side view

The crown throttle has a trapezoidal shape and gets pierced, as shown in Figure 51, by a round opening (DN 500). The opening is needed to aerate the resulting rear part of the chamber. The dimensions of the crown throttle as well as the elevation at the top are shown in Figure 52.

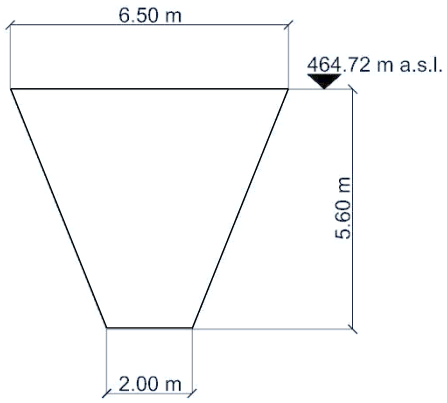

Figure 52 - Cross section of the crown throttle

The crown throttle has an influence on the whole mass oscillation. Not only is the effect of the sloshing and the combined spraying of the air water mix influenced. Additional is it investigated that the extension chamber in some way shares effects which else can be found at the upper chambers. This way the crown throttle improves the differential effect of the surge tank system with the extension chamber. The rather small de-aeration opening creates a so called semi-air cushion in the rear part which has a significant impact on the water level in the inlet area of the chamber. The effect of the semi-air cushion will be further explained in the following analysis of the simulation results.

5.5.2 Results and Findings V3

The impact of the crown throttle can be noticed right at the beginning of the simulation. The separation into two parts, a front and rear one, of the chamber can already be noticed after a short period of time.

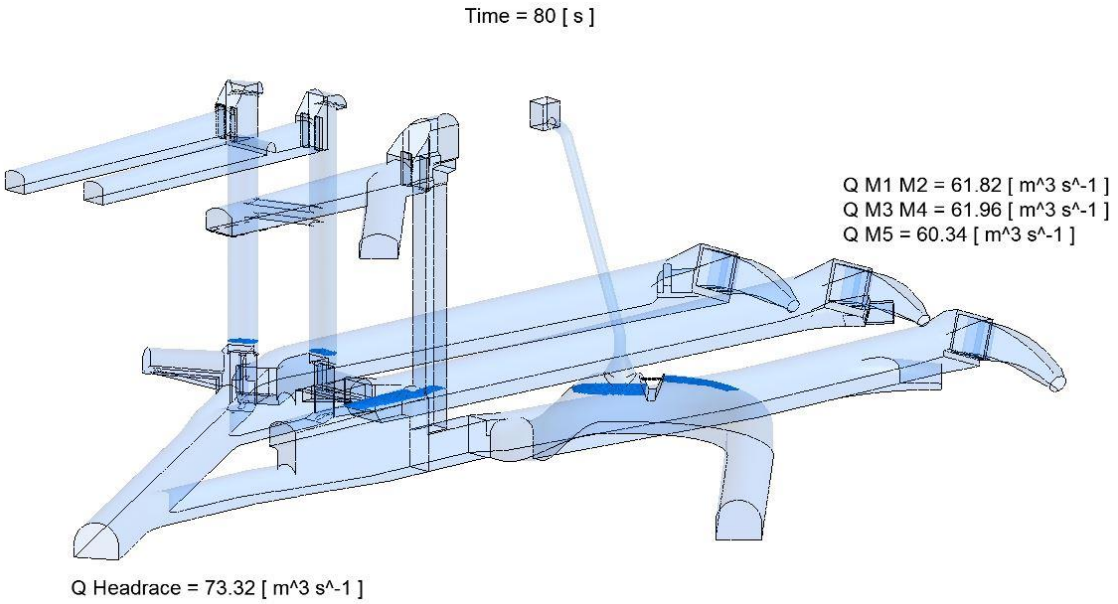

Figure 53 - Effect of crown throttle at start-up (V3- full system)

As mentioned several times in the foregoing chapters, provides the extension chamber water for all three start-up chambers. After about 80 seconds (Figure 53) is the water level lowered to a point where the extension chamber parts into two sections. The water level at the aeration pipe in front of the throttle is lowered faster due to the bigger area of the connection to the existing system. The rear water level stays at a higher level and the flow situation approaches to an outflow under a gate. The reduced cross section leads to an accelerating of the outflow below the throttle. The flow velocity is higher until the point where the water levels are balanced out between the two parts. After the balancing, the level is lowered over the whole route of the chamber. This observation already gives consensus with the considerations of the semi-air cushion effect during the mass oscillation.

The previous simulations stated already that free-surface flow in the sand traps is avoided at any point. This is also the case for V3 with the additional installed aerated crown throttle.

5.5.2.1 Semi-air cushion effect

The semi-air cushion effect is best explained at the first upswing of the mass oscillation. The upswing starts after the closing of the turbines at 360 seconds and can be noticed by a differential filling of the parts before and after the crown throttle. Figure 54 shows a two-minute sequence with steps of 40 seconds.

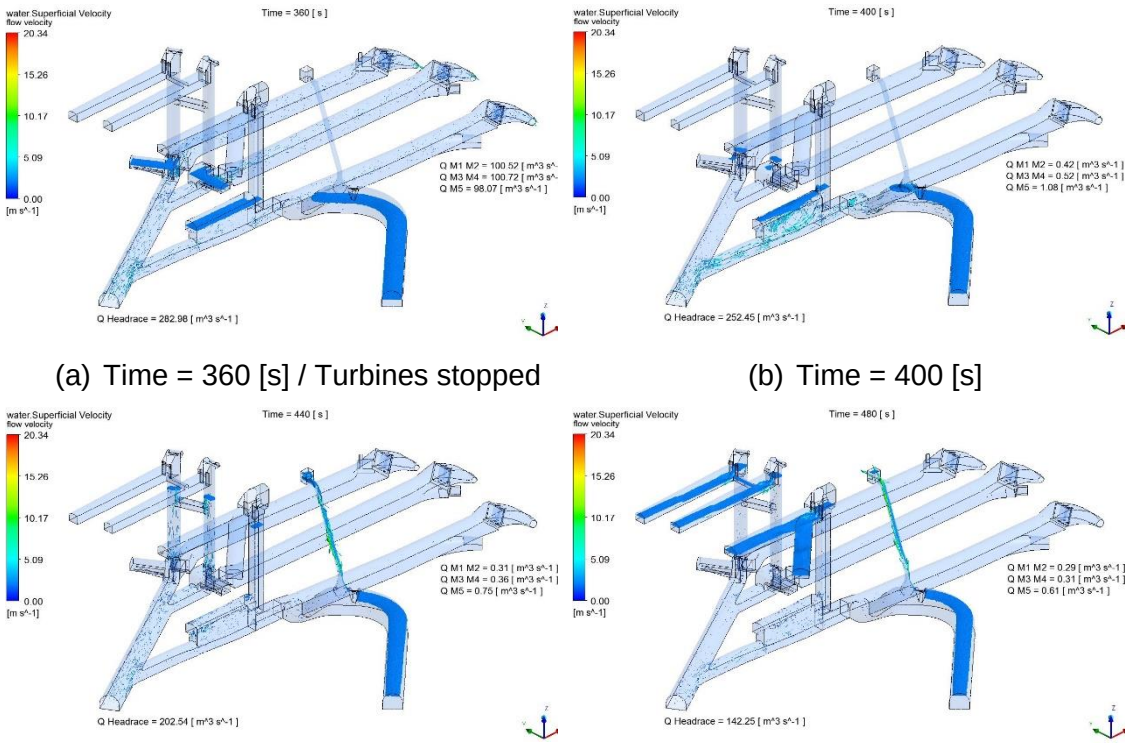

(a) Time = 360 [s] / Turbines stopped (b) Time = 400 [s]

(c) Time = 440 [s] (d) Time = 480 [s] / ~max. upsurge

Figure 54 - Sequence of mass oscillation (V3 - full system)

Figure 54a shows that the water level is at its lowest just as the turbines are stopped. The lowest water level is the same as for the foregoing simulations due to the fact that the dimension of the chamber is not changed and that the input data for the transient load case is the same. The water level is rising in the whole system simultaneously until the crown throttle is reached. After surpassing the bottom of the throttle, the water level in the rear part is rising at a slower rate than in the front part due to the limited run-off through the throttle. This behaviour creates a pressure inside the semi-air cushion. The semi-air cushion can be seen as fully adiabatic because the time exposed is relatively short. This means no heat exchange with rock. The rising of the water level in the system can be seen in Figure 54b and Figure 54c. In both figures, the mentioned effect of the limited

run-off can be seen, indicated by the different water level with respect to the level in the rear part of the chamber. The maximum upsurge at the system noticed is shown in Figure 54d. At this point can it be observed that the extension chamber somehow works just the same as the upper chambers – except the pressure by elevation it is an air pressure that is creating the delayed filling. The limited run-off at the upper chambers generates a higher water level in the surge shaft. The same effect can be seen one to one at the crown throttle. The water level in the front part is much higher than in the rear part. Therefore, an additional water mass is provided which helps to slow down the flow in the main tunnel. The term semi-air cushion for this effect is based on the small de-aeration opening. Due to this the volume can be used instead of volume in an upper chamber. This way the semi-air cushion increases the safety of the upper chamber volume.

The sequence of the mass oscillation shows that the issue concerning the spraying of the air water mix out of the pipe into the cavern could not be fully eliminated. But the air escape with spraying and pulsation was significantly mitigated. The semi-air cushion effect based on the throttle has such a positive impact on the system that it nearly overshadows this fact. The sloshing of the water into the aeration cone is fixed but due to the changed pressure situation the aeration pipe needs to be revisited.

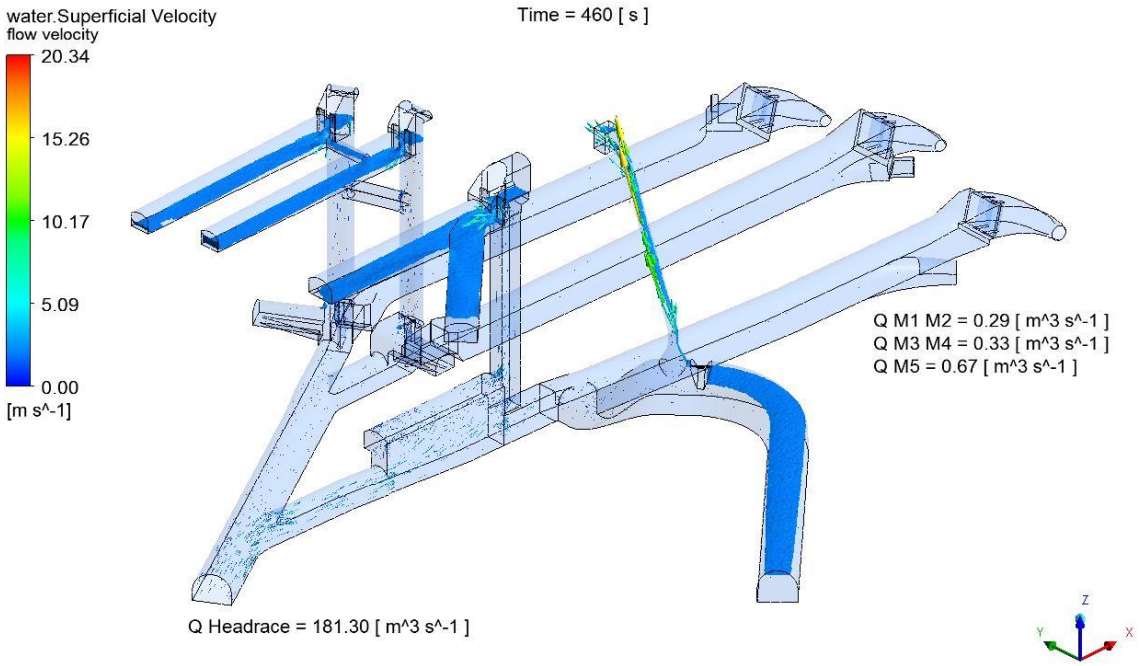

Figure 55 - Maximum upsurge after 460 seconds (V3 - full system)

Figure 55 shows the system at the maximum upsurge. It shows that the velocity of the air water mix in the ventilation pipe is very high. This leads to the assumption that the air needs to be fully separated from the water. The rising water level compresses the entrapped air in the chamber. The rather small opening (DN 500) leads to the forming of an air jet at the aeration opening. The air jet blasts the water into the ventilation pipe and upwards resulting in a higher water level in the aeration pipe and further on in the spraying of the air water mix.

It appears that the solution for this problem is an independent aeration for the rear part of the chamber. An additional aeration pipe generates two separate air situations in the chamber. The generating of an air jet due to the compressed air is therefore eliminated. During the mass oscillation, the pipe only has to transport air and the aeration of the front part only has to aerate the small front section.

6. Discussion extension chamber

After the simulation of three different variants V1, V2 and V3 of the surge tank system the collected knowledge is reflected on the impact of the extension chamber and all the adaptions taken up to this point.

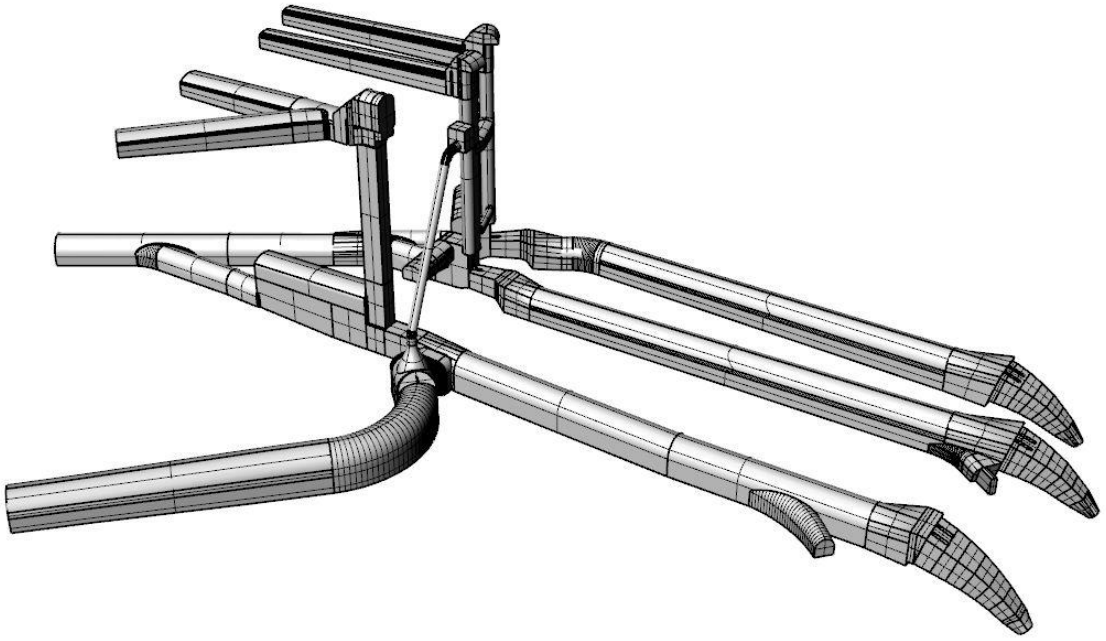

Figure 56 - Perspective view of V3

Figure 56 shows the system with all adaptions taken up to this point of the thesis. The issue of the air water mix spraying out of the aeration pipe couldn't be solved completely but an approach for the elimination of the problem is provided in the foregoing chapter 5.5.2.1, which is a separate de-aeration pipe and de-watering pipe.

The discussion is mainly divided into two parts. The first part is about the layout and the second part about the adaptions taken. In the first part the discussion will focus on the improvement potential of the layout with the exception of the route. The second part is additionally split into the two main adaptions, the aeration with the associated retention cavern and the crown throttle.

6.1 Layout

The route of the extension chamber is excluded in this discussion due to the already discussed problems and associated solution approach in chapter 5.4.1. The focus at this point lies more on the potential for improvement in means of the volume of the chamber.

The simulation results of all three variants V1, V2 and V3 show that the water level during steady operation at the maximum discharge is sufficiently high, since the crown of the sand trap has an elevation of 450 m a.s.l. which is the absolute limit that must always be submerged. It is very important, that there are still some meters left since the simulations are made at capacity level. But the discharge and power upgrade should also work for lower levels than the maximum water level in the reservoirs. The following Figure 57 gives an idea of the case mentioned. The figures show the steady operation situation at V3 as an example.

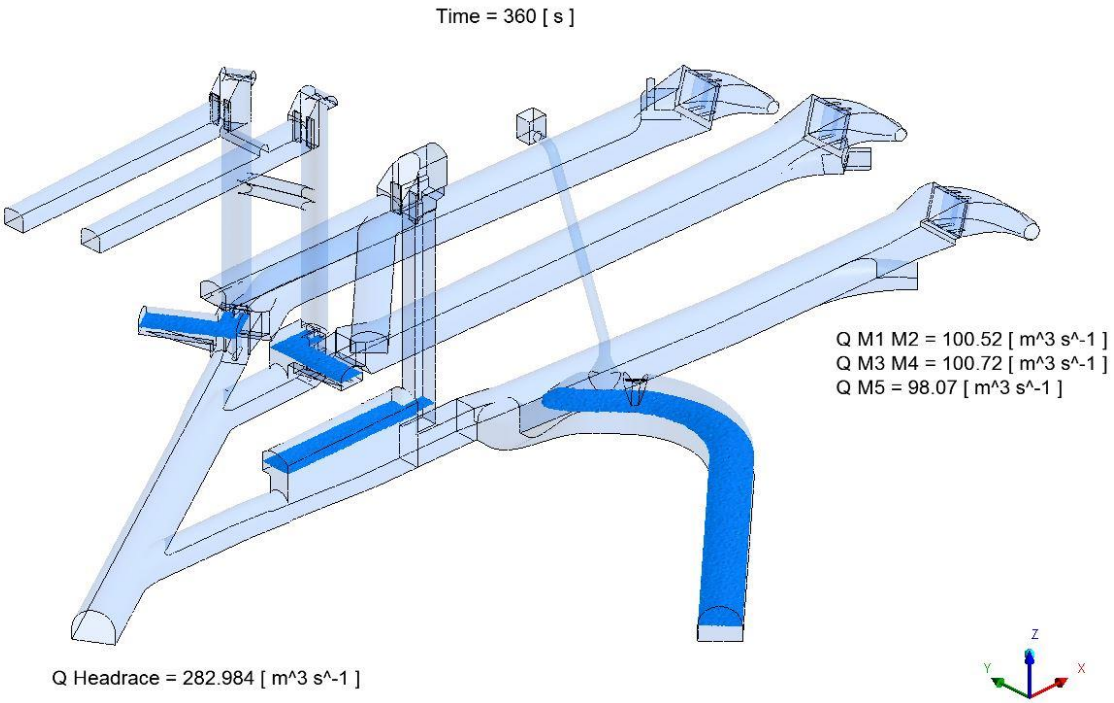

Figure 57 - Water level at steady operation (V3 - full system)

The water level of approximately 457 m a.s.l. shortly before the stopping of the turbines is sufficiently high for this case. The connection has a length of about 30 m and a flow area of 137 m^2. The resulting volume of the connection is not accounted in the drafting of the main chamber. The cross sections were adjusted to a more frequent used layout and to provide an inclination at the crown and

invert over the whole route. Thus, is the cross section at the start of the chamber bigger than it would be only based on the calculation from the initial volume.
It is needed for safety reasons that the chamber provides a bigger volume than based on the calculation. However, it doesn't need to be that big because the construction of tunnels or chambers is always bound to expenses and it would be favourable to reduce the excavation material.

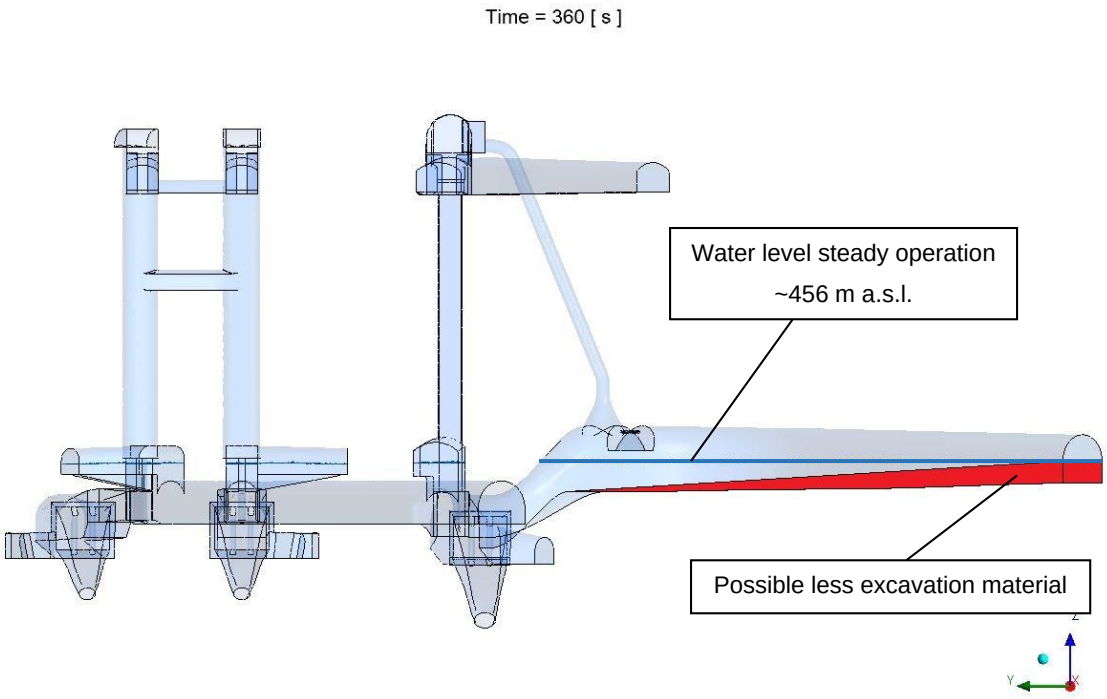

Figure 58 - Possible change of layout (V3 -rear view)

A possible adaption of the layout is discussed in Figure 58. The layout has sort of the same trapezoidal shape but with a steeper inclination at the chamber invert. The cross section at the end is reduced to the point where the shown actual water level is situated. This change reduces the volume but a safety volume of water is still provided due to the larger cross section at the beginning. In any cases it will be needed to, further investigate or simulate the system with the changed extension chamber to provide a sound objective statement about the changes.

6.2 Adaptions

For now, the adaption of the additional aeration pipe for the rear part of the chamber is not simulated. This adaption will be part of the simulation of V4 with respect to the implementation of Fleksible Sandfang (FlekS) in the next chapter.

6.2.1 Aeration pipe and retention cavern

The curved design of the aeration pipe is based on the consideration of connecting the end of the pipe to the existing access tunnel of the upper chamber at surge tank no.3. In the end, it is also possible to construct a straight design. The difference is that a straight pipe needs a longer cavern at the top than a curved pipe. Nevertheless, the changed design has no impact on the results of the simulations. The changed diameter in contrast to the design leads to different results. The change of the diameter requires further investigations and simulations. The retention cavern is developed based on necessity and as protection against the air water mix spraying out of the pipe and thus into the access tunnel of the upper chamber. Principally, it can be said that the larger the pipe in diameter the better. For now, an investigated pipe with 3 m seems to be sufficient.

6.2.2 Crown throttle

The crown throttle has a positive effect on the system although it doesn't solve the problem with the air water mix completely. The semi-air cushion provides an additional water storage effect that is a valuable benefit. The throttle implemented is considered to be made out of concrete. The construction has to be evaluated. The trapezoidal shape and the associated small width at the bottom is linked to great effort in relation to formwork. The establishing of a connection between the concrete and the planned unlined tunnel crown is additional bound to great effort due to the high forces acting at the throttle. The extension chamber is planned, due to the rock quality, to have unlined walls. The invert of the chamber has to be constructed with a concrete layer and is intended to be one of the few parts made of concrete.

A possible solution for the emerging issues mentioned would be to widen the crown throttle along the route of the chamber (Figure 59). This change would make it possible to substitute the concrete by rock to establish the throttle. The excavated cross section in the area of the throttle is simply reduced and realised as change in cross section. Therefore, is the throttle made out of unlined rock and a resulting positive effect is that the excavated material is reduced. Additional might it be easier to realise the throttle due to the ceasing of the complex processes of concrete placement and connection establishing. Only the de-aeration pipe needs to be significantly longer. However, the greater length has not really an influence on the semi-air cushion effect. An exact statement about the situation with a changed length needs to be based on further investigations and simulations. The following Figure 59 illustrates the idea of the lengthening of the throttle. The figure represents a schematic cross section of the extension chamber and the associated connection to sand trap no.3.

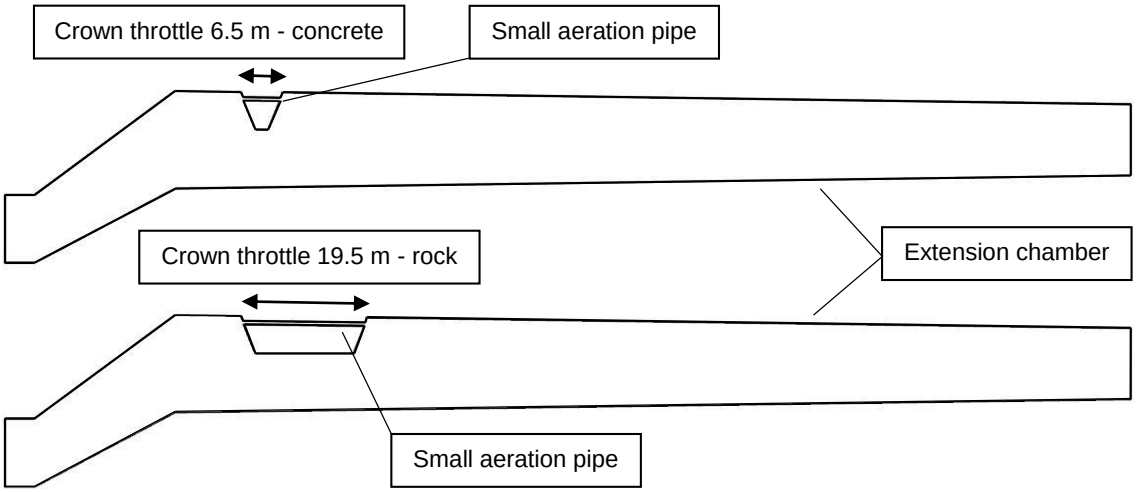

Figure 59 - Comparison of crown throttle length if concrete or rock type

The first cross section represents the implemented crown throttle with a length of 6.5 m, due to the length is it needed that the throttle has to be made of concrete. The lengthening of the throttle, for example to 19.5 m, makes it possible to realise the throttle as a cross section reduction. Therefore, can the throttle be made out of unlined rock.

7. Outlook - Implementation of Fleksible Sandfang (FlekS)

The research project "Fleksible Sandfang" (FlekS) deals with the upgrading of existing sand traps. The research is based on literature studies and connected hydraulic scale modelling plus CFD simulations. The reason for the initiating of the project are the challenges experienced at various large hydro power plants in Norway. The goal of the project is to increase the trap efficiency as well as capabilities of automated sluicing systems. On the basis of this research would it be possible to increase the capacity of existing power plants and maybe even modify them into pumped storage plants.
The first hydraulic scale model is based on the sand traps of the Tonstad sand trap no.3. The preliminary results are mainly based on CFD simulations made at the Graz University of Technology. Different structural measures are simulated to improve the efficiency of the sand trap. The structural measures investigated are for example: a flow diffusor at the beginning of the sand trap, a lowering of the tunnel invert with additional trenches and baffles in the middle. The results or findings of the simulations show that the flow diffusor in combination with the calming structures have a positive effect on the trap efficiency (Vereide , et al., 2017) and (Richter , et al., 2017).

The topicality of this research project is the reason for the simulation of a fourth variant V4 of the system. On the one hand is the impact of a flow calming structure at the beginning of the sand trap in respect to the mass oscillation from interest. On the other hand, the compatibility of the findings from the research project in relation to the topic of upgrading an existing power plant is of interest. The structural measures at the tunnel floor are neglected in the oncoming variant due to the low relevance in the case of mass oscillation.

The modelled flow calming structure is situated at the area of the extension chamber intake or widening of the cross section at the beginning of the sand trap. Thus is the entry area of the chamber reduced by half. The calming structures layout can be seen in Figure 60. The structure consists of 61 round openings, each with a diameter of 1.0 m and a length of 4.0 m.

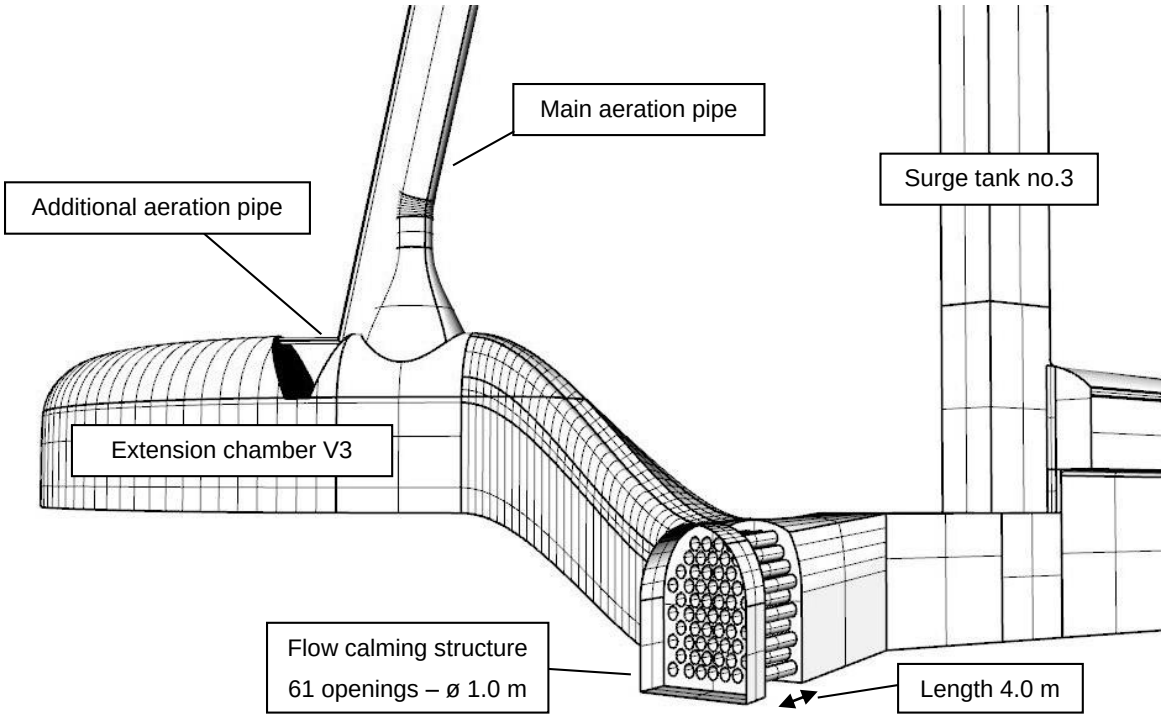

Figure 60 - Implementation flow calming structure sand trap entry

The cross section change at the beginning of the sand trap represents a gradual expansion. The flow calming structure changes the situation in a smoother expansion that distributes the flow more evenly. Due to the calmed down flow it is possible to extend the length were the sedimentation can happen.
Additionally to the calming structure, the adaption of an independent aeration pipe for the rear part of the extension chamber is implemented (Figure 60). The position of the aeration pipe is slightly changed in contrast to V3. In V4, the pipe is slightly higher situated and therefore nearer to the tunnel crown. The whole system of V4 is shown in Figure 61 and Figure 62.

The simulation has the same procedure as for the V1 – V3. The input data as well as most of the boundary conditions stay the same for the oncoming simulation. A small exception is done at the boundary conditions. The calming structure consists of concrete in the simulation and therefore represent additional concrete surfaces which have to be taken into account via the affiliated roughness value. No big difference is seen between a simulation with steel pipes or concrete pipes in this case.

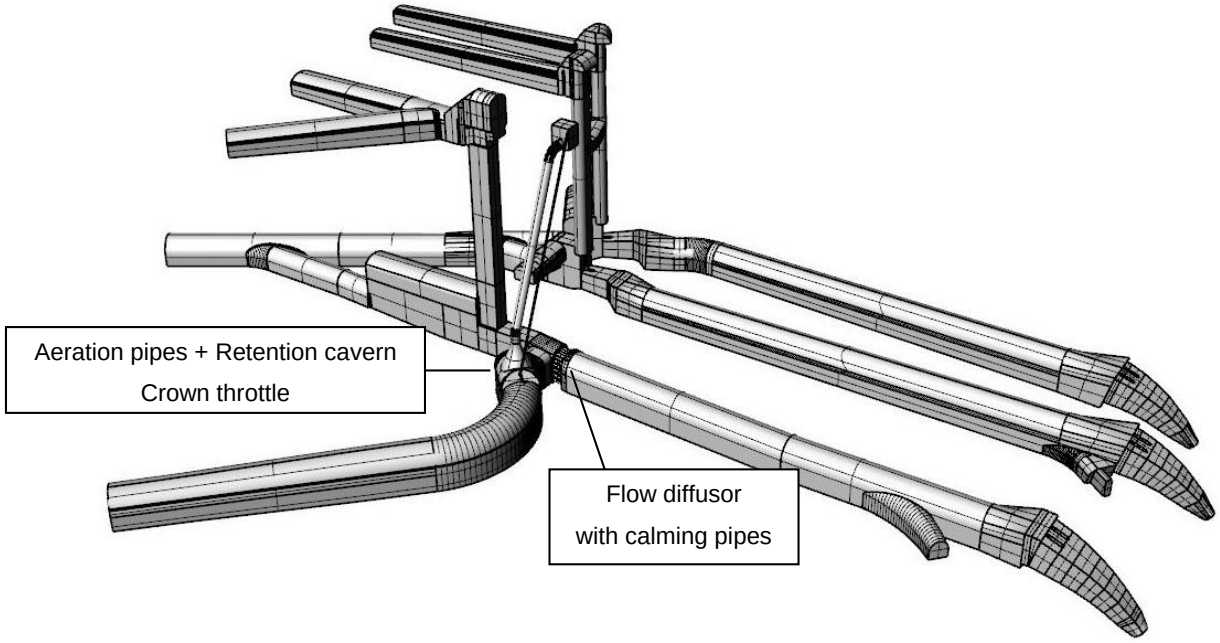

Figure 61 - Perspective view of V4

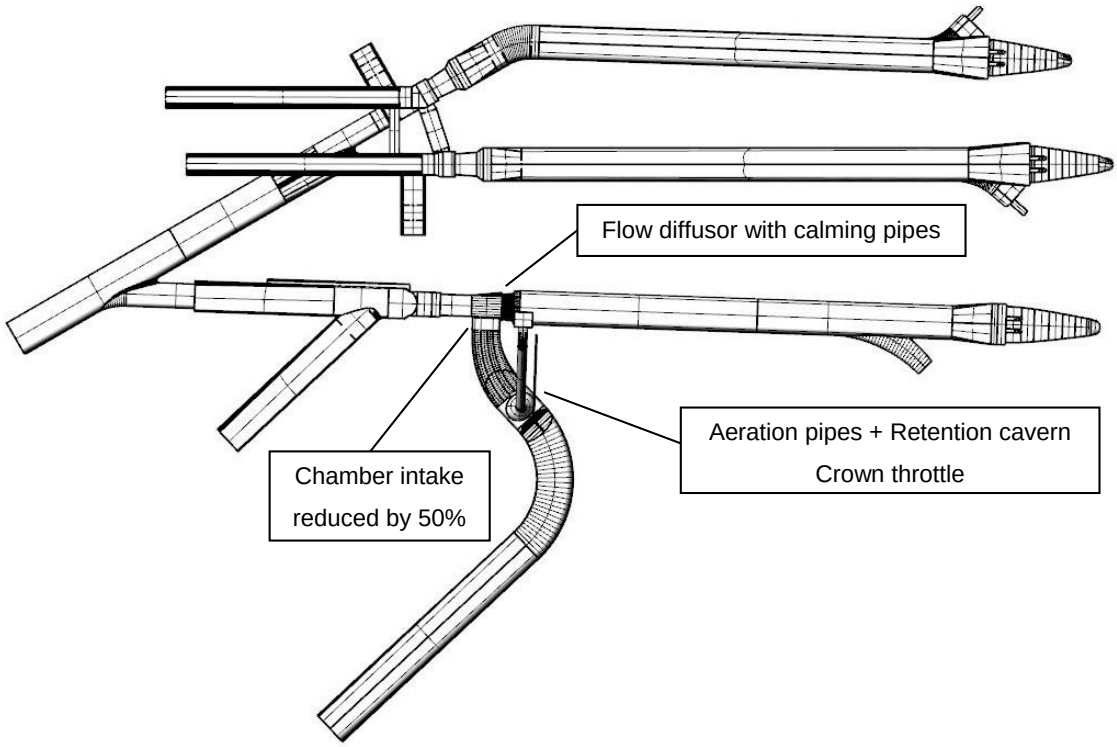

Figure 62 - Ground view of V4

7.1 Results and Findings V4

The situation during the starting up of the turbines looks ordinary and is the same as for the foregoing variants. A negative effect due to the flow diffusor cannot be noticed. The lowering of the water level happens nearly in the same way as for V3. In Figure 63 the system is shown at the time step of 80 seconds after the start of the simulation. The turbines are starting up and the water in the headrace gets accelerated.

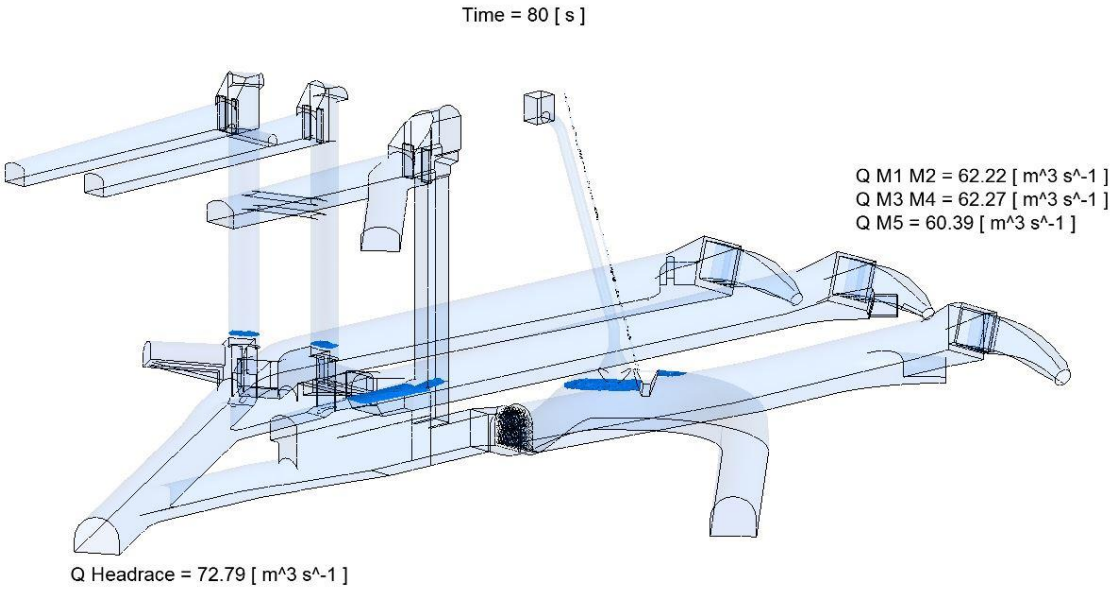

Figure 63 - Water level at start-up (V4 - full system)

As above, the first mass oscillation is investigated over a time sequence of two minutes, starting at the exact moment were the stopping of the turbines is initiated.

The Figure 64a represents exactly this moment. The water level is at its lowest and is high enough to ensure no free surface flow in the sand traps. The additional installation of the flow diffusor has therefore no real impact in the case of steady operation. The water level starts to rise due to the stopping of the turbines, this situation can be seen in Figure 64b. The semi-air cushion effect behaves exactly the same as in V3 of the system. The impact of the additional aeration pipe for the rear part of the chamber can already be seen just 40 seconds after the stopping. Figure 64c shows that the positive effect of the extra aeration pipe lasts on for the whole upswing event. The water levels are nearly the same in all three surge tanks and in the aeration pipe of the front part. In Figure 64d the system is

shown two minutes after the stopping of the turbines. Nearly the maximum water level in the system is reached. The system showed over this two-minute sequence no negative effects or situations. Therefore, a combination of the two upgrades seem realisable.

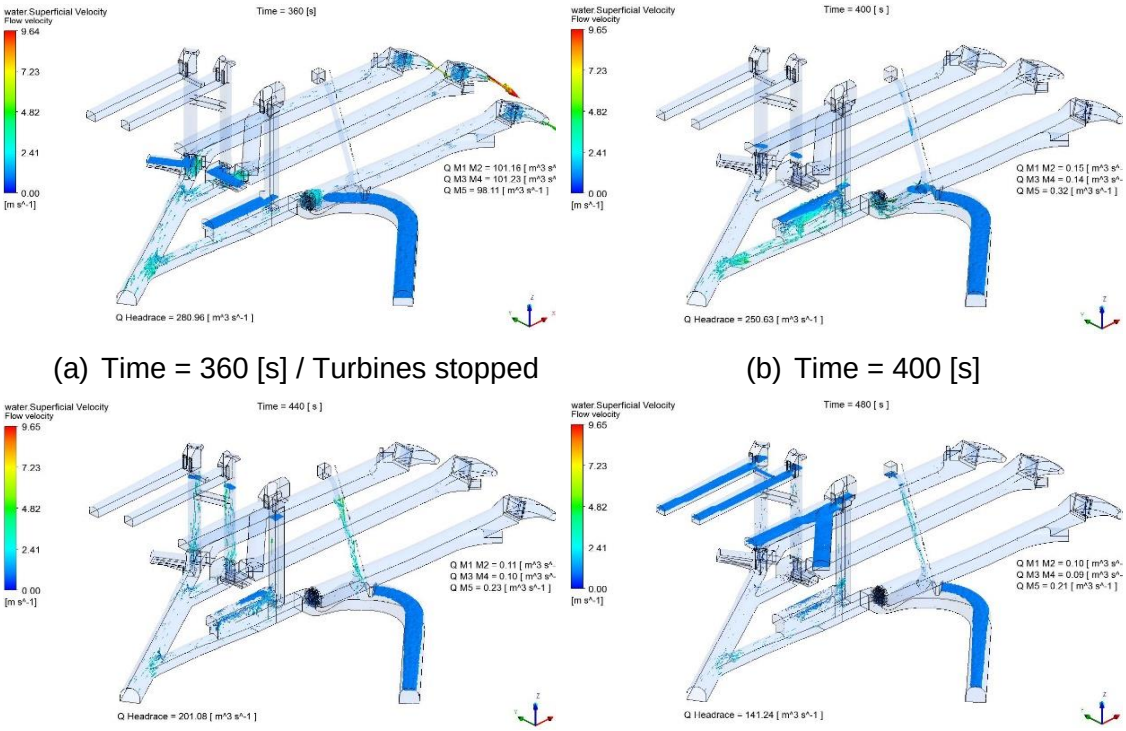

(a) Time = 360 [s] / Turbines stopped (b) Time = 400 [s]

(c) Time = 440 [s] (d) Time = 480 [s] / ~ max. upsurge

Figure 64 - Sequence of mass oscillation (V4 - full system)

The point of the maximum upsurge is reached at about 460 seconds and can be seen in Figure 65. This time step is further analysed to make a statement about the additional aeration pipe and the retention cavern.

The main aeration pipe works very fine without pulsations and water spraying now. Also the small extra aeration pipe functions very well. Although still some spraying can be detected. The solution for this is that the extra pipe will be bended inside the small retention cavern. So water is kept in the system without any spill and air can fully access the pipe and the air cushion.

The retention cavern is still necessary which can be seen in Figure 64d and Figure 65. In both figures is the floor of the cavern covered with water.

The positive effect is that the amount of water sprayed or spilled into the cavern is much lower than before. The size of the retention cavern is sufficiently large.

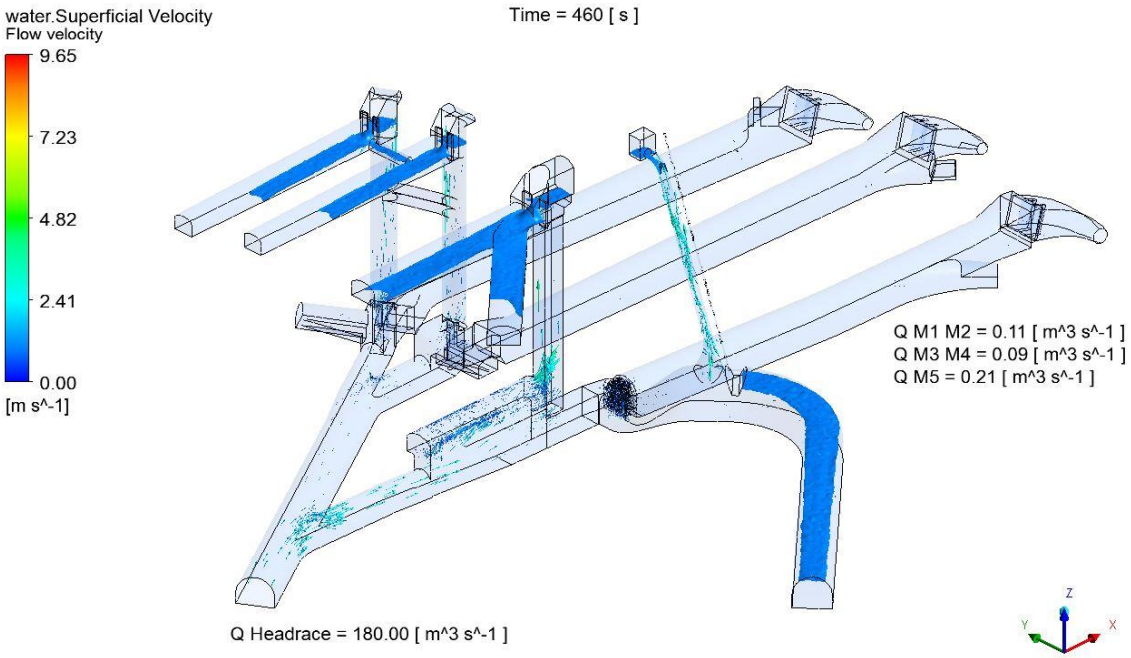

Figure 65 - Maximum upsurge after 460 seconds (V4 - full system)

The simulation of V4 shows that the combination of an upgraded discharge and sand trap is compatible and realisable. The flow diffusor is just one structural measure from the preliminary results. The next step would be to implement more of the structural measures of the preliminary results and further investigate the effects in a bigger scale than just for the sand trap no.3.

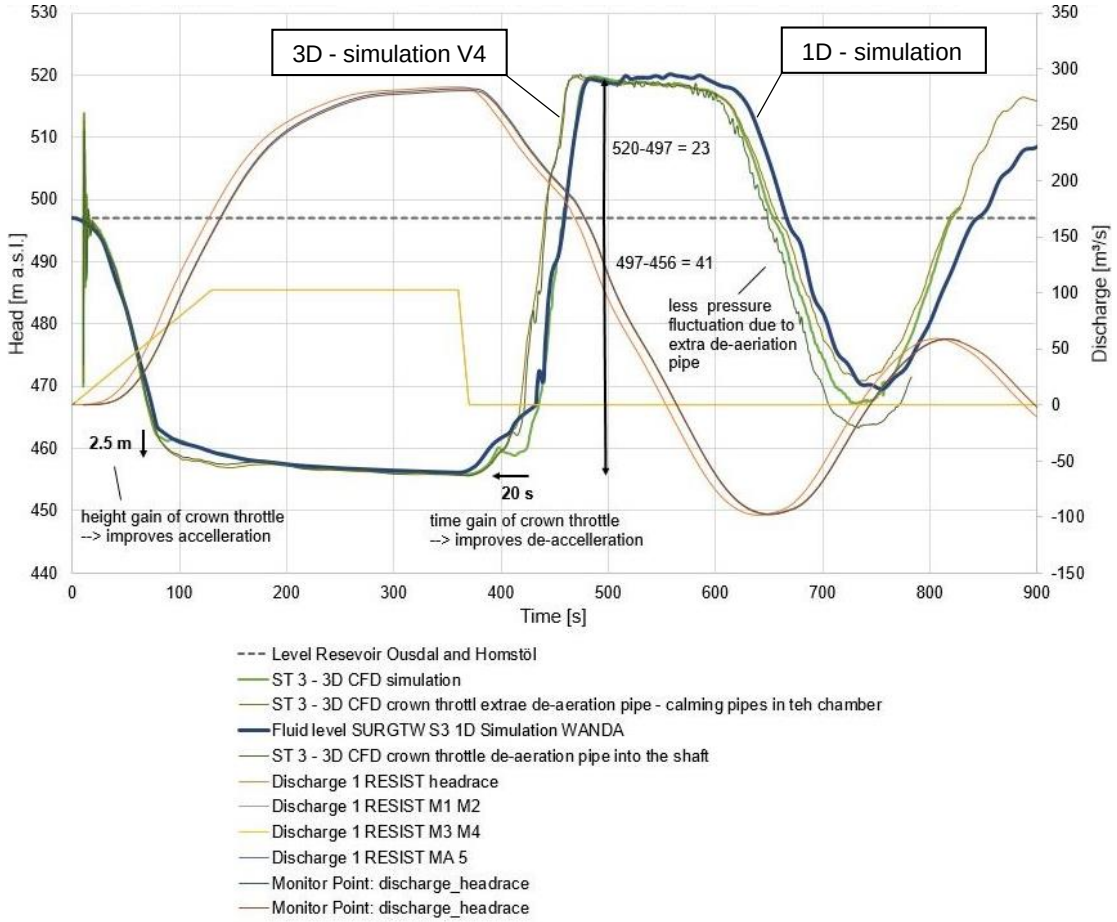

Figure 66 - Comparison of 3D and 1D simulation at the example of V4

Figure 66 shows the comparison of the 1D simulations and the 3D simulations. A very well accordance can be seen. The difference and shift in some simulations with the crown throttle show the positive behaviour onto the mass oscillation. Three effects can be identified.

1. Faster down surge due to the crown throttle to faster accelerate the mass flow
2. Faster upsurge to faster react on the flow to slow it down
3. Volume of the semi-air cushion to be used instead of upper chamber

8. Conclusion

As a summing up of the results and findings of the simulations, it can be concluded that a discharge increase for Tonstad as in this case of 25% is realisable if the needed adaptions and measures are made. The simulations were made at a capacity level of 497.6 m a.s.l. Since there is an additional margin in the lower chamber also deeper reservoir levels are qualified for discharge and this power upgrade. But for this different capacity levels further tests have to be carried out.

The problem for increased discharges are mainly the associated hydraulic losses which have to be taken into account. In the course of this thesis, an extension chamber was the chosen tool of choice to take on the increased losses by limiting the risk the risk of free surface flow in the sand traps. The results for such an upgraded discharge in combination with an extension chamber are very promising. For sure is this just the first step as these simulations have to be seen as a feasibility analysis. The whole structure of the extension chamber might further be improved and adapted. Some of the possible improvements can be for example, the possible reduction of the provided volume of the chamber and further improvement of the design and layout of the aeration or the chamber itself. Such feasibility analyses can be realised in a "short" time by the use of 3D CFD simulations as tool of choice. In comparison with the hydraulic scale models which are bound to large effort. In the simulation it is much easier to install different modifications or as example change surface roughness's as in a physical model. In addition, it is possible to model as in this thesis a power plant with all its components which wouldn't be possible as a hydraulic scale model.

Of course are hydraulic scale models additionally needed to finally clarify the system behaviour.

It was shown that the complex two-phase 3D CFD simulation with a rather coarse mesh and also a coarse time step resolution can reveal very valuable results to investigate the transient behaviour of a large surge tank facility. Due to the upgrade at the surge tanks it is possible to increase the energy output as well as the flexibility of a hydropower plant. Finally, the gained results and findings may encourage an upgrade of existing hydropower plants by simply upgrading the surge tank.

Bibliography

Bollrich, G., 2013. *Technische Hydromechanik 1, Grundlagen.* 7th ed. Berlin: Beuth Verlag.

Bråtveit, K. & Olsen, N. R. B., 2015. *Calibration of Horizontal Acoustic Doppler Current profilers by three dimensional CFD simulations,* s.l.: s.n.

Brevik, O., 2013. *3D numerisk modellering av deler av vassvegen til Tonstad kraftverk.* Master thesis: NTNU trondheim.

European Commission , n.d. *A fully-integrated internal energy market.* [Online] Available at: https://ec.europa.eu/commission/priorities/energy-union-and-climate/fully-integrated-internal-energy-market_en [Accessed 12 February 2018].

Giesecke , J., Heimerl, S. & Mosonyi, E., 2014. *Wasserkraftanalagen. Planung, Bau und Betrieb.* 6th ed. Berlin: Springer Berlin.

Idel'chik, I. E., 1994. *Handbook of Hydraulic Resistance.* 3rd ed. Danbury: Begell House.

Kjørholt, H., 1991. *Gas Tightness of Unlined Hard Rock Caverns.* Dissertation, NTH Trondheim.

Lecheler, S., 2014. *Nummerische Strömungsberechnung. Schneller Einstieg durch anschauliche Beispiele mit Ansys 5.0.* 3rd ed. Berlin: Springer Berlin.

Møller, I., 2009. *Norwegian dams, volume I.* Oslo: Energi Forl.

Palmstrom, A., 1987. *Norwegian design and contruction of unlined pressure shafts and tunnels.* Oslo, Proceedings of the International conference on Hydropower, Norway.

Richter , W., Vereide , K. & Zenz , G., 2017. Upgrading of a Norwegian pressurized sand trap combined with an open air surge tank. *Geomechanics and Tunneling ,* 10(5), pp. 620-624.

Schwarze, R., 2013. *CFD-Modellierung. Grundlagen und Anwendungen bei Strömungsprozessen.* 1st ed. Berlin: Springer Berlin.

Sira-Kvina Kraftselskap, n.d. *Tonstad kraftverk.* [Online] Available at: https://www.sirakvina.no/ tonstad-kraftverk/tonstad-kraftverk-article260-919.html
[Accessed 18 October 2017].

Statkraft, n.d. *Hydropower.* [Online] Available at: https://www.statkraft.com/energy-sources/ hydropower/
[Accessed 10 January 2018].

Statnett & Fingrid, 2016. *Challenges and opportunities for the Nordic power system,* s.l.: s.n.

Vereide , K. et al., 2017. *Upgrading of Sand Traps in Existing Hydropower Plants.* Sevilla, Proceedings of the Hydro conference.

Vereide, K., Svingen , B. & Guddal, R., 2015. *Case study: Damaging effects of increasing the installed capacity in an existing hydropower plant.* Dublin , BHR Pressure Surges.

List of figures

List of tables

List of symbols and abbreviations

Capital letters

A	[m^2]	Area
D	[m]	Pipe diameter
H	[m]	Total Height [m]
L	[m]	Pipe Length
R_e	[-]	Reynolds number
T_R	[s]	Reflection time

Small letters

a	[m/s]	Propagation velocity of the pressure wave
g	[m/s^2]	Gravitational force
h_a	[m]	water hammer
h_v	[m]	Hydraulic head loss
k	[mm]	Surface roughness
k_s	[$m^{1/3}/s$]	Manning Strickler roughness coefficient
l	[m]	Length to the nearest water surface
p	[N/m^2]	Pressure
t_s	[s]	Closing time
v	[m/s]	flow velocity
z	[m]	Height above reference plane

Greek letters

β	[°]	Divergence angle
γ	[kN/m^3]	Specific weight
ζ	[-]	Coefficient of inlet loss
η	[-]	Reduction factor
λ	[-]	Friction factor
ν	[m^2/s]	Kinematic viscosity

Abbreviations

atm	Physical (standard) atmosphere pressure
CFD	Computational Fluid Dynamics
FlekS	Fleksible Sandfang
HVDC	High-Voltage Direct-Current
HPP	Hydropower plant
UK	United Kingdom of Great Britain and Northern Ireland
SST	Shear Stress Transport
TSO	Transmission System Operator

Appendix A

List of the design plans used for the modelling of the Tonstad surge tanks. All plans were provided via the Sira-Kvina power company.

Plan number	Name
KT1.321.001.B03062	Tonstad Kraftverk Sandfang 1.
KT1.321.002.B03063	Tonstad Kraftverk Sandfang II
KT1.322.000.B00699	Tonstad Kraftverk ùvre fordelingsbasseng med trykksjakter. Oversikt.
KT1.323.000.B00325	Tonstad Kraftverk Fordelingsbasseng og inntak trykksjakter. Plan og snitt.
KT1.323.000.B00350	Tonstad Kraftverk Topp trykksjakter. Sprengning
KT1.323.001.B00864	Tonstad Kraftverk Konus trykksjakt I. Forskaling.
KT1.323.002.B01401	Tonstad Kraftverk Konus trykksjakt II. Forskaling.
KT1.841.001.B00345	Tonstad Kraftverk Stigesjakter og utjevningsbasseng. Sprengningsplan.
KT2.321.000.B06018	Tonstad Kraftverk Hovedstikningsplan. Oversikt, lengdesnitt.
KT2.321.001.B06019	Tonstad Kraftverk Tverrslag toppen. Stikning, sprengning.
KT2.322.001.B06023	Tonstad Kraftverk Tillõpstunnel. Nedre svingkammer. Stikning, sprengning.
KT2.322.001.B06050	Tonstad Kraftverk Tillõpsttunnel. ùvre svingkammer med lukekammer. Stikning, sprenging.
KT2.323.000.B06028	Tonstad Kraftverk Varegrindparti topp trykksjakt.Oversikt, sprengning.